AD NUMBER

AD881982

LIMITATION CHANGES

TO:

Approved for public release; distribution is unlimited.

FROM:

Distribution authorized to U.S. Gov't. agencies and their contractors; Critical Technology; JAN 1971. Other requests shall be referred to U.S. Army Air Mobility Research and Development Laboratory, Fort Eustis, VA 23604. This document contains export-controlled technical data.

AUTHORITY

USAAMRDL ltr, 10 Sep 1971

The following notice applies to any unclassified (including originally classified and now declassified) technical reports released to "qualified U.S. contractors" under the provisions of DoD Directive 5230.25, Withholding of Unclassified Technical Data From Public Disclosure.

NOTICE TO ACCOMPANY THE DISSEMINATION OF EXPORT-CONTROLLED TECHNICAL DATA

1. Export of information contained herein, which includes, in some circumstances, release to foreign nationals within the United States, without first obtaining approval or license from the Department of State for items controlled by the International Traffic in Arms Regulations (ITAR), or the Department of Commerce for items controlled by the Export Administration Regulations (EAR), may constitute a violation of law.

2. Under 22 U.S.C. 2778 the penalty for unlawful export of items or information controlled under the ITAR is up to ten years imprisonment, or a fine of $1,000,000, or both. Under 50 U.S.C., Appendix 2410, the penalty for unlawful export of items or information controlled under the EAR is a fine of up to $1,000,000, or five times the value of the exports, whichever is greater; or for an individual, imprisonment of up to 10 years, or a fine of up to $250,000, or both.

3. In accordance with your certification that establishes you as a "qualified U.S. Contractor", unauthorized dissemination of this information is prohibited and may result in disqualification as a qualified U.S. contractor, and may be considered in determining your eligibility for future contracts with the Department of Defense.

4. The U.S. Government assumes no liability for direct patent infringement, or contributory patent infringement or misuse of technical data.

5. The U.S. Government does not warrant the adequacy, accuracy, currency, or completeness of the technical data.

6. The U.S. Government assumes no liability for loss, damage, or injury resulting from manufacture or use for any purpose of any product, article, system, or material involving reliance upon any or all technical data furnished in response to the request for technical data.

7. If the technical data furnished by the Government will be used for commercial manufacturing or other profit potential, a license for such use may be necessary. Any payments made in support of the request for data do not include or involve any license rights.

8. A copy of this notice shall be provided with any partial or complete reproduction of these data that are provided to qualified U.S. contractors.

DESTRUCTION NOTICE

For classified documents, follow the procedure in DoD 5220.22-M, National Industrial Security Program, Operating Manual, Chapter 5, Section 7, or DoD 5200.1-R, Information Security Program Regulation, Chapter 6, Section 7. For unclassified, limited documents, destroy by any method that will prevent disclosure of contents or reconstruction of the document.

USAAVLABS TECHNICAL REPORT 70-69

AN EXPERIMENTAL/THEORETICAL CORRELATION OF MODEL AND FULL-SCALE ROTOR PERFORMANCE AT HIGH ADVANCING-TIP MACH NUMBERS AND HIGH ADVANCE RATIOS

By

Bruce B. Charles

January 1971

EUSTIS DIRECTORATE

U. S. ARMY AIR MOBILITY RESEARCH AND DEVELOPMENT LABORATORY

FORT EUSTIS, VIRGINIA

CONTRACT DAAJ02-69-C-0098

BELL HELICOPTER COMPANY

FORT WORTH, TEXAS

Statement #2 to remain
per Mrs Gillam (H. Curtis)
927-3002

R Newsom
4-2-71

DISCLAIMERS

The findings in this report are not to be construed as an official Department of the Army position unless so designated by other authorized documents.

When Government drawings, specifications, or other data are used for any purpose other than in connection with a definitely related Government procurement operation, the United States Government thereby incurs no responsibility nor any obligation whatsoever; and the fact that the Government may have formulated, furnished, or in any way supplied the said drawings, specifications, or other data is not to be regarded by implication or otherwise as in any manner licensing the holder or any other person or corporation, or conveying any rights or permission, to manufacture, use, or sell any patented invention that may in any way be related thereto.

DISPOSITION INSTRUCTIONS

Destroy this report when no longer needed. Do not return it to the originator.

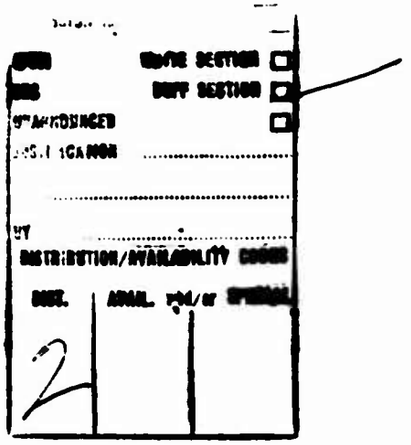

DEPARTMENT OF THE ARMY
EUSTIS DIRECTORATE
U.S. ARMY AIR MOBILITY RESEARCH AND DEVELOPMENT LABORATORY
FORT EUSTIS, VIRGINIA 23604

This report has been reviewed by the Eustis Directorate, U.S. Army Air Mobility Research and Development Laboratory, and is considered to be technically sound. The purpose of this investigation was (1) to determine if the performance derived from small-scale tests in a Freon atmosphere adequately represents full-scale behavior by comparing small-scale (Freon) tests with full-scale wind tunnel tests and HPH flight test rotor performance, and (2) to correlate the model results with calculated rotor performance using current-state-of-the-art analytical techniques.

Task 1F162204A13903
Contract DAAJ02-69-C-0098
USAAVLABS Technical Report 70-69
January 1971

AN EXPERIMENTAL/THEORETICAL CORRELATION OF MODEL AND FULL-SCALE ROTOR PERFORMANCE AT HIGH ADVANCING-TIP MACH NUMBERS AND HIGH ADVANCE RATIOS

Bell Helicopter Company Report 576-099-055

By

Bruce D. Charles

Prepared by

Bell Helicopter Company
Fort Worth, Texas

for

EUSTIS DIRECTORATE
U.S. ARMY AIR MOBILITY RESEARCH AND DEVELOPMENT LABORATORY
FORT EUSTIS, VIRGINIA

SUMMARY

Aerodynamic performance of two reduced-scale model rotors has recently been obtained in a Freon atmosphere in the NASA-Langley Transonic Dynamics Tunnel. The results are compared with existing full-scale wind tunnel and inflight rotor performance data to substantiate this method of testing rotors. Additionally, current state-of-the-art analytical techniques are employed to calculate the model performance. Overall, the model and full-scale results show good agreement when compared nondimensionally on an equal resultant force coefficient basis. Expected differences (due to rotor airfoil section differences) at conditions near rotor stall and at high advancing tip Mach numbers were not found in the test data. Possible implications are that a rotor tested in Freon may experience less severe stall and compressibility effects than would be shown by a corresponding rotor tested in air.

FOREWORD

The comparison of scale model (Freon atmosphere) with full-scale (air atmosphere) wind tunnel results and the comparison of scale model (Freon atmosphere) wind tunnel results with theory are presented in this report. The project was performed under Contract DAAJ02-69-C-0098, Task 1F162204A13903, under the technical cognizance of Patrick Cancro, Project Engineer, Eustis Directorate, U.S. Army Air Mobility R&D Laboratory.

The author also wishes to recognize the technical assistance of R. S. Todd, R&D Aerodynamicist, and W. H. Tanner, R&D Group Engineer, Advanced Technology, of the Bell Helicopter Company in the preparation of this report.

TABLE OF CONTENTS

TABLE OF CONTENTS (CONT'D)

LIST OF ILLUSTRATIONS

LIST OF SYMBOLS

a	Speed of sound, ft/sec
A_{1_s}	Lateral cyclic pitch with respect to the shaft axis, deg
b	Number of blades
B_{1_s}	Longitudinal cyclic pitch with respect to the shaft axis, deg
c	Blade chord, ft
C_D/σ	Rotor drag coefficient, $C_D/\sigma = D/\rho\, bcR(\Omega R)^2$
C_L/σ	Rotor lift coefficient, $C_L/\sigma = L/\rho\, bcR(\Omega R)^2$
C_Q/σ	Rotor torque coefficient, $C_Q/\sigma = Q/\rho\, bcR^2(\Omega R)^2$
D	Drag, the component of the resultant force parallel to the relative wind direction, positive in the downwind direction, lb
L	Lift, the component of rotor resultant force perpendicular to the relative wind direction in the plane of the relative wind and the shaft, positive up, lb
M	Mach number, $M = V/a$
$M_{(1.0,\ 90)}$	Advancing tip Mach number, $M_{(1.0,\ 90)}=(V + \Omega R)/a$
M_s	Instantaneous bending moment applied to shaft
$\overline{M}_s$	Average bending moment applied to shaft
$M_{\parallel}$	Bending moment on shaft resulting in bending parallel to axis of blades
$M_{\perp}$	Bending moment on shaft resulting in bending perpendicular to axis of blades
P_R	Prandtl number
q	Dynamic pressure at vehicle velocity, $q = 1/2\rho V^2$, lb/ft^2
Q	Shaft torque, the moment about the shaft Z_s axis, positive when torque tends to accelerate the rotor, ft-lb

R	Rotor radius, ft
T_W/T_1	Ratio of local wall and freestream temperatures
V	Forward speed, ft/sec
W	Weight of rotor blades and hub, lb
z	Distance from rotor hub along shaft to strain gage location, ft
α	Local airfoil section angle of attack, deg
α_s	Shaft angle of attack, the angle between the relative wind and a plane normal to the shaft axis, positive in nose-up direction, deg
α_c	Control axis angle of attack, the angle between the relative wind, the shaft axis, and the projection of the control axis on the plane of the relative wind axis, positive in nose-up direction, deg
γ	Ratio of specific heats
$\theta_{.75R}$	Blade collective pitch angle measured at 0.75R, deg
μ	Advance ratio, $\mu = \frac{V}{\Omega R}$
ρ	Density of fluid medium, slugs/ft^3
σ	Rotor solidity, $\sigma = \frac{bc}{\pi R}$
ψ	Azimuth position, deg
Ω	Rotor shaft angular velocity, rad/sec

Systems of Axes

1. Wind axis system:

x_w	Longitudinal Wind Axis. Axis lying along the airstream or relative wind direction.
z_w	Normal Wind Axis. Axis perpendicular to the longitudinal wind axis in the plane of the wind axis and the shaft centerline.
y_w	Lateral Wind Axis. Axis perpendicular to the x_w and z_w axes.

2. Shaft axis system:

z_s Shaft Axis. Axis coincident with the shaft centerline.

x_s Longitudinal Shaft Axis. Axis perpendicular to the shaft axis, in the plane of the shaft axis and relative wind direction.

y_s Lateral Shaft Axis. Axis perpendicular to the x_s and z_s axes. The axis is coincident with the lateral y_w wind axis.

3. Control axis system:

z_c Control Axis. Axis of no feathering. Axis with reference to which there is no first harmonic pitch change with azimuth angle. This axis may be tilted with respect to the shaft longitudinally (with $B1_s$) and laterally (with $A1_s$), separately or in combination.

x_c Longitudinal Axis. Axis perpendicular to the control axis in the plane of the control axis and relative wind direction.

y_c Lateral Axis. An axis perpendicular to the x_c and z_c axes.

INTRODUCTION

With the increasing speed requirements of future rotary-wing aircraft, the need for new rotor performance testing methods and improved analytical prediction techniques is evident. The high-performance spectrum has been probed in several full-scale rotor tests conducted in the NASA-Ames 40- by 80-foot Large-Scale Wind Tunnel. However, speed limitation of this tunnel prevents rotor operation at high advancing-tip Mach number/high advance ratio conditions. High-speed rotor performance results are available from inflight testing of compound helicopters such as the Army/Bell High Performance Helicopter (HPH). Unfortunately, for correlation purposes it is usually necessary to have a closely controlled wind tunnel environment where the range of conditions to be examined is not severely restricted by flight spectrum requirements.

To solve these problems, experimental efforts have recently turned to scale model testing in a Freon atmosphere at the NASA-Langley Transonic Dynamics Tunnel. The low speed of sound ($\approx$ 525 fps) and other Freon properties allow a scaled model to operate close to full-scale Reynolds numbers in the high advance ratio/high advancing-tip Mach number regime. Recently, two small-scale model rotors have been tested in the Freon wind tunnel through a range of conditions corresponding to and extending those obtained in previous full-scale wind-tunnel tests (References 1-3). Also, results corresponding to some conditions obtained in the HPH flight test program (Reference 4) were recorded.

Since the use of Freon for rotor aerodynamic testing is relatively new, and Freon has several properties significantly different from air, it is necessary to substantiate the results obtained by this method of testing. Therefore, in the present work, the Freon model, full-scale wind tunnel, and HPH flight test rotor performance are compared to determine if the performance derived from small-scale tests in Freon adequately represents full-scale behavior. In particular, since Freon has a lower ratio of specific heats than air (γ_F = 1.13, γ_{AIR} = 1.4), attention is given to comparisons at high Mach numbers and conditions near stall, as some differences between air and Freon may exist in compressibility and boundary layer flow characteristics.

A second purpose of this report is to correlate the model results with calculated rotor performance using current state-of-the-art analytical techniques. The theoretical comparisons are presented as an additional aid in substantiating the model performance. Further, the calculated performance is compared with test data over a wide range of conditions which present an opportunity to determine where analytical predictions can

be used with confidence. In this regard, three separate analyses are included. The basic method calculates performance utilizing a rigid-blade uniform-inflow theory (References 1-3 use this method). The second method accounts for non-uniform-inflow effects using a free-trailing tip vortex model. Finally, the third method accounts for the influence of local unsteady aerodynamics.

EXPERIMENTAL ROTOR DATA

DESCRIPTION OF ROTOR SYSTEMS

The Freon model rotor tests were originally designed to obtain dynamic and aerodynamic results for a Bell 540 doorhinge rotor system. At present, full-scale wind-tunnel data are not available for this system. As a result, the model/full-scale comparisons are made with nonsimilar rotors. The two Freon rotors tested are one-quarter scale models of the AH-1G (540) rotors having 0-degree- and -10-degree-twist. Of the two rotors, only the -10-degree-twist model is dynamically scaled (in flapwise bending only).

The 0-degree-twist model performance is compared with that of a full-scale UH-1B (modified) rotor for high Mach numbers and moderately high advance ratios. Both wind tunnel and inflight (HPH) data are available for the modified UH-1B rotor. Also, full-scale performance at high advance ratios and low Mach numbers has been recorded using a low-twist UH-1D modified rotor. These data are used only to make theoretical comparisons. Table I lists the geometric characteristics of these rotors.

TABLE I. GEOMETRIC CHARACTERISTICS OF THE 0-DEGREE-TWIST MODEL AND LOW-TWIST FULL-SCALE ROTORS

Rotor Parameter	1/4-Scale Freon Model	UH-1B (Modified)	UH-1D (Modified)
Twist	0 deg	-1.83 deg	-1.42 deg
Diameter	11 ft	44 ft	34 ft
Chord	6.75 in.	21 in.	21 in.
Solidity	0.0651	0.0506	0.0656
Airfoil Section and Tip Configuration	Bell 540 from root to 0.8R; linearly tapered to 6% at tip	NACA 0012 from root to 0.8R; linearly tapered to NACA 0006 (mod.) at tip	NACA 0012 from root to tip

The -10-degree-twist model performance is compared with standard and thin-tip UH-1D rotor data. Table II lists the geometric characteristics of the three rotors.

TABLE II. GEOMETRIC CHARACTERISTICS OF THE -10-DEGREE-TWIST MODEL AND FULL-SCALE ROTORS

Rotor Parameter	1/4-Scale Freon Model	Standard UH-1D	Thin-Tip UH-1D
Twist	-10 deg	-10.9 deg	-10.9 deg
Diameter	11 ft	48 ft	48 ft
Chord	6.75 in.	21 in.	21 in.
Solidity	0.0651	0.0464	0.0464
Airfoil Section and Tip Configuration	Bell 540 from root to tip	NACA 0012 from root to tip	NACA 0012 from root to 0.8R; linearly tapered to NACA 0006 (mod.) at tip

RANGE OF DATA AVAILABLE FOR MODEL AND FULL-SCALE ROTORS

The 0-degree- and -10-degree-twist Freon rotors were tested at the advancing-tip Mach numbers and advance ratios shown in Figures 1 and 2, respectively. Also, the conditions at which the full-scale rotors were tested in the NASA-Ames 40- x 80-foot wind tunnel, and points at which sufficient data are available from the HPH program, (Reference 4) are shown.

At each condition presented in these figures, the shaft angle and collective pitch were varied to obtain an envelope of data points. In the Freon model tests, the shaft angle was varied in even increments, and at each setting the collective pitch was adjusted to obtain given lift values. The maximum values were limited by stall or rotor loads and vibration. In the full-scale wind-tunnel tests, both shaft angle and collective pitch were varied in even increments. For all wind-tunnel data, the first harmonic flapping (with respect to the shaft) was minimized by application of cyclic pitch control.

THEORETICAL ROTOR PERFORMANCE METHOD

Theoretical rotor performance for the Freon model rotors is calculated using a rigid blade, uniform-inflow analysis. This basic analysis has been further modified in two separate programs. These include a free-trailing tip vortex for wake effects and an unsteady-aerodynamics analysis for oscillating airfoil effects.

UNIFORM-INFLOW ANALYSIS

The basic rotor performance program utilizes a single, rigid blade with a flapping hinge at the center of rotation. Steady two-dimensional wind-tunnel airfoil data are utilized which include Mach number and Reynolds number effects. These data include angles of attack up to 180 degrees for the reverse flow region. Tip loss effects are included. The hub and root portion of the blade is removed to be compatible with wind-tunnel data in which these effects are accounted for through tares. Angle-of-attack distributions in the basic method are calculated using the uniform induced velocity assumption.

NONUNIFORM-INFLOW ANALYSIS

Crimi's free-trailing tip-vortex analysis (Reference 5) has been integrated into the basic program to provide nonuniform-inflow effects. In this analysis, the rotor blades are replaced by single-bound vortices with strength varying harmonically with azimuth position. The wake is represented by a free vortex segment trailing from the tip of each blade-bound vortex.

To determine self-induced effects, the tip vortex segment is assumed to have a core size of five percent of the rotor radius. The core size of each segment is allowed to change as the wake distorts, but circulation strength is not allowed to decay. Two revolutions of the wake have been found necessary to obtain a periodic variation of the wake shape above 0.15 advance ratio. Once the periodicity of the distorted wake is established, the Biot-Savart relationship is integrated over the wake and bound vortex to determine induced velocities at any point in the flow. The induced velocities include vertical, tangential, and radial components. The analysis utilizes the first two components in determining angle-of-attack and Mach number effects, while the radial component is utilized in determining radial flow angles.

UNSTEADY-AERODYNAMICS ANALYSIS

Oscillating airfoil effects have been included in the basic uniform-inflow analysis using the method developed by Harris in Reference 6. Harris modified Theodorsen's oscillating airfoil analysis to account for stall hysteresis and three-dimensional flow effects. The method utilizes static two-dimensional airfoil data in conjunction with an empirically derived reference angle of attack to obtain the stall hysteresis. The reference angle of attack is a function of the quasi-steady blade element angle of attack and its time derivative. It also depends on Mach number and the experimental dynamic stall delay characteristics of the particular airfoil used. Three-dimensional flow effects on the lift coefficients above stall are corrected by the cosine rule for swept wings. Unsteady-aerodynamic effects on the airfoil drag are difficult to measure, and no instantaneous drag measurements are available. The analysis assumes that the drag coefficients are unaffected by unsteady aerodynamics below stall. At and above stall, static drag coefficients are utilized, but are taken from two-dimensional data at the reference angle of attack.

AERODYNAMIC DATA

Steady, two-dimensional airfoil data (obtained in air) are available for the 540 airfoil section from 0.3 to 0.8 Mach numbers at corresponding Reynolds numbers from 3 to 6 million. At low Mach numbers these Reynolds numbers are approximately equal to 10 million times the Mach number. (The Reynolds numbers decrease at higher Mach numbers due to temperature effects.) Similarly, for the quarter-scale model tests, the Reynolds numbers were approximately 9.2 million times the Mach number based on standard Freon density and viscosity. Therefore, the effects of Reynolds number differences between the Freon test data and the airfoil data used in the calculations are expected to be small.

The 540 airfoil data do not extend above α = 12 degrees. To account for higher angles of attack, these data were faired into NACA 0012 data (Reference 7), extending the angles of attack to 30 degrees. Further, since no 540 data were available above 0.8 or below 0.3 Mach numbers, curves needed outside this range were estimated from Reference 7. A 0.1 Mach number 0012 curve for $\alpha \leq 180$ degrees is utilized for the reverse flow region.

Aerodynamic characteristics for the thin-tip portion of the 0-degree-twist rotor were determined by the method described in Reference 2. It assumes that the improved supercritical flow characteristics of the thinner sections can be simulated

by reducing the local Mach numbers in accordance with the variation of drag divergence Mach number.

The reference angle-of-attack function used in the unsteady-aerodynamics analysis has been adopted from Reference 8 utilizing Vertol 23010-1.58 airfoil data. This was done since the 540 airfoil has not been tested for oscillating airfoil effects.

TWO-DIMENSIONAL CHARACTERISTICS OF THE BELL 540 AND NACA 0012 AIRFOILS

The Bell 540 airfoil section (shown in Figure 3) is derived from a 21-inch chord NACA 0012 profile. The leading edge portion of the 21-inch chord 0012 profile is mated to an extended straight trailing edge section aft of the spar location, yielding a 27-inch chord symmetrical airfoil. The differences between the two airfoils are summarized in the following tabulation:

	NACA 0012	540
Thickness	12% Chord	9.34% Chord
Maximum Thickness	30% Chord	23.3% Chord
Nose Radius	1.58% Chord	1.58% (Based on original 21-inch chord)

Several important differences exist between the 540 and 0012 aerodynamic characteristics as a result of profile differences. In Figure 4, the lift curve slope and maximum lift coefficients of the profiles are compared as functions of Mach number. Note that the Reynolds numbers shown for each set of data closely approximate the values at which the model and full-scale rotors were tested. As expected, the thinner profile (at lower Reynolds numbers) shows lower lift curve slopes and stalling lift coefficients. The supercritical flow characteristics of the two profiles are compared in Figure 5. Drag divergence is reached at lower Mach numbers with the 540 profile as a consequence of its forward maximum thickness location. (See Reference 9 for thickness distribution effects in supercritical flow.)

These aerodynamic characteristics may be expected to cause some differences in the model and full-scale comparisons. For example, when the performance is compared at equal rotor resultant force coefficient values, a particular airfoil section of the model rotor will generally operate at higher angles of attack than the corresponding full-scale rotor section due to the lift curve slope differences. Therefore, the model rotor is expected to show evidence of stall either at lower resultant force coefficients or lower advance ratios than the full-scale rotor. By the same reasoning, comparisons at high Mach numbers are also expected to reveal higher power requirements for the model rotor as portions of it exceed the drag divergence Mach number. These points will be important in the discussion presented in the remainder of this report.

EXPERIMENTAL AND THEORETICAL PERFORMANCE CORRELATION

0-DEGREE-TWIST MODEL ROTOR VERSUS FULL-SCALE UH-13 (MODIFIED) ROTOR PERFORMANCE

A complete sample of the 0-degree-twist Freon model performance at $\mu = 0.44$, $M_{(1.0,\ 90)} = 0.77$ is presented in Figure 6, showing the various control positions. In the upper figures, the model data are compared directly with full-scale wind tunnel performance of the UH-1B (mod.) rotor. (Corrections for solidity differences using Reference 7 were found to be small and have been neglected.) The model data are presented again in the lower figures for comparison with calculated model performance using the uniform-inflow analysis. These figures are included to give an indication of test versus test and test versus theory control position agreement. They also serve as a step to illustrate how the performance will be derived later as functions of advancing-tip Mach number and advance ratio.

The model rotor performance was measured at constant shaft angles for various lift values, yielding the smooth curves indicated by lines with solid symbols. Agreement with the full-scale rotor shaft angle data shown on the lift curves (Figure 6a) is good. However, this agreement deteriorates on the drag and torque curves (Figures 6b and 6c) with large differences shown. Agreement of the model and full-scale collective pitch lines is also good. Note that the model collective pitch was not varied in even increments. Consequently, the pitch lines shown in Figure 6a have been obtained from a graph of the lift coefficient (C_L/σ) versus three-quarter-radius collective pitch ($\theta_{.75R}$) at several constant shaft angles. A considerable scatter of the data was evident on these auxiliary graphs; therefore, the values presented in Figure 6a are subject to some error. The model collective pitch lines are omitted in Figures 6b and 6c for clarity.

Comparison of the experimental and calculated model control positions in the lower graphs of Figure 6 reveals trends similar to the test-to-test comparisons in the upper graphs (except where the theory shows abrupt slope changes indicative of rotor stall). At low and positive shaft angles in Figure 6a, for example, theory overestimates lift while the reverse is true above $\alpha_s = -10°$. In Figure 6b for a given lift coefficient, theory underestimates rotor propulsive force (negative C_D/σ) except at the extreme shaft angles, $\alpha_s = -15°$ and $\alpha_s = +5°$. At a given lift coefficient, theory also underestimates rotor torque as shown in Figure 6c.

Figures 7 and 8 are the result of crossplotting the experimental and theoretical curves in Figure 6 at constant lift coefficients to compare the performance on the basis of equal resultant force coefficients rather than at equal control positions. (All performance comparisons throughout the report will be made at equal resultant force coefficients.) The model and full-scale performance shows good correlation in Figure 7 using this basis for comparison. In particular, no significant trend differences are evident. In Figure 8, however, theory shows a major disagreement with the model data at $C_L/\sigma = 0.07$ and at large negative drag coefficients for $C_L/\sigma = 0.06$. An examination of the theoretical curves in Figure 6 at these conditions reveals that the differences are caused by rotor stall.

Stall Considerations

The theory curves in Figure 6 show stall at approximately 60 percent of the maximum lift coefficients obtained in the model tests. In test-theory comparisons of this type, early stall is usually predicted and is characteristic of an analysis that utilizes steady, two-dimensional airfoil data for stall effects. A comparison of model and full-scale uniform-inflow theory calculations is presented in Figure 9, indicating that the model rotor would be expected to reach stall sooner than the full-scale rotor. These calculations bear out the differences noted earlier between the 540 and NACA 0012 airfoils. However, comparisons of the model and full-scale experimental results (Figures 6 and 7) do not show evidence of this expected behavior.

In the Freon model tests, it was necessary to run at approximately 80 percent higher rpm than in the full-scale tests in order to obtain full-scale (UH-1B) advance ratio and Mach number values. Therefore, the airfoil oscillation frequency is higher for the model rotor. Consequently, unsteady aerodynamic effects may offer a possible explanation of the apparent stall delay exhibited by the Freon test results.

A theoretical calculation showing the effects of unsteady aerodynamics for the model rotor is included in Figure 10. At low and moderate lift coefficients, the unsteady theory agrees well with the model data. Below stall, the unsteady curves show higher power requirements than the steady theory. Above stall, the unsteady effects modify the static stall characteristics to produce a less abrupt slope change. The result is an apparent stall delay. At $C_L/\sigma = 0.07$, the entire unsteady theory curve is above stall and overestimates the power required by 30 percent. However, the data and theory curves show better slope agreement for this case. It should be

noted, however, that the unsteady calculations presented were not derived from 540 airfoil data and may not be accurate for this rotor.

A second factor that may cause differences between the full-scale and model stall character is possible nonsimilarity of their boundary layer flow character. References 10 and 11 note that similarity in steady compressible laminar boundary layer flows require identical values of the Reynolds number, Prandtl number, and the quantity $(\gamma-1)M^2$. The full-scale and model airfoils are not geometrically similar, but geometry and Reynolds number effects have been noted. Further, the Prandtl number differences between Freon and air are small ($P_{R_{AIR}} \approx 0.7$, $P_{R_{FREON}} \approx 0.8$; see Reference 12). However, the quantity $(\gamma-1)M^2$ is significantly smaller in Freon (at equal Mach numbers) due to its low ratio of specific heats ($\gamma_F = 1.13$, $\gamma_{AIR} = 1.4$).

The quantity $(\gamma-1)M^2$ enters in the temperature distribution in the boundary layer. It can be shown that the ratio of wall temperature to local freestream temperature is given by the relationship $T_W/T_1 = 1 + (\gamma-1)/2\ M^2$ (Reference 11). Thus at a given Mach number, the temperature ratio in Freon will be smaller than that in air. (This relationship is valid for an adiabatic wall only. The Prandtl number is a measure of the degree to which a flow is adiabatic, $P_R = 1$ being adiabatic.) It is noted in Reference 11 that heat transfer from the wall to the flow will cause separation at a lower adverse pressure gradient than is the case with an adiabatic wall. Therefore, Freon may require a steeper pressure gradient at the same Mach number or a higher Mach number with the same pressure gradient to cause separation.

Method of Presenting Advance Ratio and Mach Number Trends

In this section, the 0-degree-twist Freon rotor performance is compared with full-scale wind-tunnel performance of the modified UH-1B rotor and the three calculating techniques. The comparisons are presented at constant advancing-tip Mach number with varying advance ratio and at constant advance ratio with varying Mach number. The presentation method shows power variation for the model and full-scale rotors at equal resultant force coefficients. To obtain these conditions, the data have been graphed in the carpet-plot format as shown in Figure 8. The model and full-scale data are included in Appendixes I through IV.

Because the model and full-scale rotors and their test media are different, the performance comparisons cannot be made directly in dimensional form. However, nondimensional performance presented at constant Mach number with varying advance ratio (or vice versa)--using the torque coefficient/solidity ratio (C_Q/σ)--does not give a true representation of power because of the changes in rpm. Therefore, a new nondimensional torque factor is introduced which is proportional to horsepower per square foot of blade area. Using this factor, a given ordinate increment represents a constant horsepower increment at any advancing-tip Mach number/advance ratio combination. It is derived in the following manner.

Using the definition for torque coefficient, C_Q/σ, rotor horsepower may be written as

$$HP = \frac{Q\Omega}{550} = \frac{\rho(\Omega R)^3 \, bcR}{550} C_Q/\sigma$$

In this relationship the tip speed, ΩR, can be expressed as a function of advancing-tip Mach number and advance ratio ($\mu = V/\Omega R$):

$$M_{(1.0,\ 90)} = (1 + \mu) \frac{\Omega R}{a} \qquad (a = \text{speed of sound})$$

$$\text{or } \Omega R = \frac{aM_{(1.0,\ 90)}}{1 + \mu}$$

Substitution yields

$$\frac{HP}{bcR} = \frac{a^3 \rho}{550} \left(\frac{M_{(1.0,\ 90)}}{1 + \mu} \right)^3 \frac{C_Q}{\sigma}$$

Therefore,

$$\frac{HP}{bcR} \sim \left(\frac{M_{(1.0,\ 90)}}{1 + \mu} \right)^3 \frac{C_Q}{\sigma}$$

The torque coefficient factor is applied to all comparisons in the following work which are presented as functions of advance ratio/Mach number. If the rotor coefficients obtained from the Freon model are assumed to be valid for a full-scale version operating in air, an ordinate increment of 0.001 represents a $\Delta HP \approx 6$ horsepower per square foot of blade area for both Freon and full-scale rotors using standard air density and speed of sound.

It should be noted that by presenting the performance as a function of advance ratio at constant Mach number (and vice versa), the resultant force in pounds represented by a given resultant force coefficient is not constant but increases with Mach number and decreases with advance ratio due to the changes in rpm.

Advance Ratio Trends

The 0-degree-twist rotor advance ratio comparisons are presented in Figures 11 and 12 for $M_{(1.0,\ 90)}$ = 0.80, 0.85, 0.90, and 0.95. In Figures 11 and 13, the following notation is employed:

———— or ◇ — Freon Data - The solid line denotes test data which have been crossplotted from the Freon performance curves shown in the Appendix. This is referred to as Freon data in the text. A diamond symbol is used where Freon data are available only at one point.

– – – or ○ — Freon Theory - These calculations use the quasi-static uniform-inflow theory. Normally a dashed line is shown. In some graphs (Figure 11a at C_L/σ = 0.08, C_D/σ = -0.008 as an example) circle symbols are used since at higher advance ratios, theory values were calculated to be in extreme stall.

— — or □ — Full-Scale Data - Normally a long dashed line is used for the full-scale tunnel results. However, in some cases the only full-scale data available are at a single advance ratio; therefore, no line could be drawn and a square symbol is used.

Erratic behavior is displayed by the model data in Figure 11 for $M_{(1.0,\ 90)}$ = 0.80 and 0.90 at a μ value of about 0.35.

Although the experimental results have been carefully scrutinized, no explanation for this "bump" in the curves has been found. A possible reason for this behavior was thought to be that some data are not graphed at their nominal Mach numbers. For example, in Figure 11a at $\mu = 0.34$, the Mach number actually recorded is $M_{(1.0,\ 90)} = 0.81$ (see Figure 1). All other model data in Figure 11a were recorded at 0.80 Mach number. Although the Mach number is assumed to be 0.80, the torque coefficient factor for this point was calculated using $M_{(1.0,\ 90)} = 0.81$. The error caused by this assumption was evaluated analytically. At $M_{(1.0,\ 90)} = 0.81$ the torque coefficient is 0.0005, and at $M_{(1.0,\ 90)} = 0.80$ the torque coefficient has a value of 0.00048. The differences caused by this error are quite small and cannot be shown on the graph.

The erratic behavior of the Freon data was not shown at $M_{(1.0,\ 90)} = 0.85$ or at $M_{(1.0,\ 90)} = 0.95$. Also, no indication was found in the full-scale results or in the model calculations. Therefore, the Freon test data at approximately $\mu = 0.35$ were assumed to be in error, and the "bump" was faired out. The resulting Freon data curves are shown compared with various theoretical results in Figure 12.

General characteristics of the model experimental advance ratio performance trends (Figure 11) may be described as follows. At low lift coefficients ($C_L/\sigma = 0.04$), the power requirements show small variation with advance ratio for a given resultant force coefficient until moderately high advance ratios are attained. An increase in the power curve slope occurs between approximately 0.40 and 0.50 advance ratio. With increasing propulsive force values, the slope change occurs at correspondingly lower advance ratios. This behavior would be expected as the rotor approaches stall. A check of the data was made for the conditions $M_{(1.0,\ 90)} = 0.80$, $C_L/\sigma = 0.04$, $C_D/\sigma = -0.004$, $\mu = 0.49$, and $M_{(1.0,\ 90)} = 0.90$, $C_L/\sigma = 0.04$, $C_D/\sigma = 0$, $\mu = 0.55$ to determine if stall had occurred. However, a definite sign of rotor stall was not found. In some instances, the Freon data curves show an unexpected tendency to "level out" above 0.5 advance ratio.

Trends similar to those just discussed also appear in the Freon data at higher lift coefficients. Aside from the differences in magnitudes, the higher lift curves show only a small slope increase over the "linear" portion at lower advance ratios. A slight increase in slope is also evident as the Mach number is increased at constant lift coefficients.

A comparison of the model experimental advance ratio trends with those of the full-scale UH-1B (modified) rotor shows reasonable agreement. At 0.80 Mach number, the full-scale

data nearly duplicate the model performance, except for the region between 0.30 and 0.40 advance ratio. At 0.90 Mach number, the full-scale curves show a tendency for the power increase to occur at lower advance ratios than in the model data, particularly for the zero and positive propulsive force values. However, more full-scale data are needed to determine if the high advance ratio trends are significantly different. Although no curves can be drawn, the full-scale data points at 0.85 and 0.95 Mach numbers show magnitudes consistent with the 0.80 and 0.90 Mach number full-scale data and correlate reasonably well with the model data.

Finally, the small dashed line curves in Figure 11 present the theoretical Freon rotor performance using a uniform-inflow analysis. Later, the influence of theoretical nonuniform-inflow and unsteady aerodynamics on the advance ratio and Mach number trends will be examined.

Three significant trends are found in the test-theory advance ratio comparisons. Two of these may be pointed out in the 0.80 Mach number case. The theoretical performance shows good correlation with the model experimental data at C_L/σ = 0.04 for advance ratios below μ = 0.45. At higher advance ratios, the theory significantly underestimates the power required. For example, the test-theory power difference at μ = 0.55, C_L/σ = 0.04, C_D/σ = 0 amounts to roughly 1.8 horsepower per square foot of blade area--on a full-scale basis--or nearly 180 horsepower for a full-scale model.

The second major factor is theoretical prediction of early rotor stall. The observed power differences above 0.45 advance ratio are not shown at higher lift coefficients for this reason. In the C_L/σ = 0.06 curves, stall has occurred at approximately 0.45 advance ratio for C_D/σ = 0 and appears at slightly lower advance ratios as the propulsive force coefficient is increased. For the highest lift case, the entire set of theory curves shows stall at or just below 0.30 advance ratio.

These two characteristics are found in the remaining theoretical curves at higher Mach numbers. However, a third trend masks their appearance at 0.95 Mach number. An examination of the comparisons shows (particularly at low advance ratios) that with increasing Mach number, the theory begins to overestimate power requirements until a wide divergence occurs at 0.95 Mach number. Possible reasons for this behavior are noted in the Mach number trends discussion.

Except for the erratic data at μ = 0.35, the Freon model results closely approximate full-scale results. It has already

been mentioned that power coefficients are sensitive to Mach number. Considering that the Mach number for a given model data point is known only within ±.01 of the published value and that the data then must be faired and crossplotted, it can be said that the model and full-scale results are within the experimental error incurred in their measurement. Secondly, in the comparison of the test data to the uniform inflow calculations, it can be concluded that at low to moderate lift coefficients (at which rotorcraft will be flying) and for advance ratios above 0.4 to 0.5, the agreement between calculation and experiment is quite poor. Similar results have been shown in Reference 3.

Advance Ratio Trends With Nonuniform-Inflow and Unsteady Aerodynamics Theory

The 0-degree-twist rotor calculations presented in Figure 11 are compared in Figure 12 with calculations which separately include the effects of nonuniform-inflow and unsteady aerodynamics. In some cases, the wake calculations were not obtainable at high advance ratios due to program convergence difficulties.

Generally, for low lift values, the wake and unsteady effects do not change the uniform-inflow results significantly. They do show slightly higher power requirements at the high advance ratios (nonuniform-inflow theory appears to show stall at $M(1.0, 90) = 0.90$ and $C_D/\sigma = 0.004$), although no marked improvement is made in the high advance ratio test-theory differences noted earlier. For the $C_L/\sigma = 0.04$ case at $M(1.0, 90) = 0.95$, both the unsteady theory and the wake theory predict lower power requirements at low advance ratios than the uniform-inflow theory. The reason for this is unknown.

The unsteady aerodynamics and nonuniform-inflow effects show their greatest influence at $C_L/\sigma = 0.06$. At this lift coefficient, the unsteady theory shows the largest power requirements of the three theories for conditions below stall. Also, it shows a significant stall delaying effect. A comparison with the model data at 0.80 Mach number reveals that the correlation above $\mu \approx 0.40$ is much improved with this theory. At 0.90 and 0.95 Mach numbers, the difference between uniform-inflow and unsteady theories has approximately the same magnitude as is shown at $C_L/\sigma = 0.04$. As a result, correlation with the high Mach number model performance shows poorer agreement, particularly at the high propulsive force coefficients.

The calculations which include nonuniform effects show power requirements that generally lie between the uniform-inflow and

unsteady theory curves for C_L/σ = 0.06. Since the wake theory does not include unsteady aerodynamics, it approaches stall at approximately 0.45 advance ratio in a manner similar to the uniform-inflow theory results. At 0.95 Mach number, the wake calculations show closer agreement with the uniform-inflow calculations and tend to lie below these curves at low advance ratios. This effect gives a trend which agrees better with the model data. However, the magnitude of these curves still remains much larger than the model results.

Mach Number Trends

The experimental and theoretical performance of Figure 11 has been crossplotted and presented in Figure 13 as a function of advancing-tip Mach number for advance ratios of 0.31, 0.36, 0.41, and 0.45. These conditions were chosen so that a maximum number of full-scale comparisons could be made with the limited data available. However, full-scale rotor performance trends still could not be drawn for 0.31 and 0.45 advance ratios. Since the data were not all taken at the exact Mach numbers shown in Figure 11, there has been some error introduced into the curves in Figure 13 by crossplotting directly from Figure 11. For example, the model data plotted at M(1.0, 90) = 0.95 were actually recorded at M(1.0, 90) = 0.96. The result is that the power shown at 0.95 Mach number is greater than is actually the case. The trends, however, are unaffected by this error.

The full-scale rotor Mach number performance at advance ratios of 0.36 and 0.41 compares favorably with the model experimental results. Model test data at 0.80 and 0.90 Mach numbers for these advance ratios correspond to the "bumps" found in the advance ratio trends, and their power values are thought to be too high. By making this correction, the apparent decrease in power above 0.90 Mach number would be removed and better correlation with the full-scale curves would result. The low-lift curves at 0.41 advance ratio contain full-scale data for the entire Mach number range of the model data. No significant differences between the two sets of data are found at high Mach numbers.

Theoretical Mach number performance compared with the test results at 0.31 advance ratio shows that a crossover point exists between 0.80 and 0.90 Mach number. At low Mach numbers, the agreement is reasonable, but the trend is incorrect and a large power overestimation results at 0.95 Mach number. This trend continues both at higher advance ratios and at higher lift coefficients. However, as advance ratio is increased, the theoretical curves shift downward with respect to the test curves, giving the appearance of good agreement at high Mach numbers--except where the influence of stall is shown.

The large test-theory power differences at low advance ratios and high Mach numbers are evident in both the advance ratio and Mach number trend comparisons. Previous correlations with full-scale rotor data (Reference 2) have shown that theory predicts the power requirements well for these conditions. In Figure 14 (from Reference 2), for example, good agreement is shown with thin-tip UH-1D rotor performance for $\mu = 0.30$ and $M_{(1.0,\ 90)} = 0.95$. At $C_L/\sigma = 0.04$ and $C_D/\sigma = -0.004$, the calculated and experimental full-scale values agree within 80 horsepower. However, at corresponding conditions in Figure 13 ($\mu = 0.31$), theory overestimates the model power required by nearly 270 horsepower (on a full-scale basis).

If 540 airfoil data were available to use in the model calculations above 0.8 local Mach numbers instead of 0012 data, it is expected that even larger high Mach number differences would be shown. In Figure 15, theoretical Mach number trends are presented for the model at 0.30 advance ratio. The dashed line curve represents calculated performance using entirely NACA 0012 airfoil data for the 0-degree-twist model rotor. As indicated, the calculations using 540 airfoil data ($M \leq 0.8$) show slightly larger power requirements because the 540 airfoil must operate at angles of attack higher than corresponding 0012 values to provide the same rotor lift coefficient. The angle-of-attack difference would be larger yet if 540 airfoil data had been available for local Mach numbers greater than 0.8. Further, since the 540 airfoil has lower drag divergence Mach numbers, the combined effect would result in larger calculated power requirements than are shown in Figure 13. (Note in Figure 13 that a local Mach number of 0.8 is not reached until $M_{(1.0,\ 90)} = 0.88$ where $M_{(1.0,\ 90)}$ is based on V, ΩR, and the standard speed of sound. This is a consequence of varying the local speed of sound in the calculations to simulate improved Mach number characteristics of the tapered thickness tip.)

Based on the differences in airfoil characteristics and the results of the theoretical calculations, the experimental model performance would be expected to require more power at high Mach numbers than the full-scale rotor. The fact that it does not may indicate a possible difference between air and Freon testing. According to the trends shown, supercritical flow effects on rotors tested in Freon may be less severe than those on a rotor tested in air at equivalent conditions. To determine if this phenomenon is present, it will be necessary to compare the performance of a full-size rotor with that of an exact-scale model tested in Freon.

Mach Number Trends With Nonuniform-Inflow and Unsteady Aerodynamics Theory

Theoretical Mach number trends showing separately the effects of nonuniform-inflow and unsteady aerodynamics are compared with uniform-inflow calculations in Figure 16. The model test results are also included and have been smoothly faired to remove the erratic variations shown earlier. The wake and unsteady refinements to the uniform-inflow theory usually produce higher power requirements, with the most significant differences shown at high lift coefficients. Their influence on the Mach number trends causes the following behavior.

At low advance ratios ($\mu = 0.31$), the wake and unsteady theory curves generally lie slightly above the uniform-inflow theory results. The unsteady theory curves at a given drag coefficient maintain approximately a constant difference with increasing Mach number. The wake theory curves, however, approach the uniform-inflow theory curves and often cross below at high Mach numbers, indicating a relief of the compressibility effects. As the advance ratio reaches $\mu = 0.36$, the power shown by wake and unsteady theories at lower Mach numbers is considerably higher than the uniform-inflow theory values. With further increases in advance ratio ($\mu = 0.41$-0.45), the wake theory values tend to show closer agreement with uniform-inflow theory while the unsteady theory curves maintain larger power requirements (except where uniform-inflow theory shows stall - for example, at $\mu = 0.45$, $C_L/\sigma = 0.06$, $C_D/\sigma = -0.004$).

A comparison of the model experimental performance with that predicted by unsteady aerodynamics and nonuniform-inflow theories shows significant improvements in the test-theory correlation. Although theory continues to overestimate high Mach number power magnitudes, the nonuniform-inflow calculations show better high Mach number test-theory trend agreement because of the "compressibility relief" effect previously noted. The tendency for uniform-inflow theory curves to shift downward with reference to the experimental curves is also eliminated in the wake and unsteady theory calculations. For example, at $\mu = 0.36$ for $C_D/\sigma = -0.004$, the wake and unsteady calculations show excellent agreement with the model data below 0.90 Mach number. Above 0.90 Mach number, the unsteady theory curves are too steep and diverge from the test data. However, the nonuniform-inflow theory values at 0.95 Mach number differ from the test data by less than 10 percent.

HIGH ADVANCE RATIO PERFORMANCE AT LOW MACH NUMBERS

In Reference 3, the performance of a full-scale 34-foot-diameter modified UH-1D rotor was compared with uniform-inflow theory calculations for high advance ratio/low advancing-tip Mach number conditions. Figure 17 shows a test-theory comparison at μ = 0.51, M(1.0, 90) = 0.64 using Reference 3 data. For a given resultant force coefficient, the theory would yield a large underestimation of the torque coefficient. Figure 17 shows that prediction of the drag coefficient appears to be responsible since the torque coefficients agree reasonably well. Although the coefficient differences are large, the magnitudes of the drag or horsepower differences are small due to the low tip Mach number.

A similar comparison between Freon data and theory is presented in Figure 18 for the conditions μ = 0.44, M(1.0, 90) = 0.62. Large underestimations of the torque coefficients at a given resultant force coefficient will also be found as before. However, in this case, the drag coefficients agree well and large differences are shown on the C_Q/σ versus α_c graph. The reason for this reversal in the comparisons is unknown.

-10-DEGREE-TWIST MODEL ROTOR VERSUS FULL-SCALE STANDARD AND THIN-TIP UH-1D ROTOR PERFORMANCE

The -10-degree-twist Freon rotor performance is presented in Figure 19 with uniform-inflow theory and full-scale (standard tip) UH-1D rotor performance comparisons. The data were taken at 0.30 advance ratio; consequently, only Mach number trends are shown. Solidity corrections were applied to the small-scale test and theoretical results using the UH-1D rotor solidity as a reference value.

An examination of the full-scale and Freon results in Figure 19 reveals that the model rotor performs better at high Mach numbers than the UH-1D rotor, and poorer at low Mach numbers. The resulting crossover point occurs between 0.80 and 0.90 Mach number, and varies with both lift and drag coefficient values. This behavior may be caused by differences in the rotor airfoil thickness ratios.

In Figure 20, the model results are superimposed upon a comparison of standard and thin-tip UH-1D rotor performance. The thin-tip rotor is identical to a standard version except for a linear thickness ratio taper (from NACA 0012 to NACA 0006 mod.) over the last 20 percent of radius. The two full-scale Mach number trends show behavior similar to that in Figure 19. A simplified explanation for this may be given as follows.

At a given advance ratio, the effect of increasing the advancing-tip Mach number is to raise the dynamic pressure and increase compressibility. Although the thinner airfoil (0006 mod.) has a lower lift curve slope, for high Mach values it operates in an angle-of-attack range where the reduced thickness ratio offers better high Mach number performance than a thicker airfoil. For low Mach numbers, the thin profile loses its compressibility advantages at the higher angles of attack where it must operate to maintain lift coefficients equal to the thicker profile.

Notice that in Figure 20 the model rotor data lie between the full-scale results: the standard UH-1D rotor at 0.95 Mach number shows the most power required and has the largest tip-thickness ratio. Following this, the model and thin-tip results appear in descending order corresponding to their tip-thickness ratios. (The -10-degree-twist model rotor has a constant 9.3 percent thickness ratio.) This observation, based on tip-thickness ratio, seems logical. However, the model theoretical results do not support it. It is believed that the lower thickness ratios on the inboard stations of the model rotor should cause trends more like those shown by the calculations. This again raises the question of possible differences between Freon and air testing.

0-DEGREE-TWIST MODEL ROTOR VERSUS FLIGHT TEST ROTOR PERFORMANCE

Inflight rotor performance at three advancing-tip Mach number/advance ratio conditions has been obtained with the Army/Bell High Performance (Compound) Helicopter (HPH). The method of deriving the rotor performance from flight test and wind tunnel data is presented in this section and correlation with the Freon 0-degree-twist rotor is shown.

Reduction of Flight Test Data

1. Rotor Lift

The HPH rotor is physically the same hardware as that tested in the Ames 40- x 80-foot wind tunnel and described earlier as the UH-1B (modified) rotor. Therefore, the inflight rotor lift determination utilizes both HPH test measurements and the full-scale wind tunnel data in the following manner.

The flight test vehicle was instrumented to determine fuselage (shaft) angle of attack, rotor flapping angles, rotor hub flapwise bending moments and collective pitch. Several combinations of these measurements can be used in conjunction with the wind tunnel data to determine lift. However, the method chosen determines control axis angle of attack from shaft angle and rotor flapping, and the rotor lift from hub bending.

The rotor hub flapwise bending moments were also measured on the rotor in the wind tunnel (using the same strain gages). From these measurements and the tunnel balance data, the hub bending moment variation with lift and rpm was graphed. Inflight rotor lift was determined by entering this graph with the flight test rpm and hub bending moment and reading the corresponding lift. The solid symbols in Figure 21a represent the lift coefficients determined in this fashion and graphed versus control axis angle of attack for the conditions $\mu = 0.40$, $M_{(1.0,\ 90)} = 0.83$. Measured collective pitch and shaft angles at these lift values are tabulated on the graph. Agreement between the wind-tunnel (dashed lines) and inflight collective pitch values is good. Note that the line faired through the data does not represent a constant shaft angle line.

2. Rotor Drag

The HPH rotor drag is determined from measured shaft bending moments as shown in Figure 22a. The rotor lift, drag, and weight forces produce an average

resultant bending moment (assuming zero side force) in the fixed system, $\overline{M}_s$, at the strain gage location which may be expressed as

$$\overline{M}_s = -Lz \sin a_s + Dz \cos a_s + Wz \sin a_s$$

After rearranging, the drag is found to be

$$D = \frac{\overline{M}_s + (L-W)z \sin a_s}{z \cos a_s}$$

The instantaneous bending moment in the fixed system is made up of components in the rotating system which are measured by the strain gages attached to the shaft. These components are chosen parallel and perpendicular to the rotor span axis as shown in Figure 22b. Thus, the resultant instantaneous bending moment is

$$M_s = M_{\parallel} \cos\psi + M_{\perp} \sin\psi$$

Further, the parallel and perpendicular components vary with azimuth position and are assumed to have the form

$$M_{\parallel} = M_{\parallel_{MAX}} \cos\psi$$

$$M_{\perp} = M_{\perp_{MAX}} \sin\psi$$

The average resultant bending moment in the fixed reference is given by

$$\overline{M}_s = \frac{1}{2\pi} \int_0^{2\pi} (M_{\parallel} \cos\psi + M_{\perp} \sin\psi) \, d\psi$$

or substituting the components

$$\overline{M}_s = \frac{1}{2\pi} \int_0^{2\pi} (M_{\parallel_{MAX}} \cos^2\psi + M_{\perp_{MAX}} \sin^2\psi) \, d\psi$$

$$\overline{M}_s = \frac{M_{\parallel_{MAX}} + M_{\perp_{MAX}}}{2}$$

Therefore, the rotor drag may be calculated using the measured shaft bending moments and rotor lift from

$$D = \frac{M_{\parallel_{MAX}} + M_{\perp_{MAX}}}{2z \cos \alpha_s} + (L-W) \tan \alpha_s$$

The solid symbol points in Figure 21b were calculated using the drag equation. In the form shown, this equation also included shaft and hub drag which had to be subtracted to be consistent with the wind tunnel data. According to Reference 13, a good approximation for hub and shaft drag area is $f \approx 2ft^2$. The dashed line in Figure 21b shows the adjusted values.

The dotted line on the drag curve in Figure 21b has been derived from the intersection points of the flight and wind tunnel data shown on the lift curve. Assuming that the flight data are consistent with the wind tunnel data, the α_c and $\theta_{.75R}$ values at these points are marked on the drag curve. Ideally, this curve should duplicate the drag curve calculated from the shaft bending moments. However, the method of calculating drag neglects several factors which may be significant (for example, higher harmonics of the bending moments $M_{\parallel}$ and $M_{\perp}$ are neglected along with rotor side force and variation of hub drag with angle of attack).

3. Rotor Torque

The rotor shaft was instrumented with strain gages to determine shaft torque. The lower graph in Figure 21b shows the torque values at $\mu = 0.44$, $M(1.0, 90) = 0.83$ converted into coefficient form and graphed versus rotor angle of attack. The dotted line indicates values derived from the lift curves in the same fashion that the drag values were found. Note that the two curves show better agreement in this case. It is believed that the methods of determining rotor lift and rotor torque are accurate and give results consistent with the wind tunnel data.

Comparison of Model, Full-Scale, and Inflight Rotor Performance

In Figure 23, the 0-degree-twist Freon rotor performance is compared with the HPH and full-scale wind tunnel results on an equal resultant force coefficient basis. Using this method of presentation, inflight data generally show good agreement with both model and full-scale wind tunnel performance. The model, full-scale wind tunnel, and flight results all lie within a band $\Delta C_Q/\sigma \approx 0.002$ in width.

Figure 23a shows that in flight, the rotor apparently requires more power than is shown by wind tunnel results at $\mu = 0.40$ and $M(1.0, 90) = 0.83$. However, a crosscheck of Figure 21b reveals that the calculated drag at low lift coefficients (at positive control axis angles of attack) is on the order of $D/q \approx 2ft^2$ too high.

Also, the measured torque is higher than full-scale wind tunnel values. At $C_L/\sigma = 0.08$, the calculated drag is lower than is shown by wind tunnel values, but the torque value compensates to give good agreement. In the remaining figures, at higher Mach numbers and advance ratios, the HPH and full-scale wind tunnel results show even better agreement.

The inflight HPH data that is available for comparison to the tunnel results is extremely limited. The agreement shown is good; however, this may be misleading for the following reasons:

- The method of calculating the lift is based upon tunnel measurements. The interference effects between the wind tunnel model and the rotor will certainly be different than between the HPH airframe and the flight rotor. These differences will affect the control angles at a given rotor resultant force.

- The method for calculating drag is at best only approximate. The agreement shown may be due to compensating errors and, therefore, may be fictitious.

No conclusions should be drawn from this analysis except that a wind tunnel test of the full-scale HPH is required to validate the techniques used.

CONCLUSIONS

An analysis of the experimental model and full-scale rotor performance comparisons and correlation with calculated model performance yields the following conclusions:

- The model test performance shows reasonable agreement with full-scale wind tunnel data when compared at equal resultant force coefficients as functions of advance ratio and advancing-tip Mach number.

- Theoretical calculations indicate that the Freon model rotor would be expected to show stall at lower resultant force coefficients or at lower advance ratios (for a given force coefficient) than the full-scale rotor.

- At high Mach number-low advance ratio conditions, theoretically predicted power requirements are significantly larger than those shown by the model test data. Similar test-theory comparisons using full-scale rotor data show good agreement for rotors operating in air at these conditions.

- Absence of the expected rotor stall and high advancing-tip Mach number differences from the test-to-test comparisons indicates that (due to the low ratio of specific heats) a rotor tested in Freon may possess more stable boundary-layer flow characteristics and less severe compressibility effects than a corresponding full-scale rotor tested in air.

- Calculated advance ratio trends for the model rotor at low lift coefficients and low Mach numbers ($M_{(1.0,\ 90)}$ = 0.80-0.90) show significant underestimation of rotor power above $\mu \approx 0.45$. At higher lift coefficients, the uniform-inflow and wake theories predict early rotor stall at high advance ratios. However, the unsteady theory shows a significant stall delay effect which yields improved test-theory correlation for these conditions.

- Mach number trends calculated with the nonuniform-inflow theory show lower power requirements at high Mach numbers than uniform-inflow or unsteady theories, indicating that the wake may effect a "compressibility relief." Trend agreement with the test data is improved with this theory.

LITERATURE CITED

1. Lee, Charles; Charles, Bruce; and Kidd, David, WIND-TUNNEL INVESTIGATION OF A QUARTER-SCALE TWO-BLADED HIGH PERFORMANCE ROTOR, Bell Helicopter Company, Fort Worth, Texas; USAAVLABS Technical Report 70-58, U. S. Army Aviation Materiel Laboratories, Fort Eustis, Virginia, to be published.

2. Tanner, W. H., and Van Wyckhouse, J. F., WIND-TUNNEL TESTS OF FULL-SCALE ROTORS OPERATING AT HIGH ADVANCING TIP MACH NUMBERS AND ADVANCE RATIOS, Bell Helicopter Company, Fort Worth, Texas; USAAVLABS Technical Report 68-44, U. S. Army Aviation Materiel Laboratories, Fort Eustis, Virginia, July 1968, AD 674188.

3. Charles, Bruce D., and Tanner, Watson H., WIND-TUNNEL INVESTIGATION OF SEMIRIGID FULL-SCALE ROTORS OPERATING AT HIGH ADVANCE RATIOS, Bell Helicopter Company, Fort Worth, Texas; USAAVLABS Technical Report 69-2, U. S. Army Aviation Materiel Laboratories, Fort Eustis, Virginia, January 1969, AD 684396.

4. Sonneborn, Walter G. O., HIGH MACH NUMBER/HIGH ADVANCE RATIO FLIGHT TEST PROGRAM WITH THE HIGH-PERFORMANCE UH-1 COMPOUND HELICOPTER, Bell Helicopter Company, Fort Worth, Texas; USAAVLABS Technical Report 71-2, U. S. Army Aviation Material Laboratories, Fort Eustis, Virginia, to be published.

5. Crimi, Peter, THEORETICAL PREDICTION OF THE FLOW IN THE WAKE OF A HELICOPTER ROTOR, CAL Report No.'s BB-1994-S-1 and BB-1994-S-2, Cornell Aeronautical Laboratory, Incorporated, Buffalo, New York, September 1965.

6. Harris, Franklin D.; Tarzanin, Frank J., Jr.; and Fisher, Richard K., Jr., ROTOR HIGH SPEED PERFORMANCE, THEORY VS TEST, a paper presented at the V/STOL Technology and Planning Conference Sponsored by the Air Force Flight Dynamics Laboratory, 23-25 September 1969, Las Vegas, Nevada; The Boeing Company, Vertol Division, Philadelphia, Pennsylvania.

7. Tanner, Watson H., CHARTS FOR ESTIMATING ROTARY WING PERFORMANCE IN HOVER AND AT HIGH FORWARD SPEEDS, Sikorsky Aircraft Division of United Aircraft Corporation, Stratford, Connecticut; NASA CR-114, National Aeronautics and Space Administration, Washington, D. C., November 1964.

8. Gross, David W., and Harris, Franklin D., PREDICTION OF INFLIGHT STALLED AIRLOADS FROM OSCILLATING AIRFOIL DATA, American Helicopter Society 25th Annual National Forum, Presented at the Sheraton-Park Hotel, Washington, D. C., May 14, 15, 16, 1969; The Boeing Company, Vertol Division, Philadelphia, Pennsylvania.

9. Hoerner, S. F., FLUID-DYNAMIC DRAG, 2nd Edition, Midland Park, New Jersey, Hoerner, 1965, P. 15-16.

10. Kuethe, A. M., and Schetzer, J. D., FOUNDATIONS OF AERODYNAMICS, 2nd Edition, New York, John Wiley & Sons, Inc., January 1963, pp 260-1.

11. Schlichting, H., BOUNDARY LAYER THEORY, 4th Edition, New York, McGraw-Hill Book Company, Inc., June 1962.

12. Huber, Paul W., USE OF FREON-12 AS A FLUID FOR AERODYNAMIC TESTING, Langley Memorial Aeronautical Laboratory, NACA Technical Note 1024, National Advisory Committee for Aeronautics, Washington, D. C., April 1946.

13. Foster, R. D., RESULTS OF THE 1/2-SCALE UH-1 AND HIGH SPEED HELICOPTER PYLON AND HUB MODEL WIND TUNNEL INVESTIGATION, Bell Helicopter Company, Fort Worth, Texas, BHC Report No. 8025-099-012, March 21, 1961.

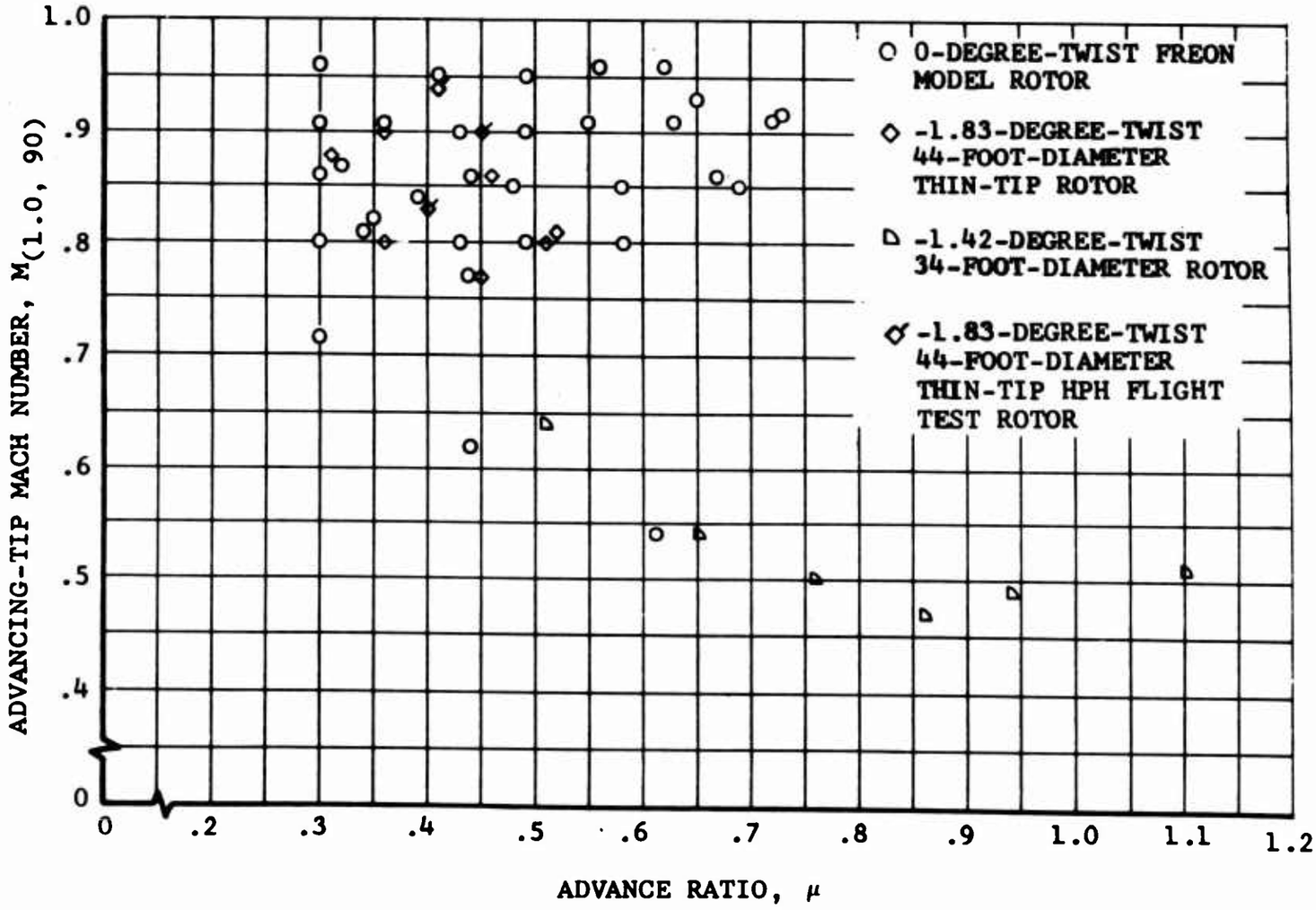

Figure 1. Advance Ratio/Advancing-Tip Mach Number Test Conditions Available for the 0-Degree-Twist Model Rotor and the Various Low-Twist Full-Scale Rotors.

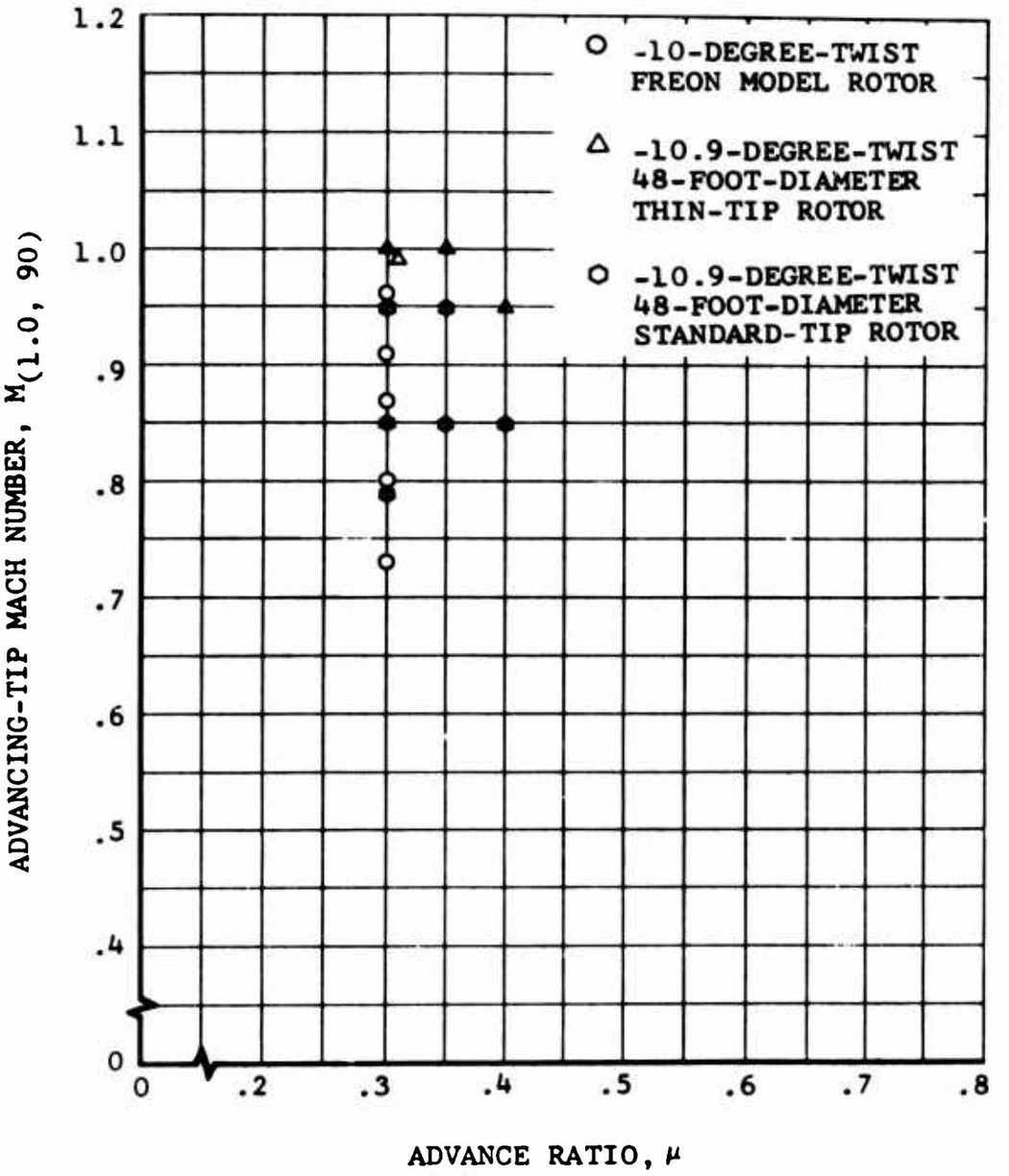

Figure 2. Advance Ratio/Advancing-Tip Mach Number Test Conditions Available for the -10-Degree-Twist Model Rotor and the Various High-Twist Full-Scale Rotors.

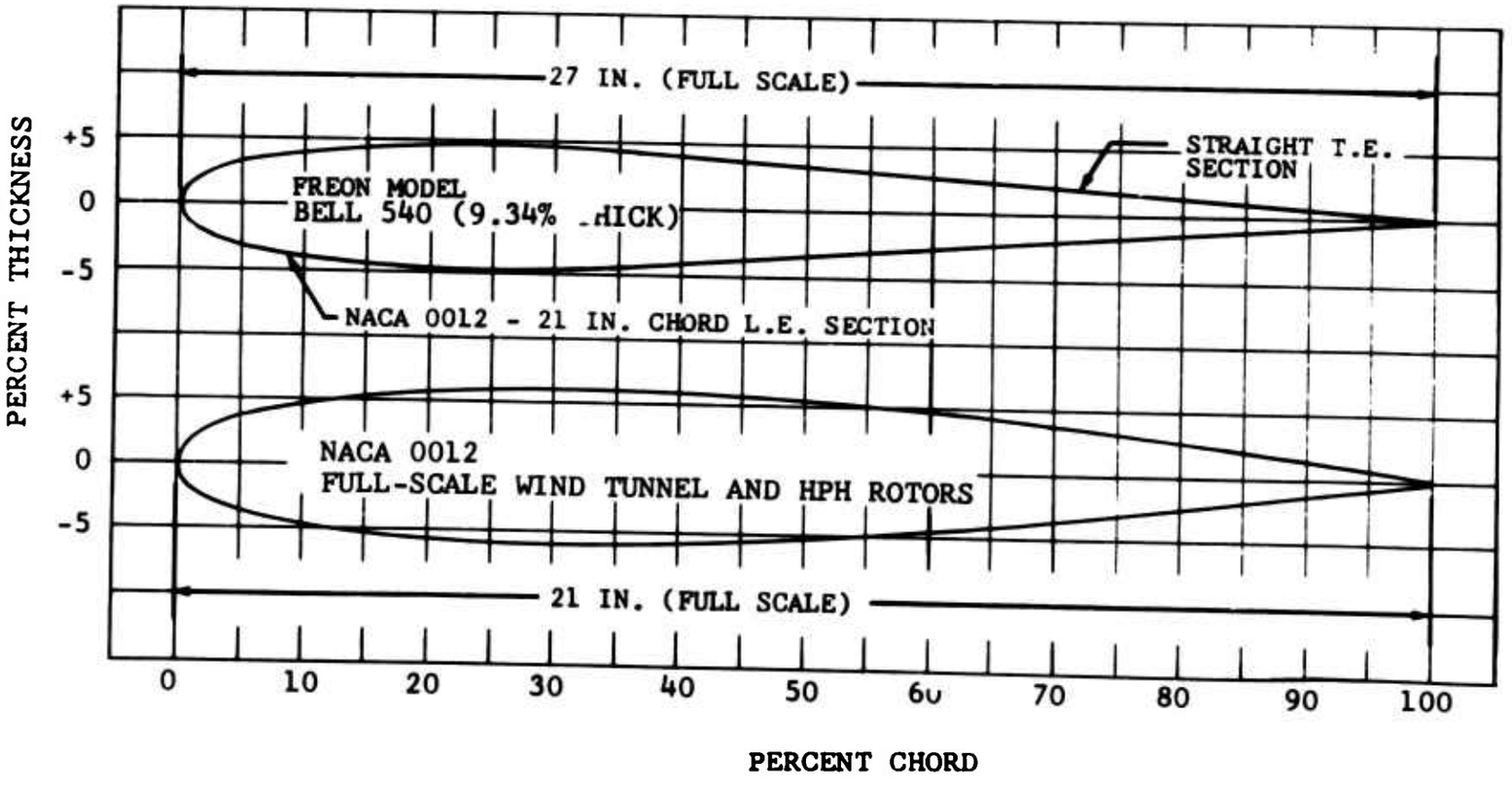

Figure 3. Airfoil Profile Sections of the Freon Model and Full-Scale Rotors.

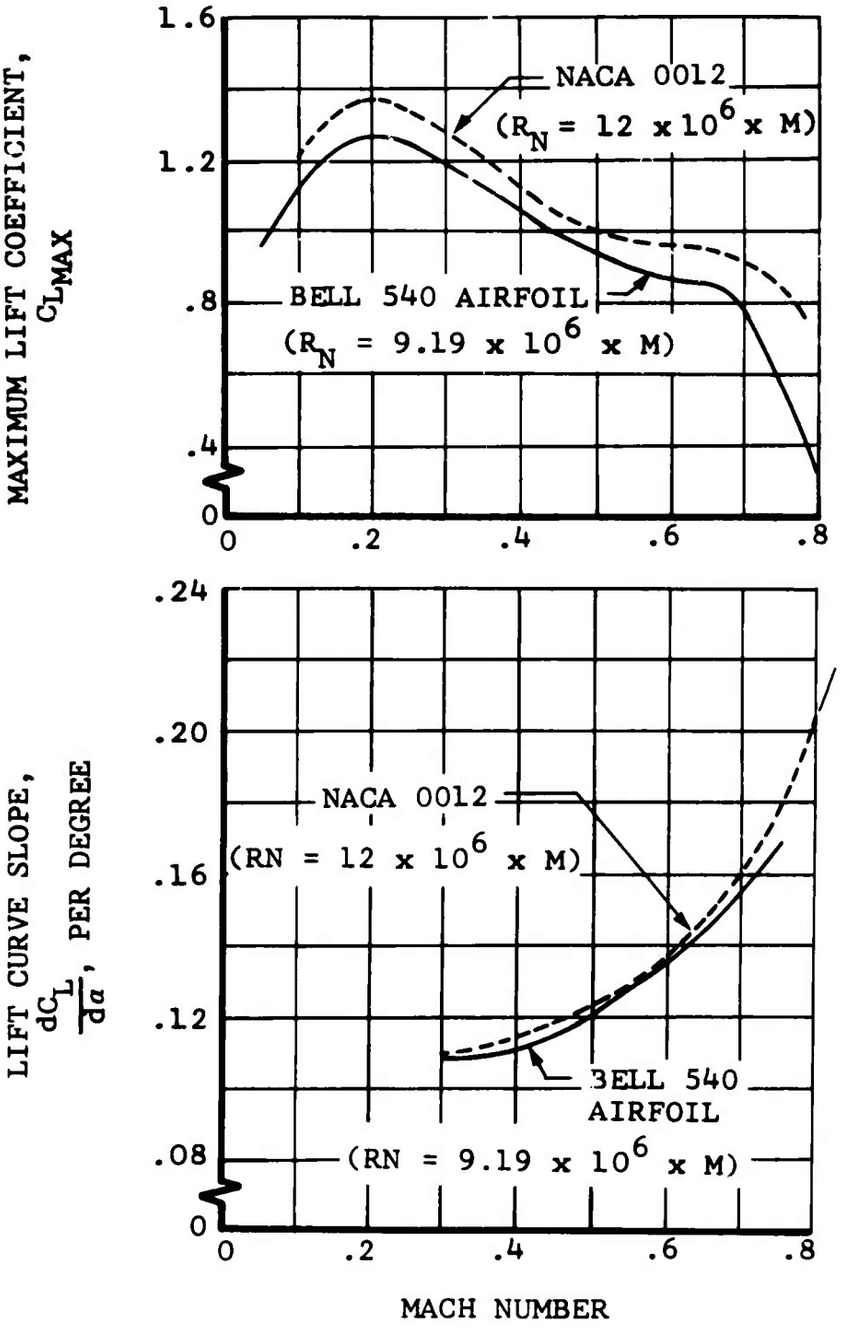

Figure 4. Lift Curve Slope and Maximum Lift Coefficient Characteristics of the Bell 540 and NACA 0012 Airfoil Sections as a Function of Mach Number.

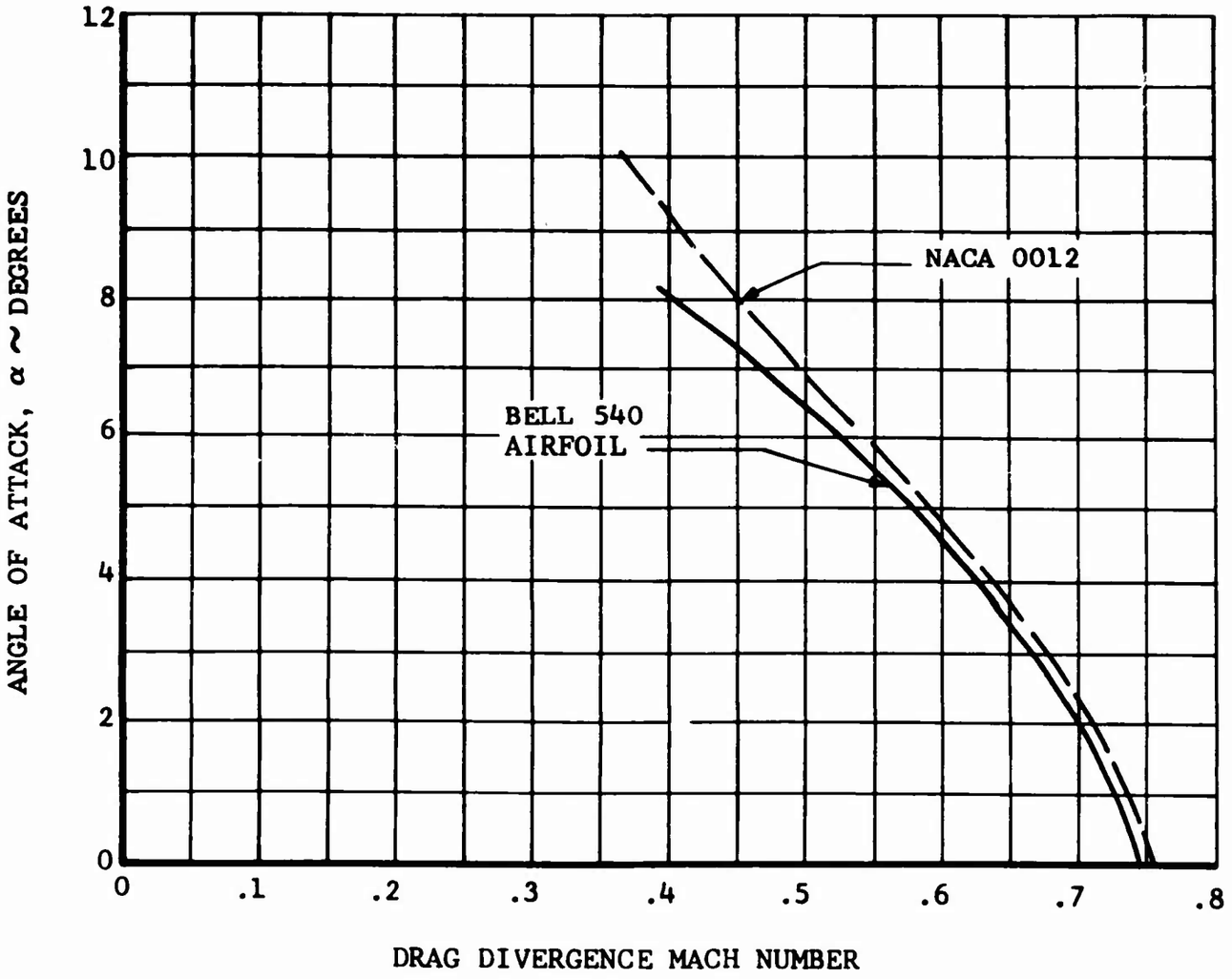

Figure 5. Supercritical Flow Characteristics of the Bell 540 and NACA 0012 Airfoil Sections.

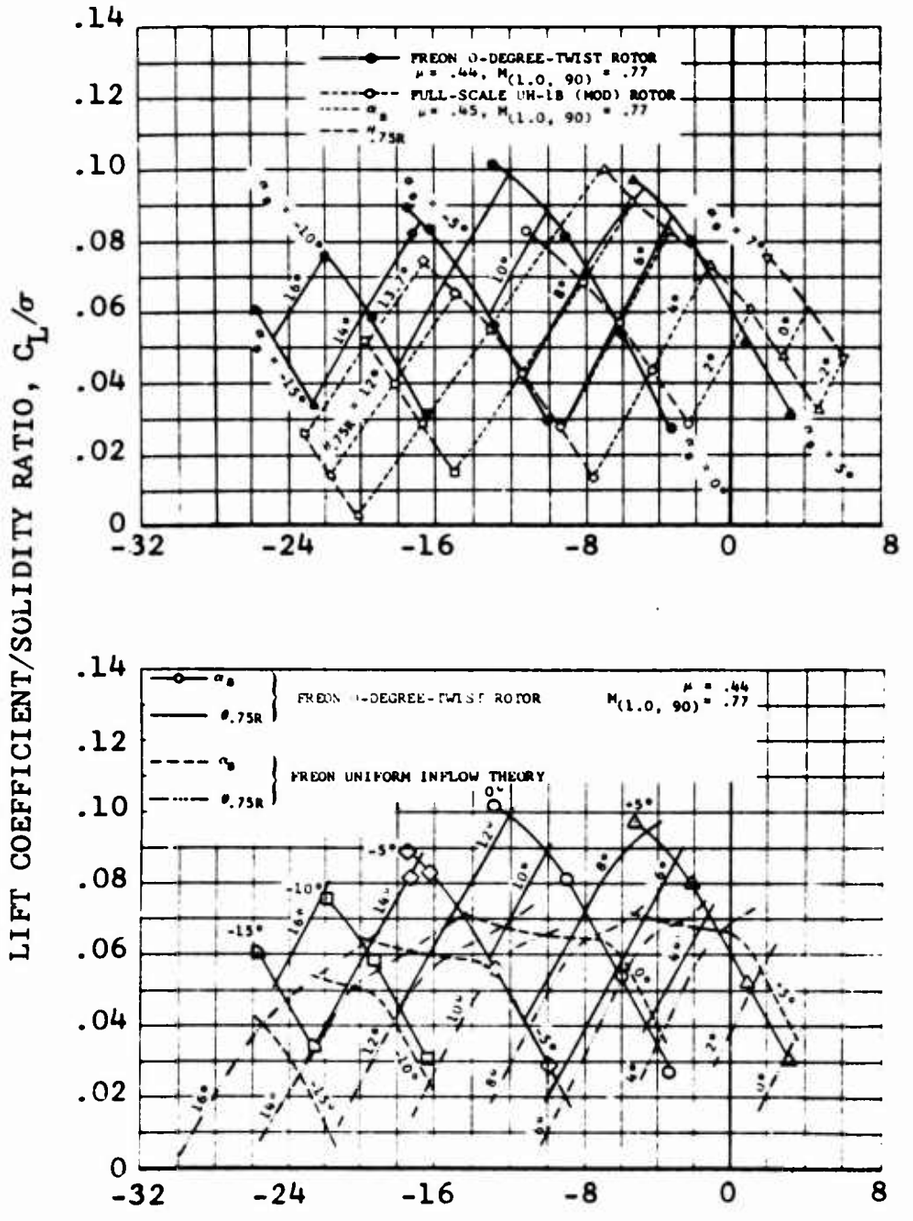

CONTROL AXIS ANGLE OF ATTACK, α_c, DEGREES

(a) C_L/σ vs α_c

Figure 6. Nondimensional Performance Comparisons of the Freon 0-Degree-Twist Rotor With Full-Scale and Theoretical Performance.

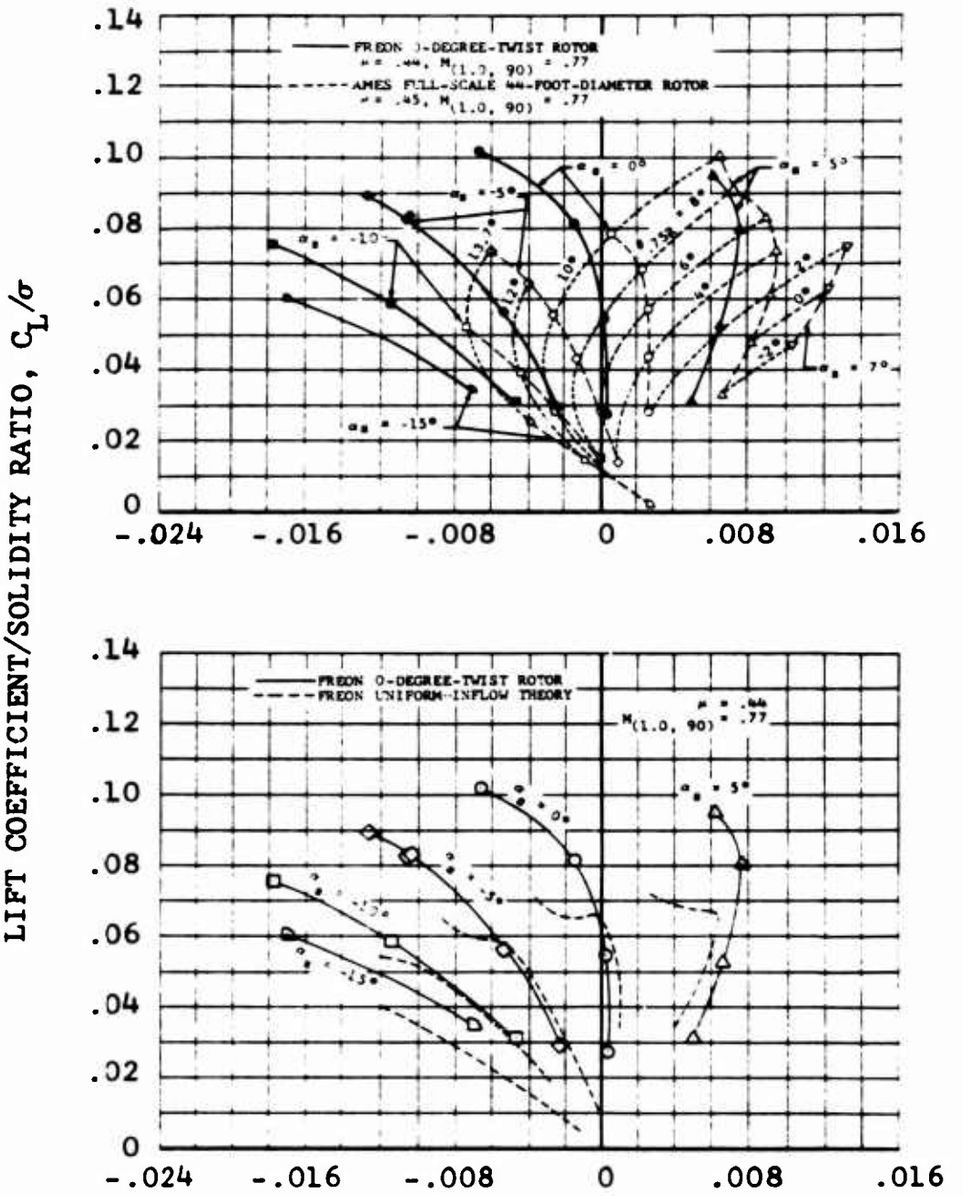

(b) C_L/σ vs C_D/σ

Figure 6. Continued.

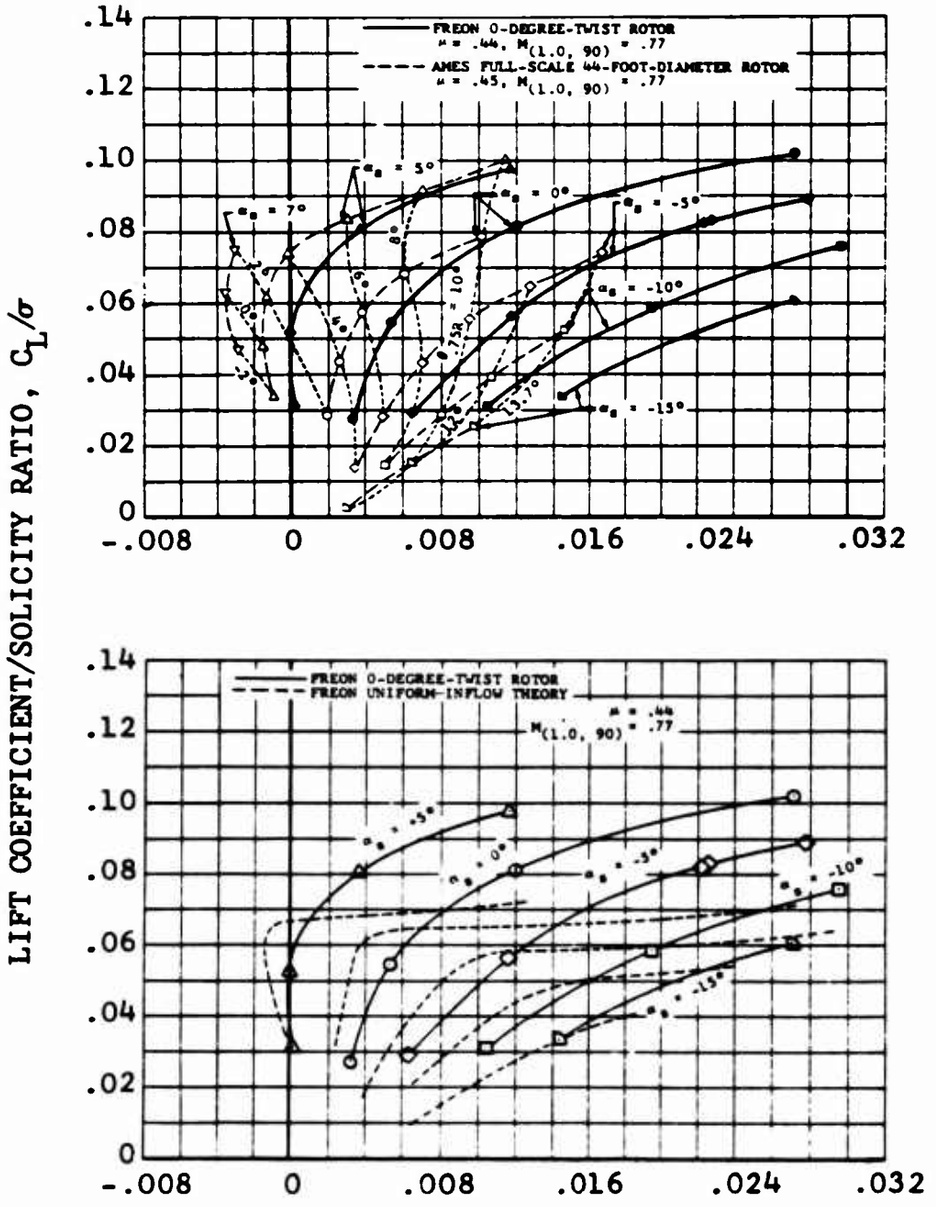

(c) C_L/σ vs C_Q/σ

Figure 6. Concluded.

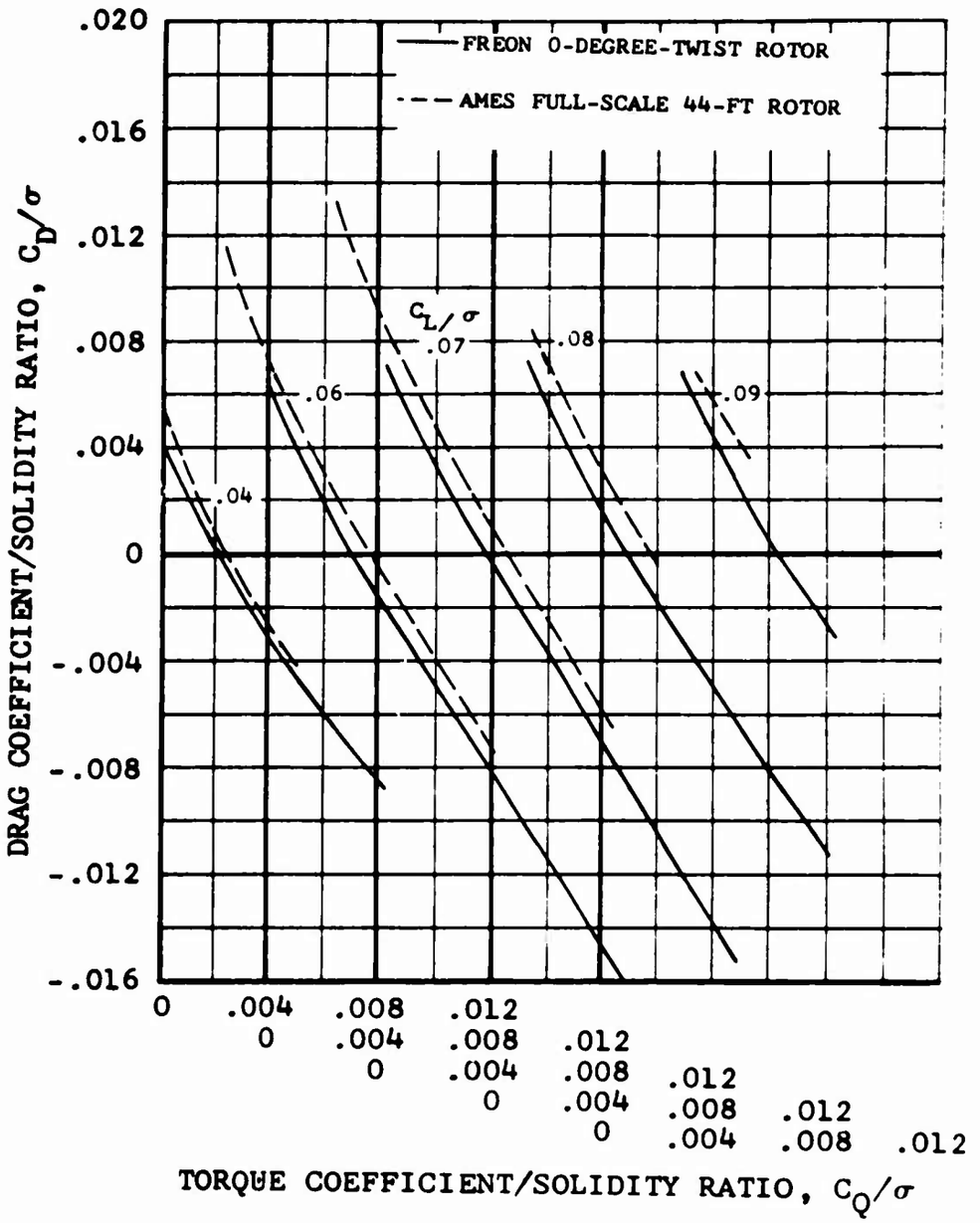

Figure 7. Nondimensional Performance Comparison of Freon 0-Degree-Twist at $\mu = 0.44$ and Full-Scale Rotor at $\mu = 0.45$, $M_{(1.0,\ 90)} = 0.77$.

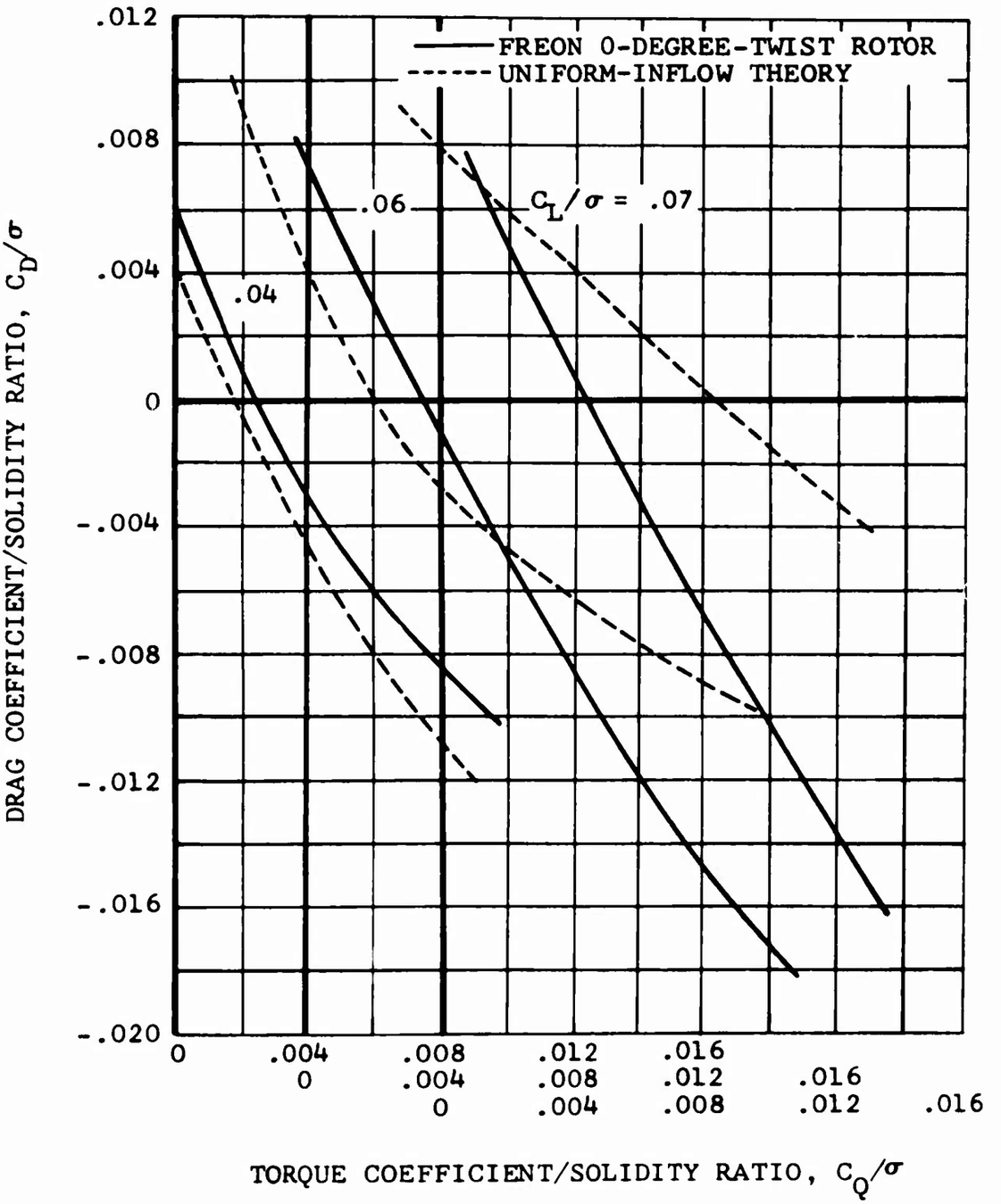

Figure 8. Nondimensional Performance Comparison of Freon 0-Degree-Twist Rotor and Freon Theory at $\mu = 0.44$, $M_{(1.0,\ 90)} = 0.77$.

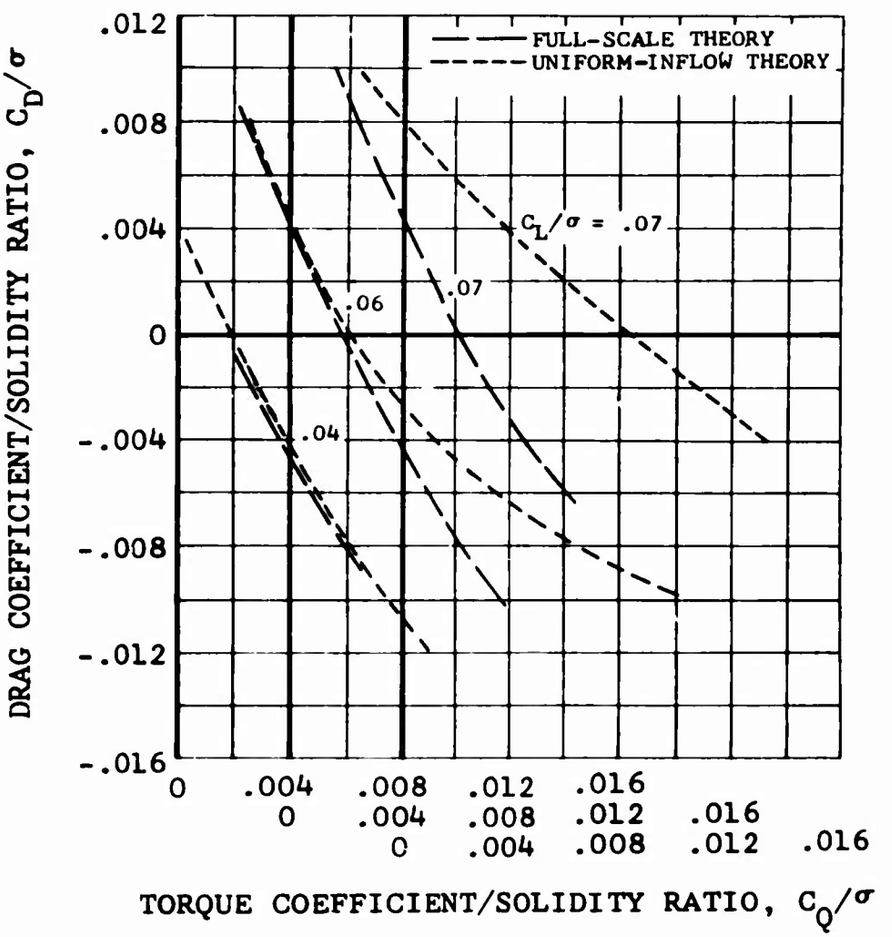

Figure 9. Nondimensional Performance Comparison of Full-Scale UH-1B (Modified) Rotor Theory With Uniform-Inflow Model Theory at $\mu = 0.45$, $M_{(1.0,\ 90)} = 0.77$.

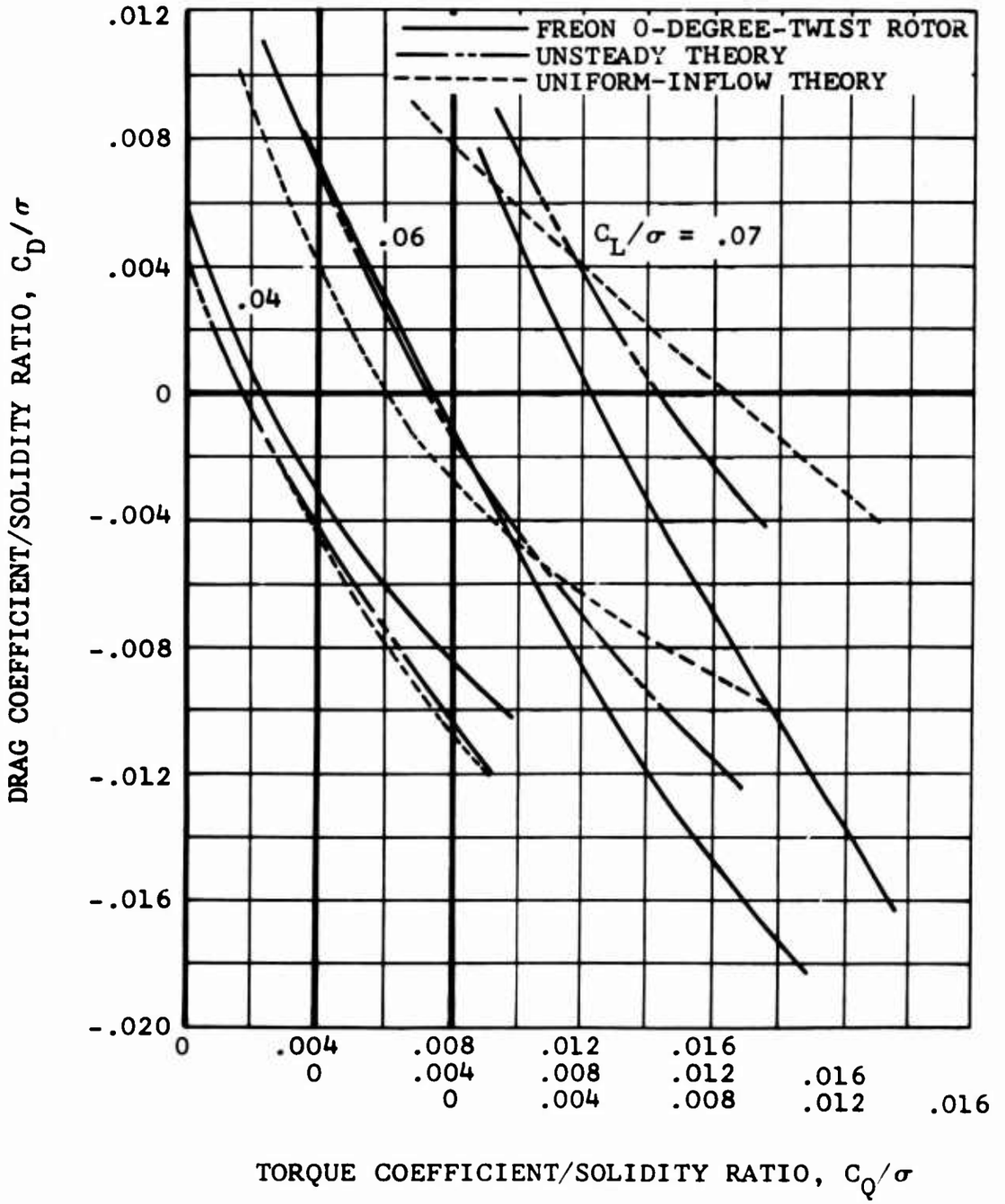

Figure 10. Nondimensional Performance Comparison of Freon 0-Degree-Twist Rotor With Uniform-Inflow and Unsteady Theory at $\mu = 0.44$, $M(1.0, 90) = 0.77$.

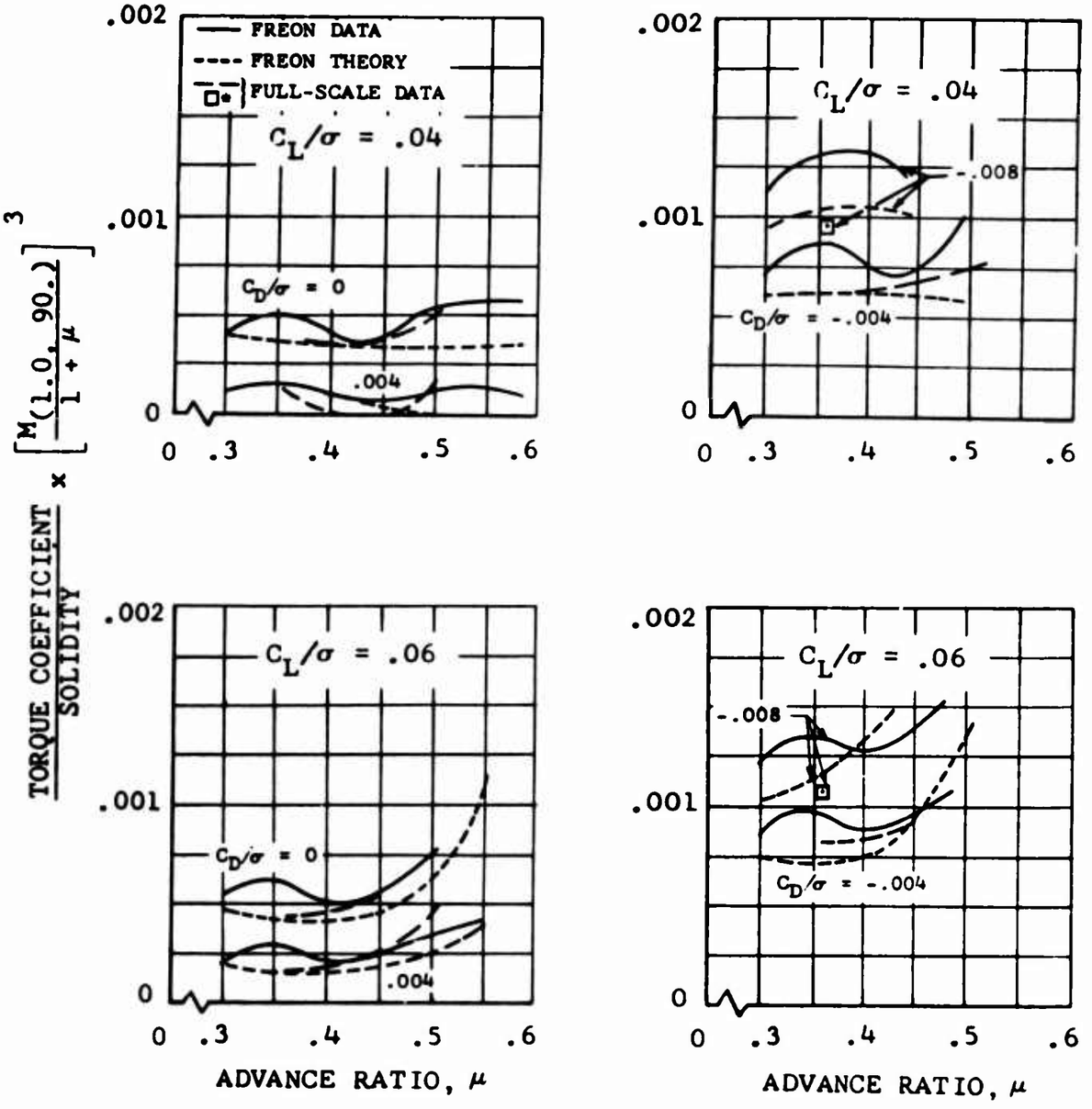

(a) $M_{(1.0,\ 90.)} = 0.80$

Figure 11. Nondimensional Performance Comparisons of the 0-Degree-Twist Model Rotor as a Function of Advance Ratio at Various Advancing-Tip Mach Numbers With Full-Scale UH-1B (Modified) Rotor Performance and Uniform-Inflow Theory. *See Text p. 13.

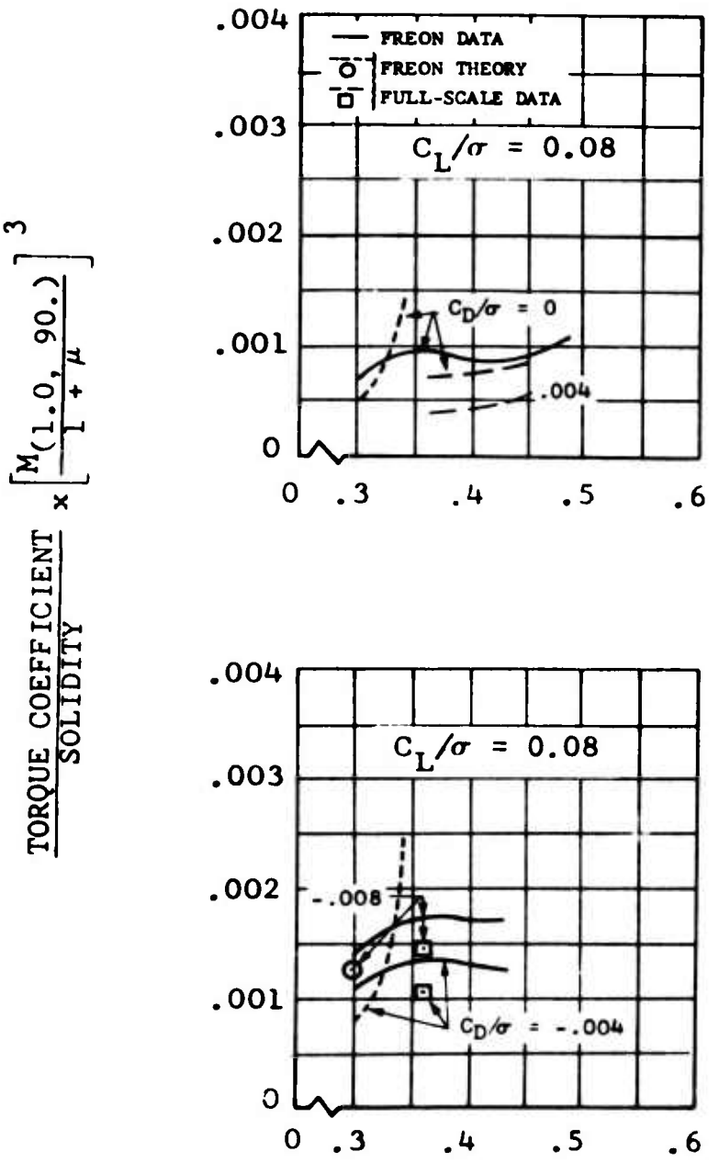

(a) Concluded.

Figure 11. Continued.

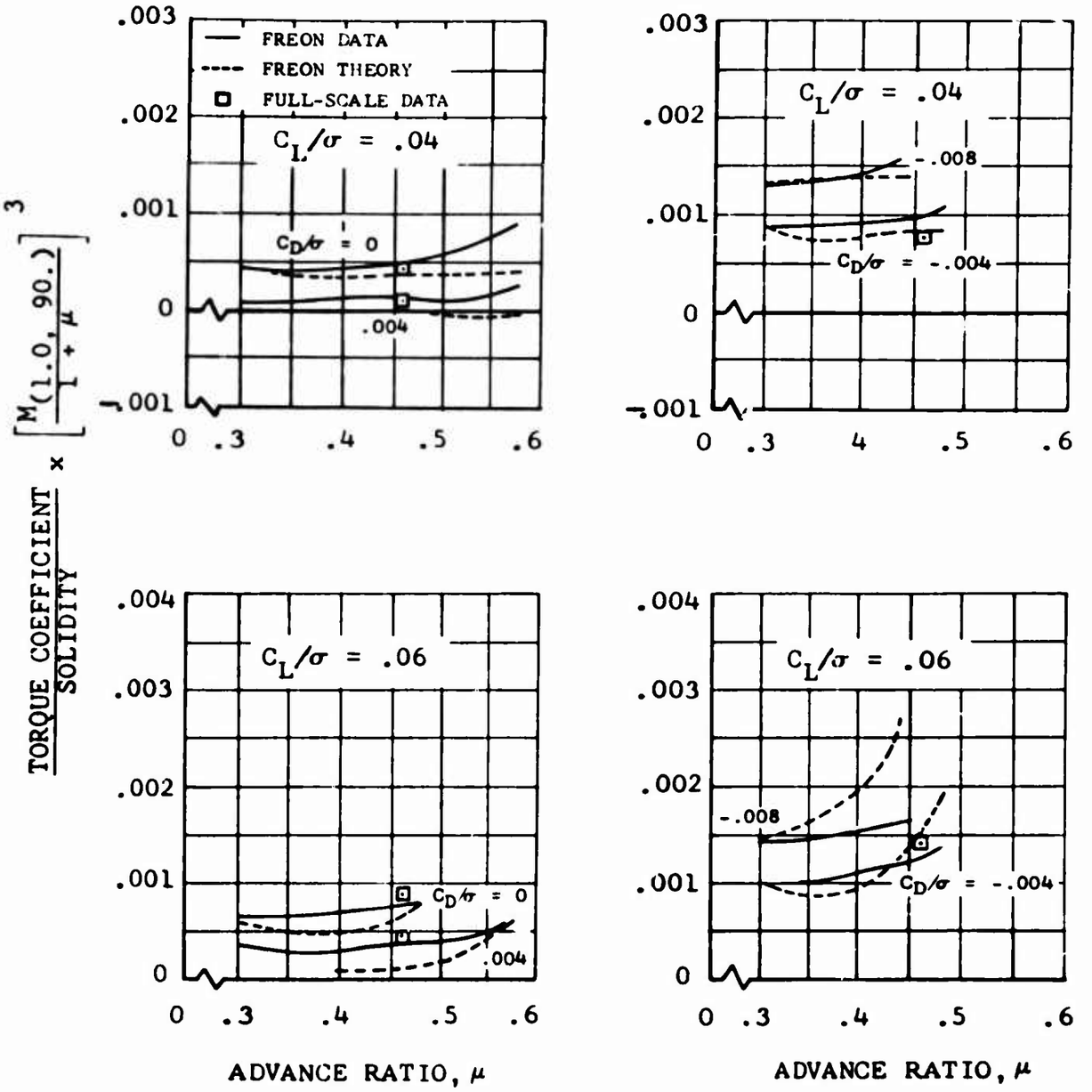

(b) $M_{(1.0,\ 90.)} = 0.85$

Figure 11. Continued.

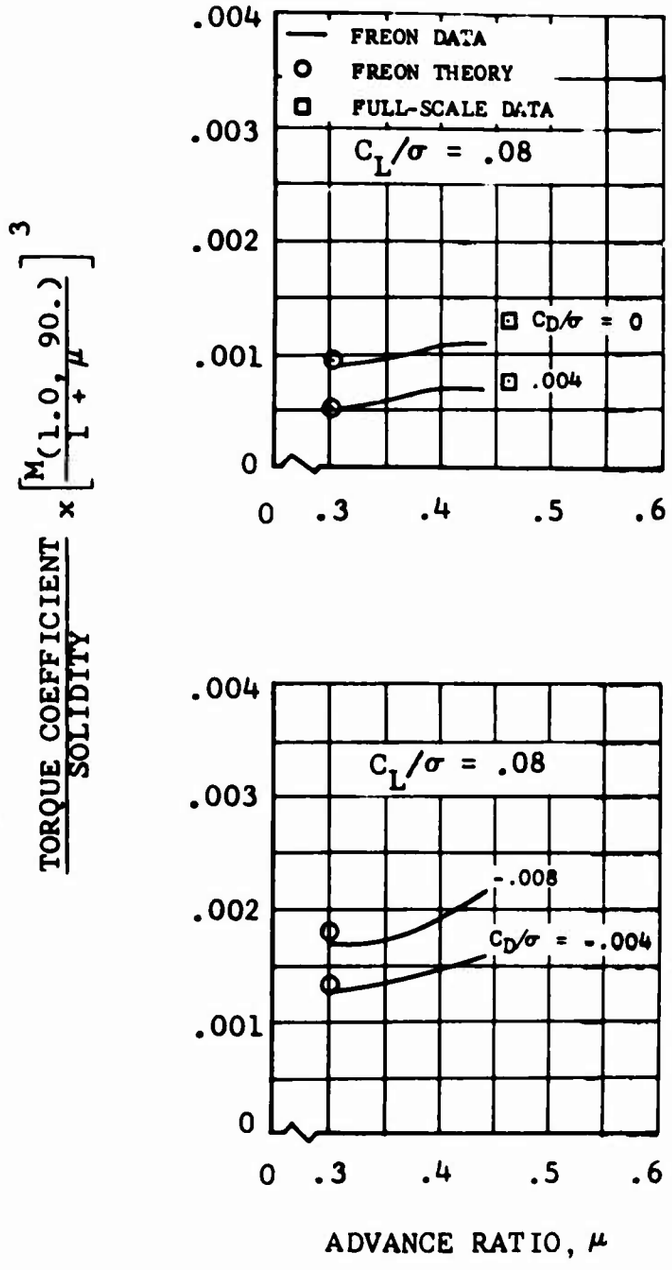

(b) Concluded.

Figure 11. Continued.

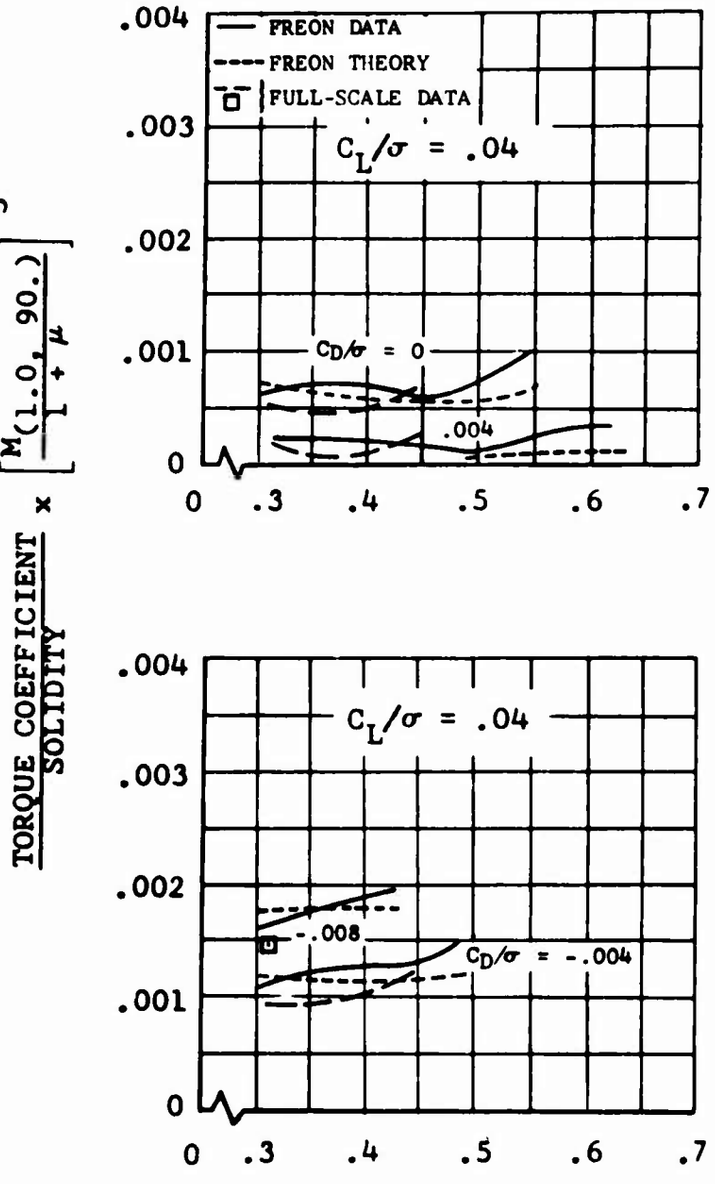

(c) $M_{(1.0,\ 90.)} = 0.90$

Figure 11. Continued.

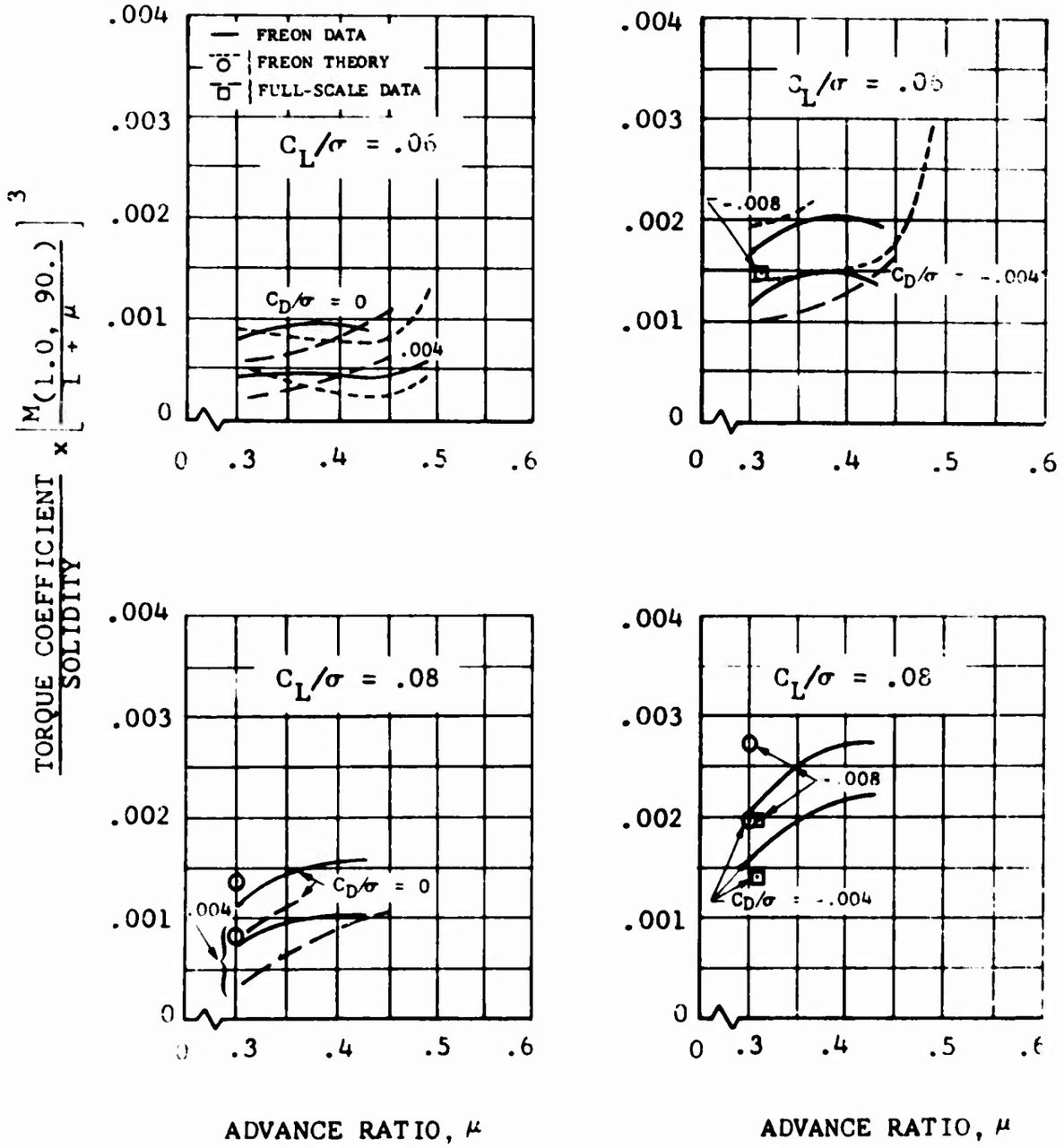

(c) Concluded.

Figure 11. Continued.

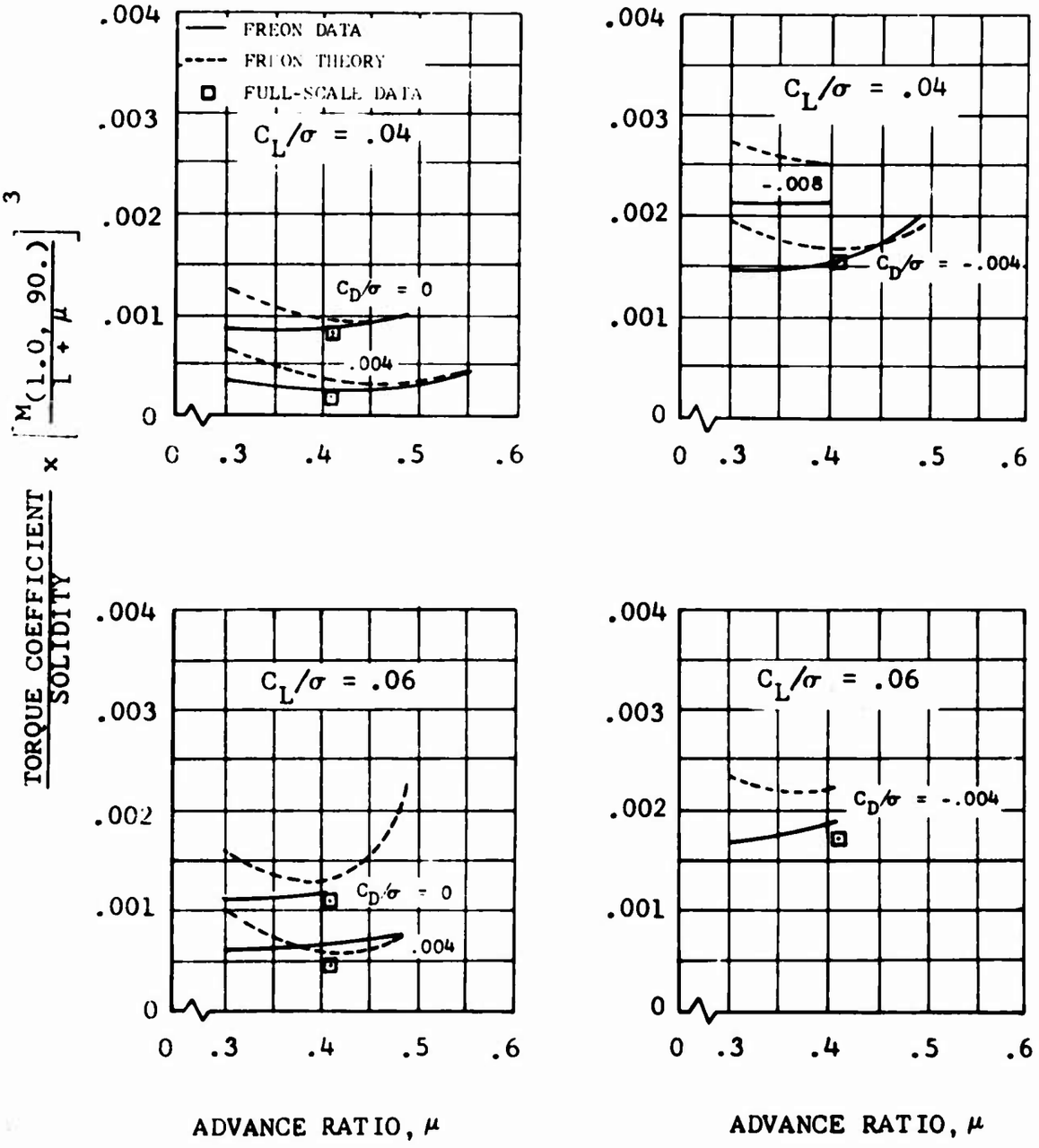

(d) $M_{(1.0,\ 90)} = 0.95$

Figure 11. Continued.

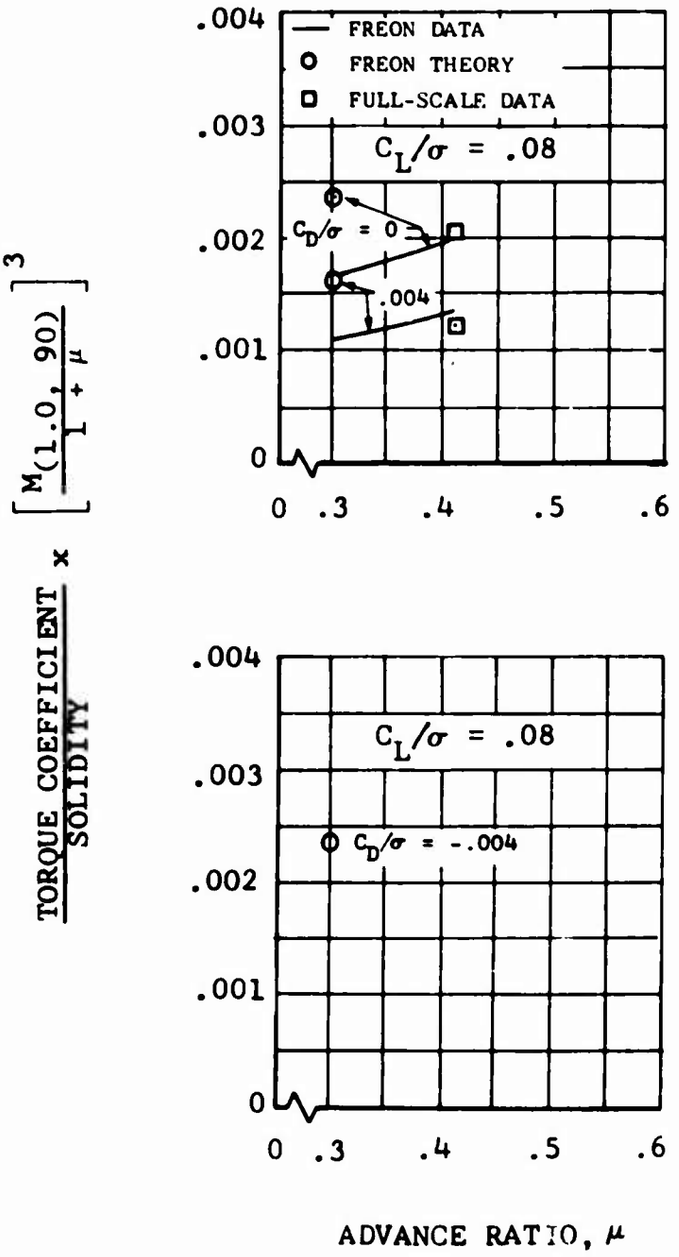

(d) Concluded.

Figure 11. Concluded.

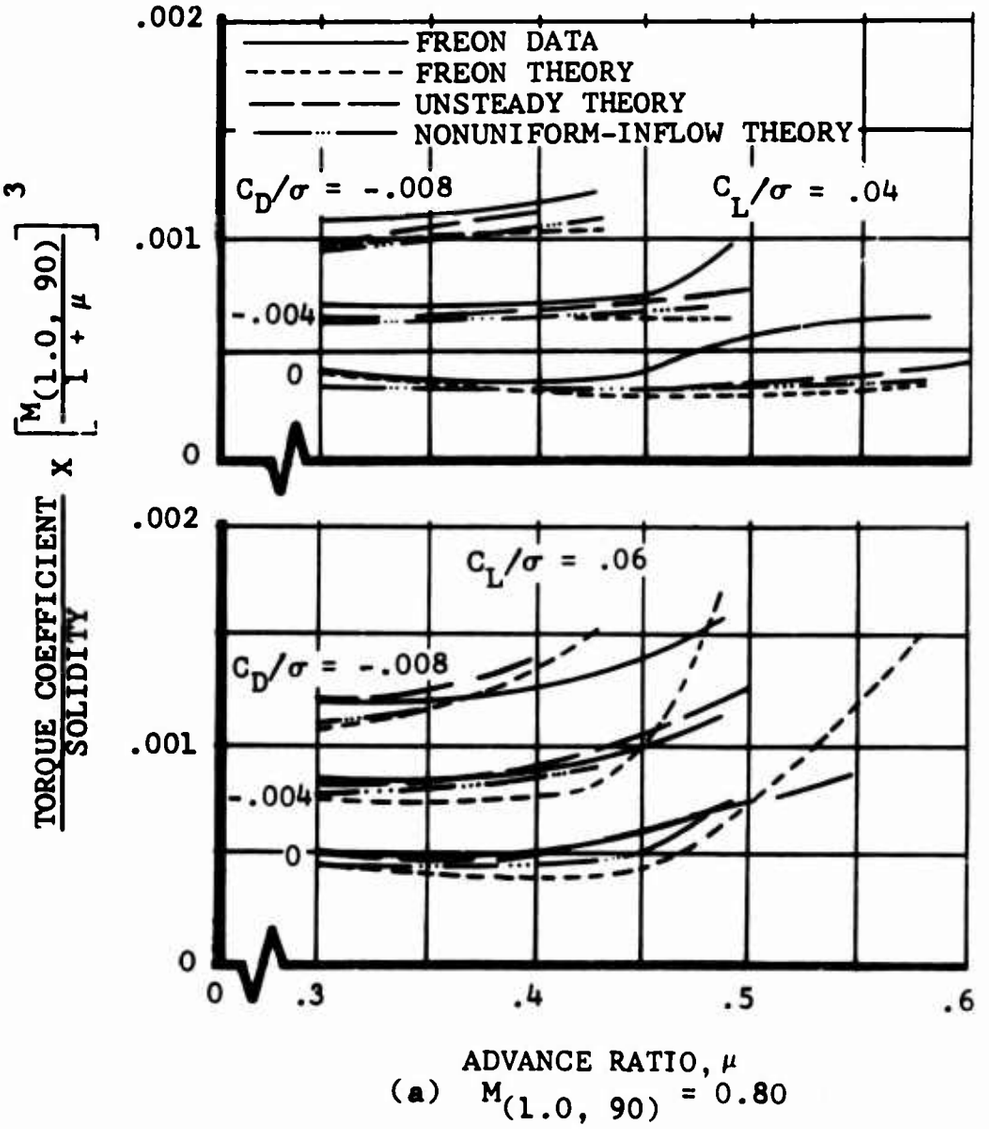

(a) $M_{(1.0,\ 90)} = 0.80$

Figure 12. Nondimensional Performance Comparison of Freon Data as a Function of Advance Ratio at Various Advancing-Tip Mach Numbers With Freon Theory, Unsteady Theory, and Nonuniform-Inflow Theory.

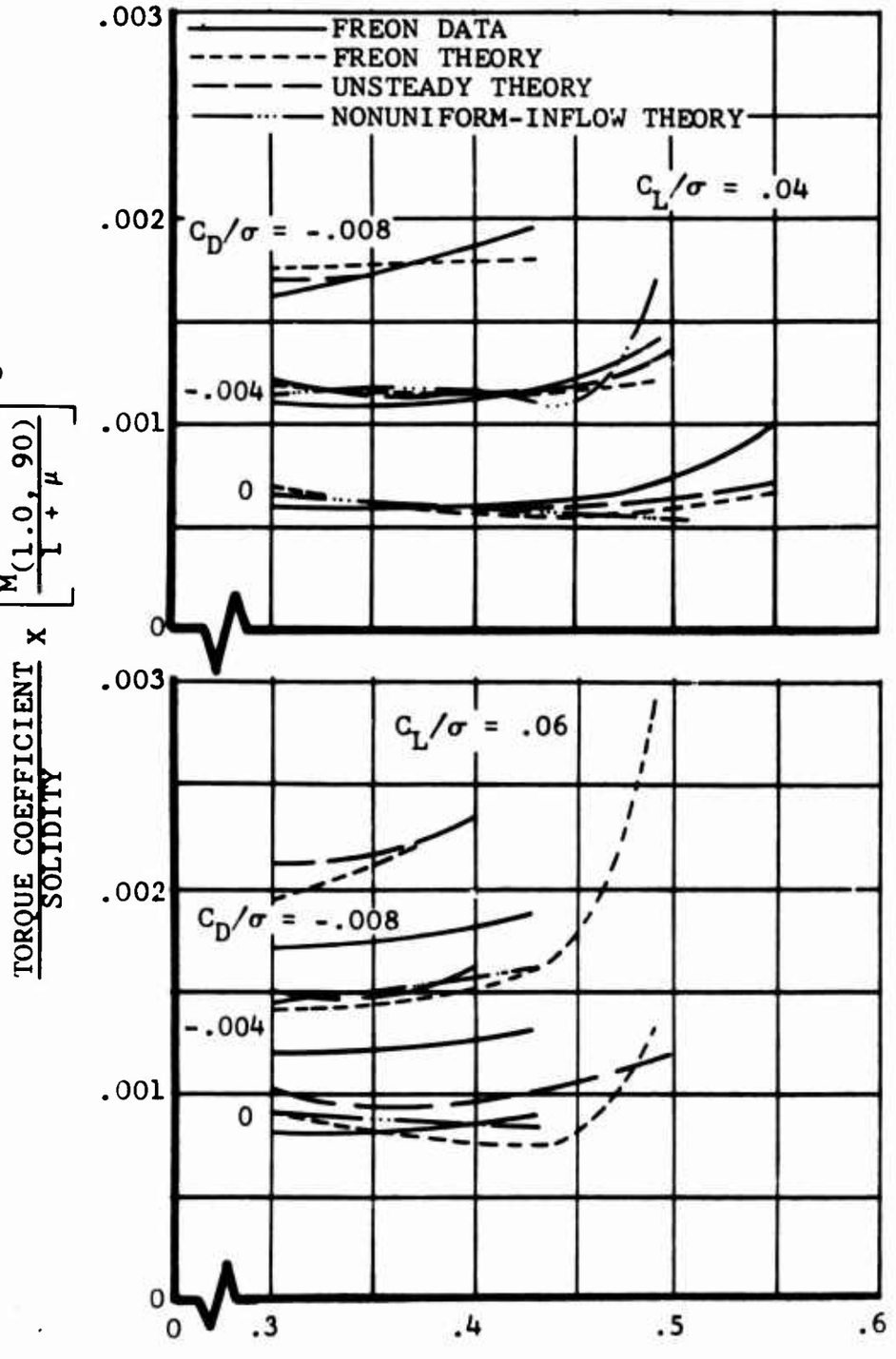

(b) $M_{(1.0,\ 90)} = 0.90$

Figure 12. Continued.

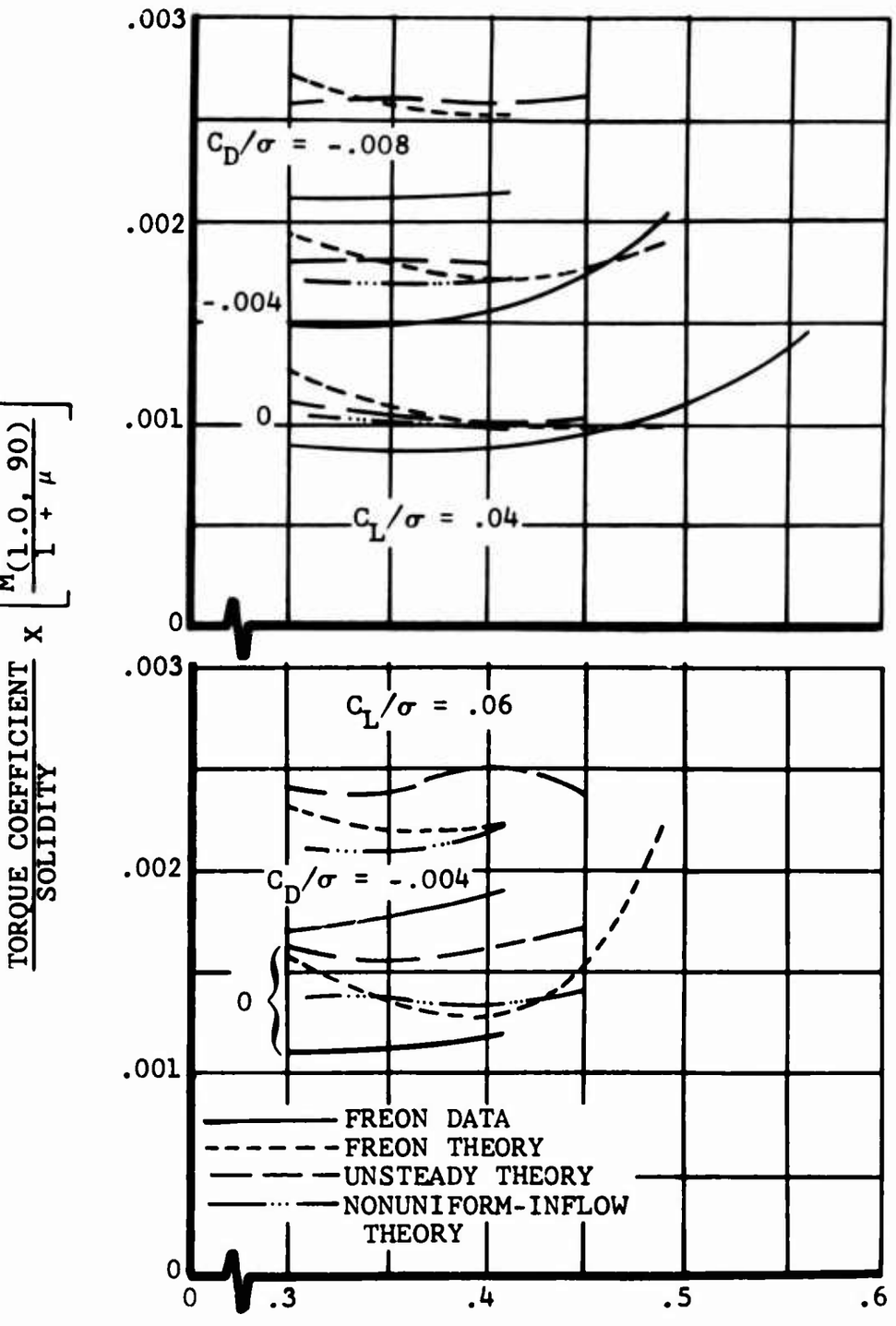

(c) $M_{(1.0,\ 90)} = 0.95$

Figure 12. Concluded.

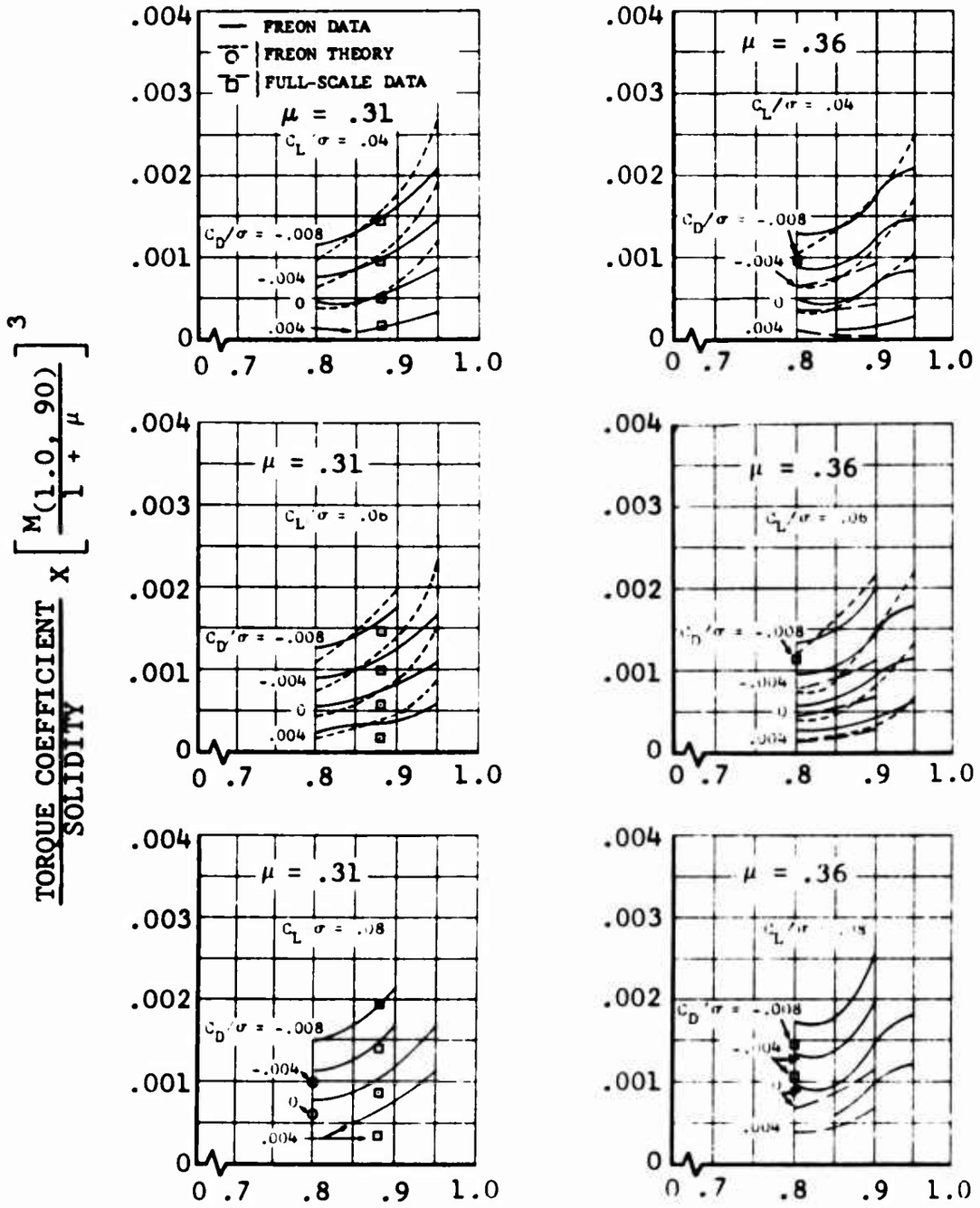

(a) μ = 0.31, 0.36

Figure 13. Nondimensional Performance Comparisons of the 0-Degree-Twist Model Rotor as a Function of Advancing-Tip Mach Number at Various Advance Ratios With Full-Scale UH-1B (Modified) Rotor Performance and Uniform-Inflow Theory.

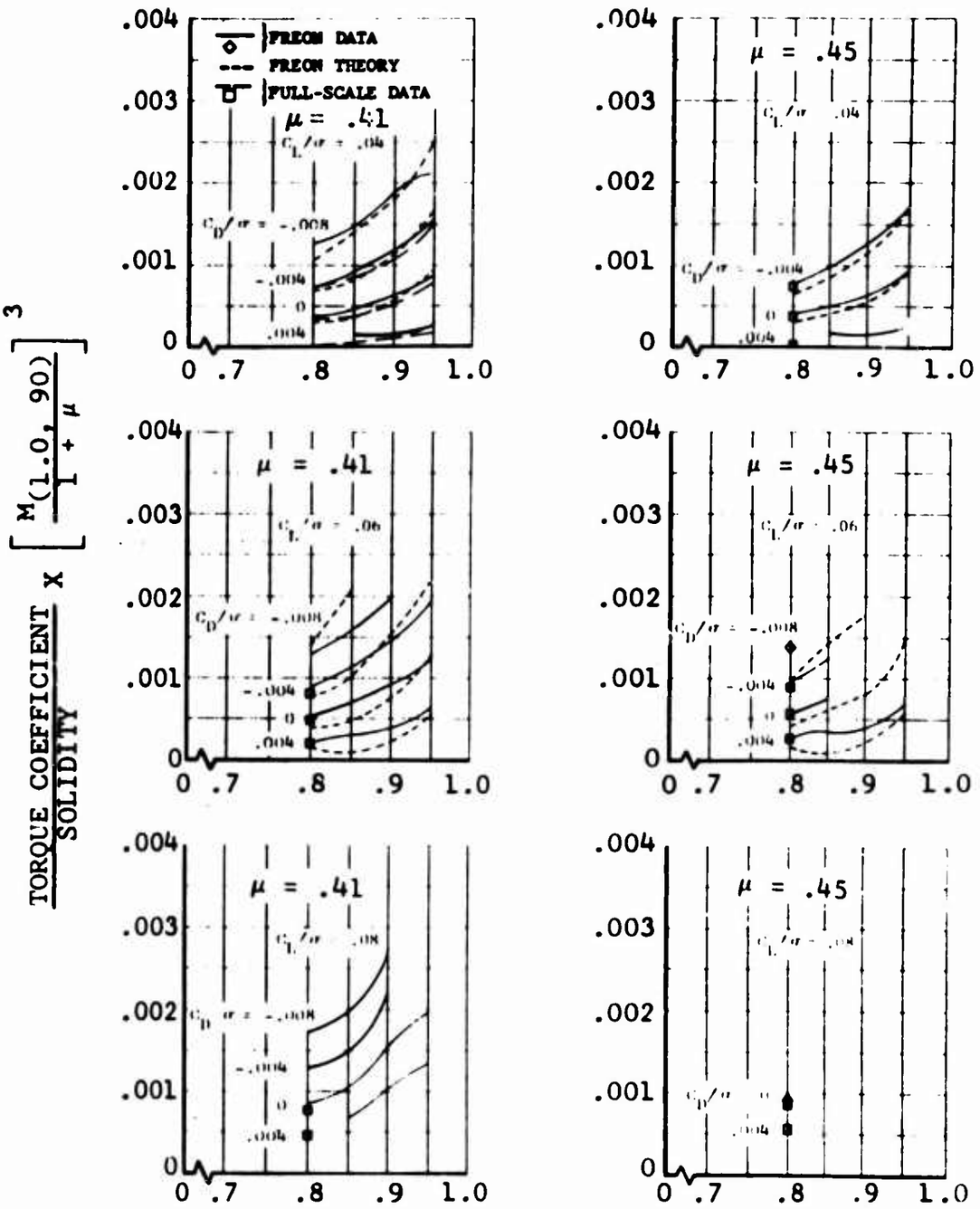

(b) μ = 0.41, 0.45

Figure 13. Concluded.

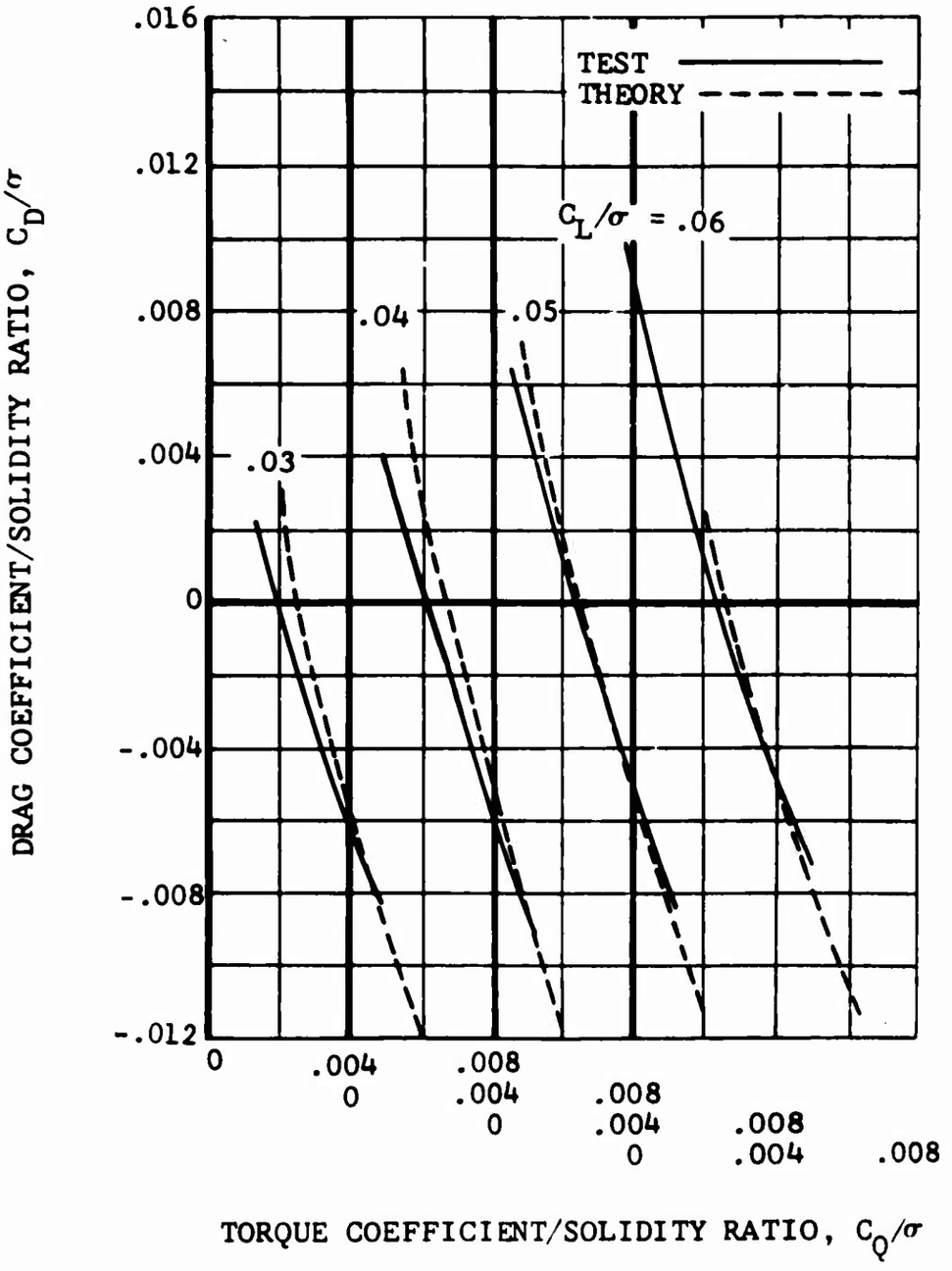

Figure 14. Nondimensional Performance Comparison of Thin-Tip UH-1D Rotor With Uniform-Inflow Theory at μ = 0.30, $M_{(1.0,\ 90)}$ = 0.95.

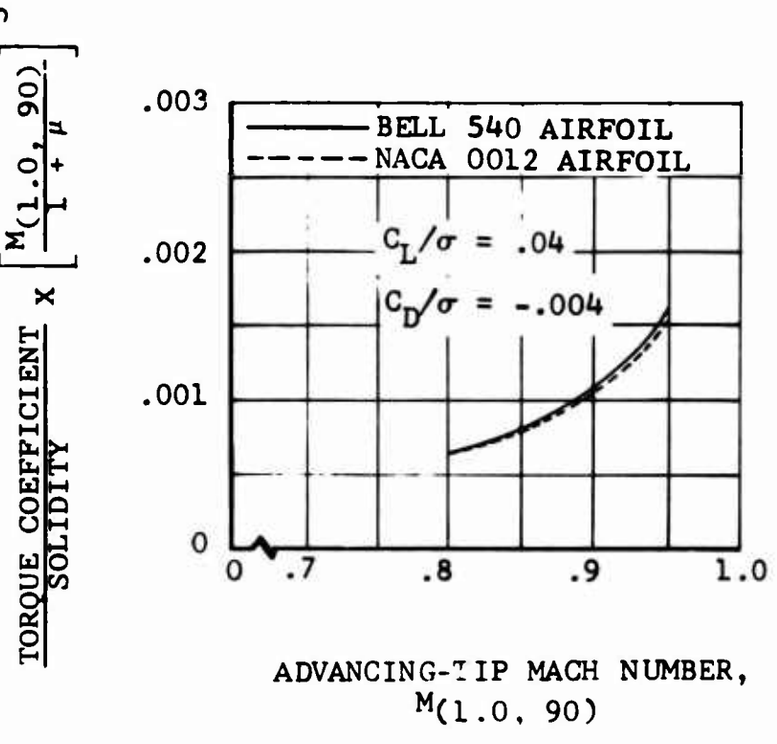

Figure 15. Nondimensional Theoretical Performance of the 0-Degree-Twist Freon Model Rotor at μ = 0.30 Showing Differences Between Bell 540 and NACA 0012 Airfoils.

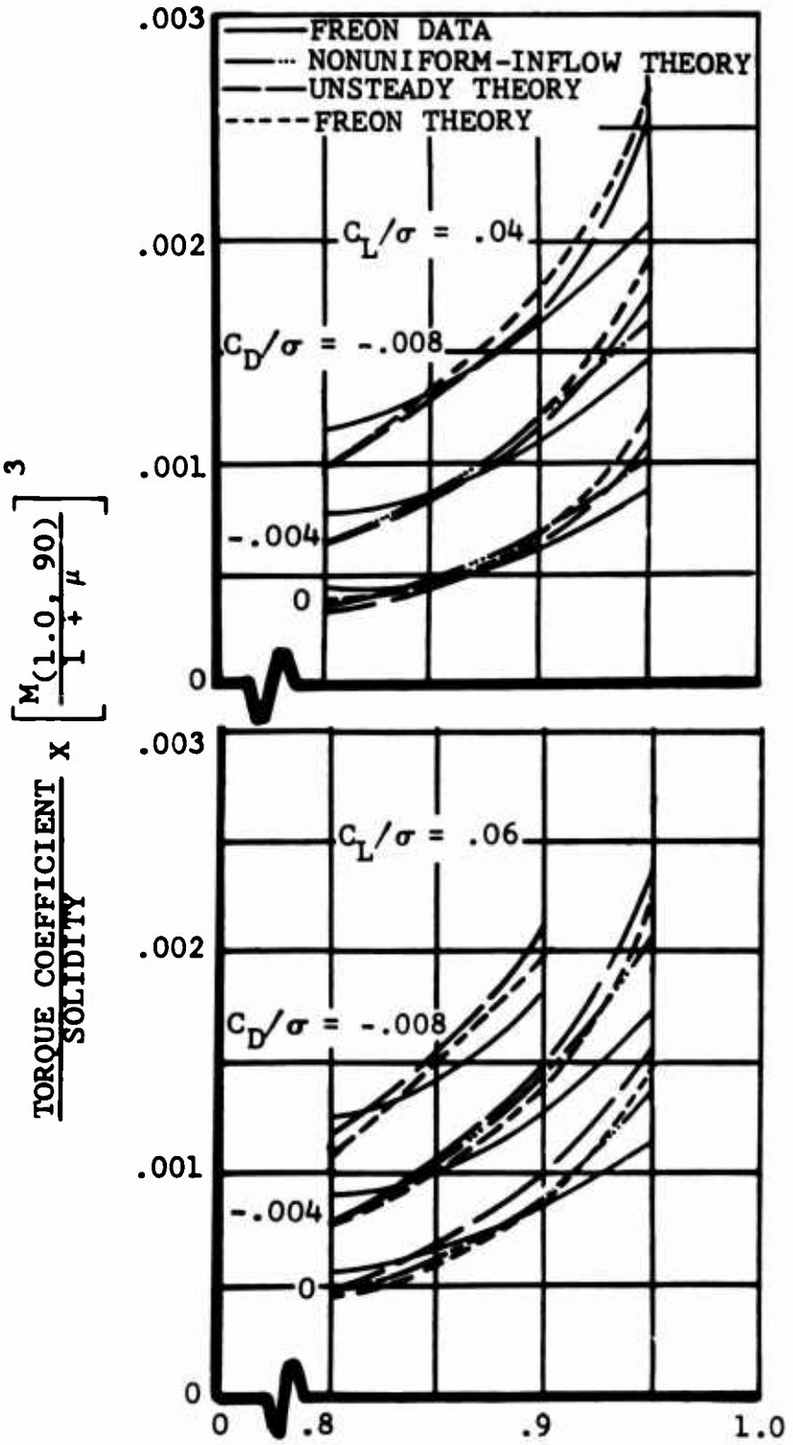

(a) μ = 0.31

Figure 16. Nondimensional Performance Comparison of Freon Data as a Function of Advancing-Tip Mach Number at Various Advance Ratios With Freon Theory, Unsteady Theory, and Nonuniform-Inflow Theory.

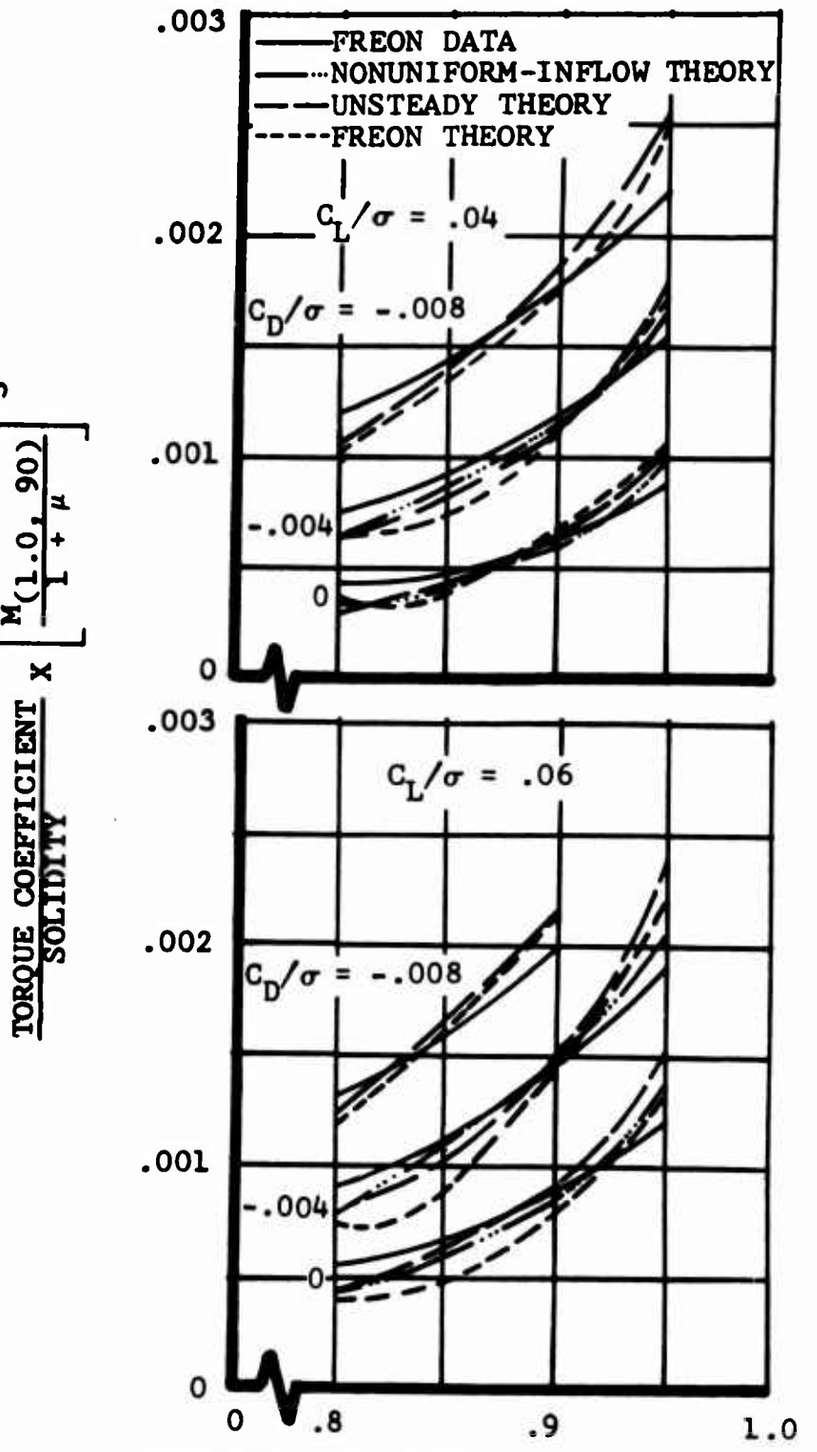

(b) μ = 0.36

Figure 16. Continued.

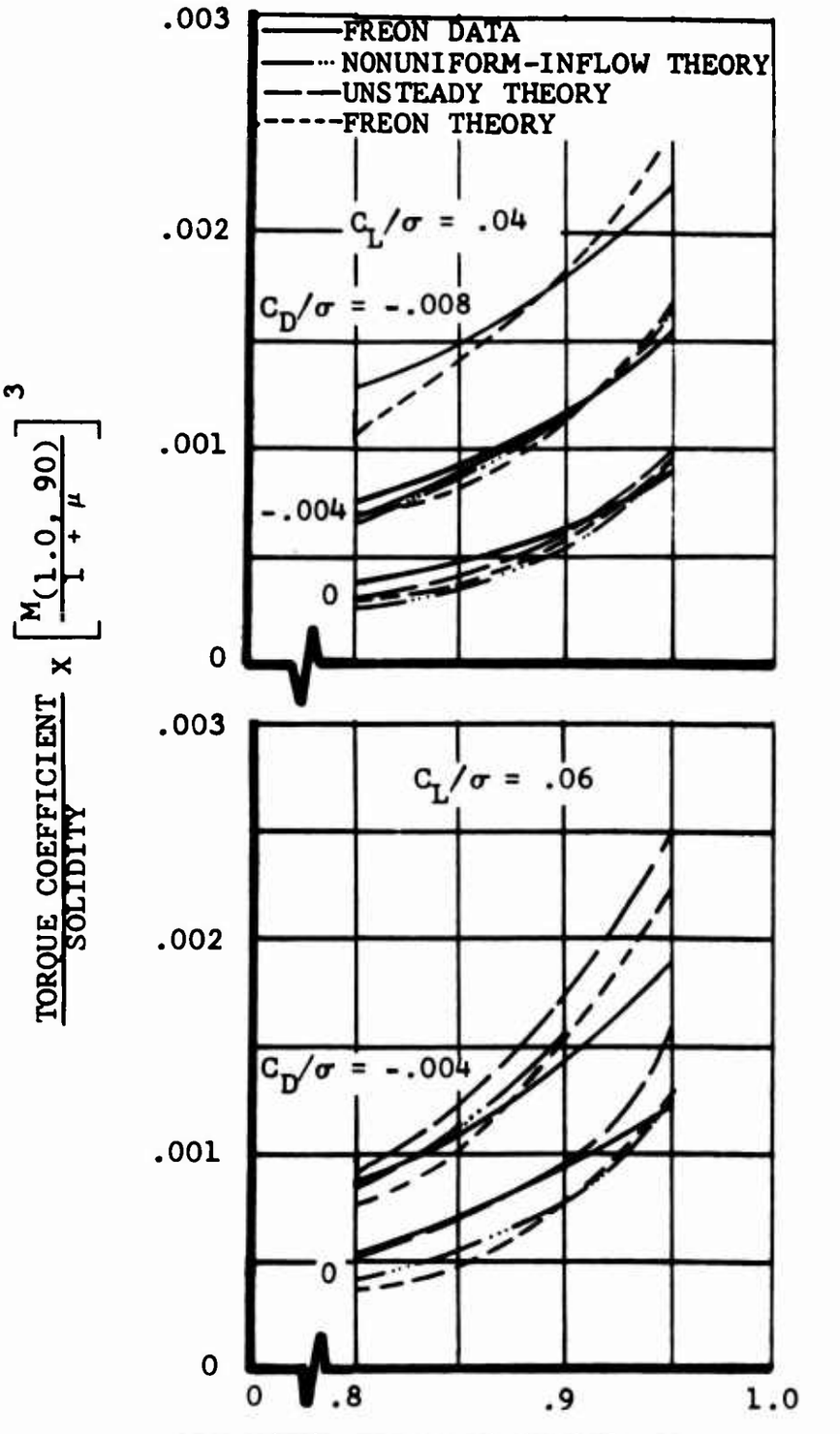

(c) μ = 0.41

Figure 16. Continued.

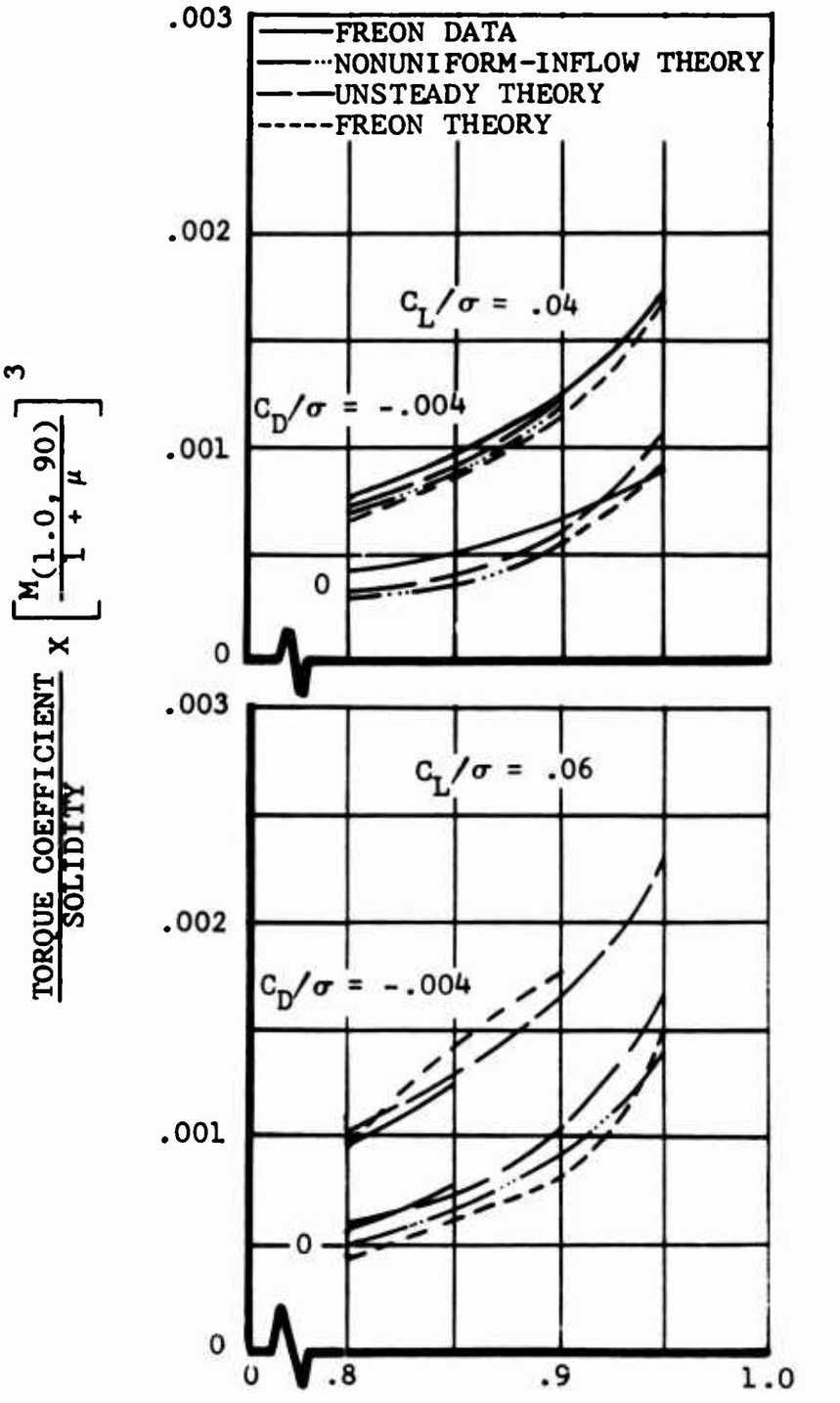

(d) μ = 0.45

Figure 16. Concluded.

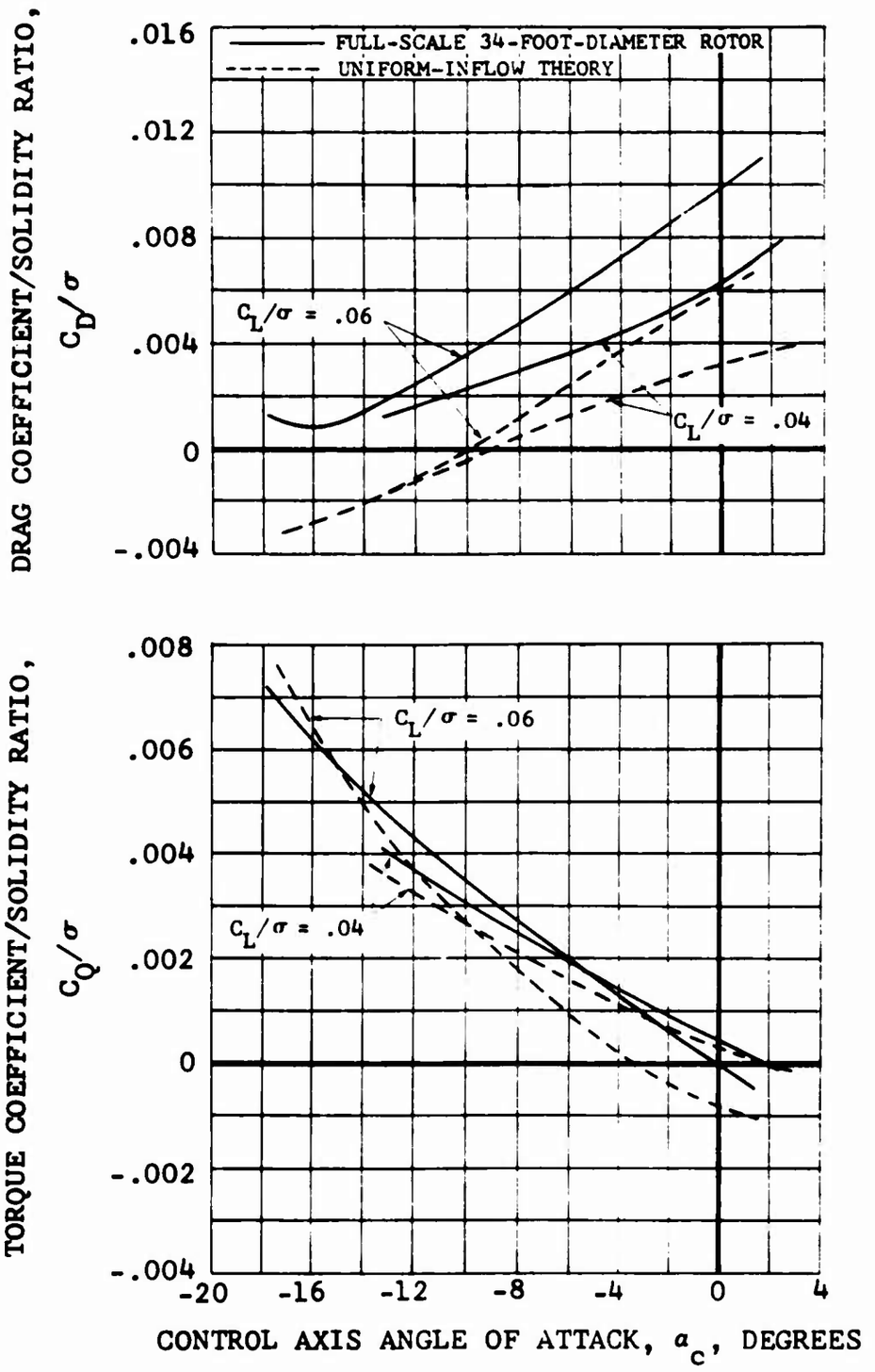

Figure 17. Nondimensional Comparison of Experimental and Theoretical Full-Scale 34-Foot-Diameter Rotor Performance as a Function of Control Axis Angle of Attack at μ = 0.51; $M_{(1.0,\ 90)}$ = 0.64.

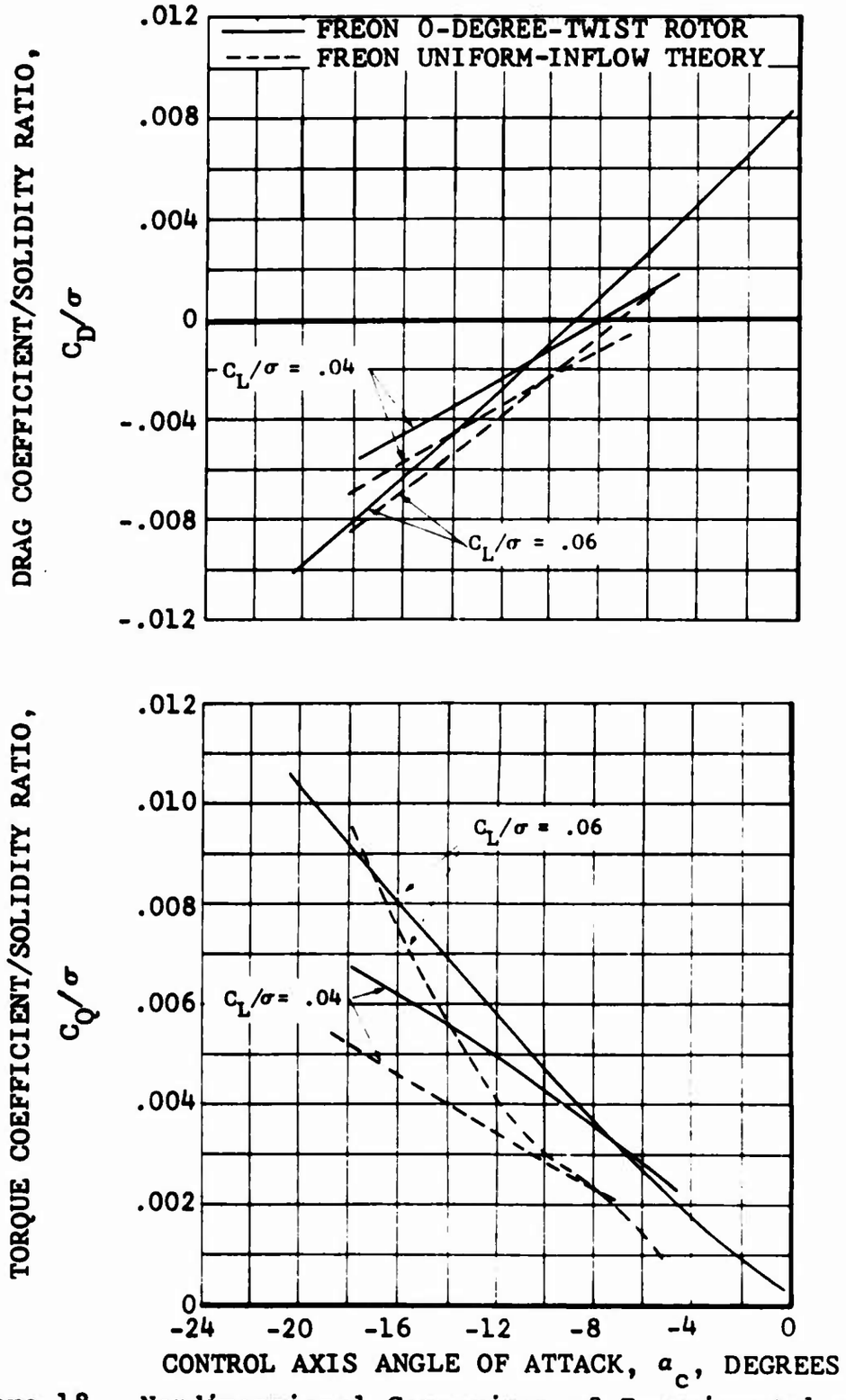

Figure 18. Nondimensional Comparison of Experimental and Theoretical 0-Degree-Twist Model Rotor Performance as a Function of Control Axis Angle of Attack at μ = 0.44; $M_{(1.0,\ 90)}$ = 0.62.

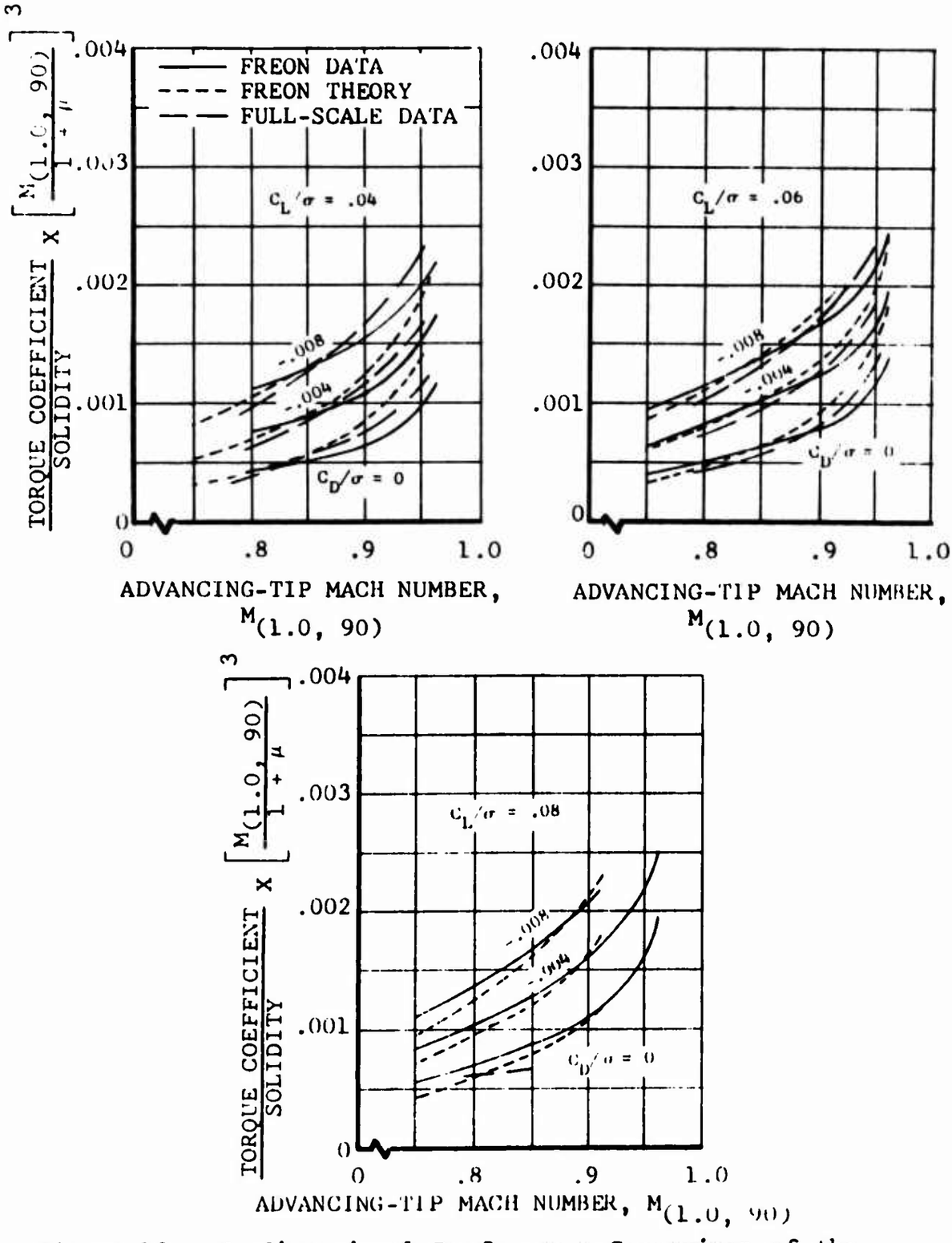

Figure 19. Nondimensional Performance Comparison of the -10-Degree-Twist Model Rotor as a Function of Advancing-Tip Mach Number at μ = 0.30 With Full-Scale UH-1D Rotor Performance and Uniform-Inflow Theory.

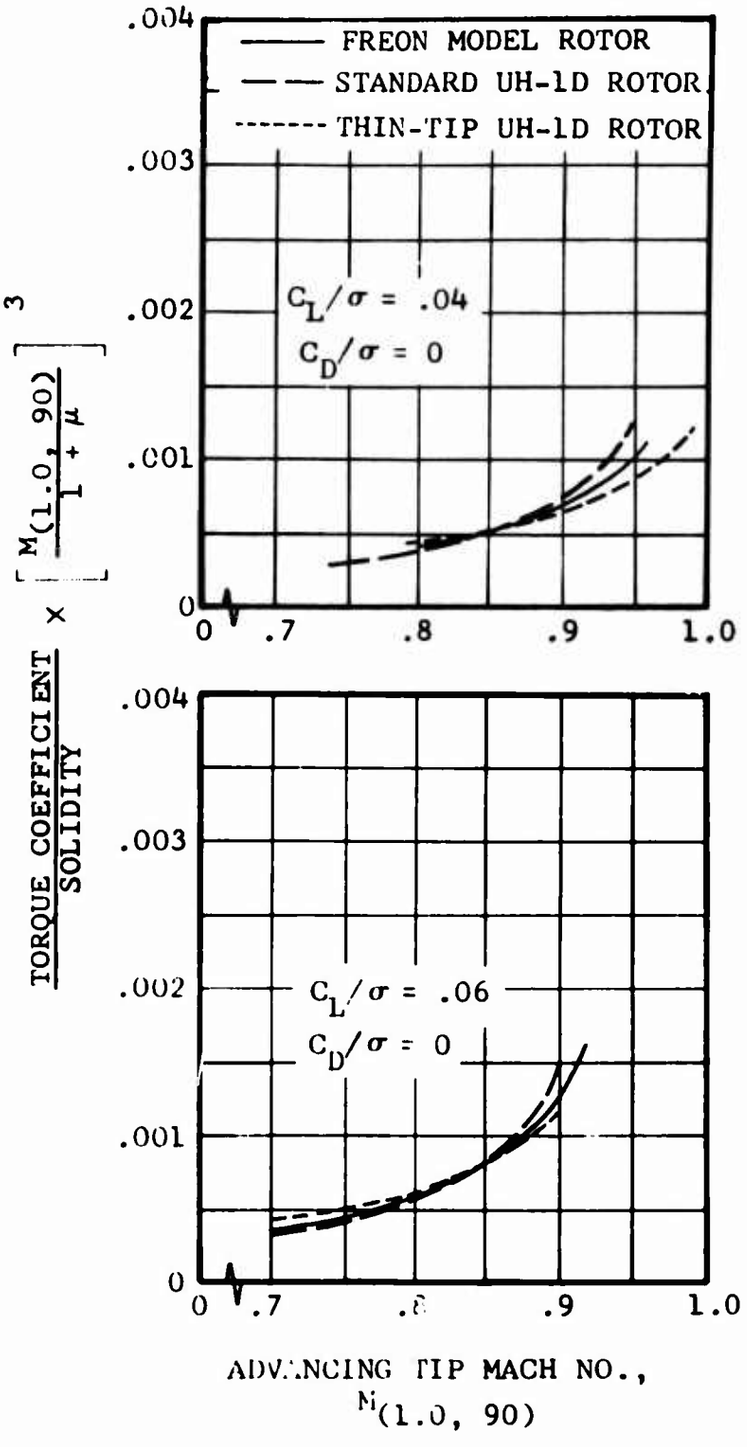

Figure 20. Nondimensional Performance Comparison of the -10-Degree-Twist Model Rotor as a Function of Advancing-Tip Mach Number at μ = 0.30 With Standard-Tip and Thin-Tip UH-1D Rotor Performance.

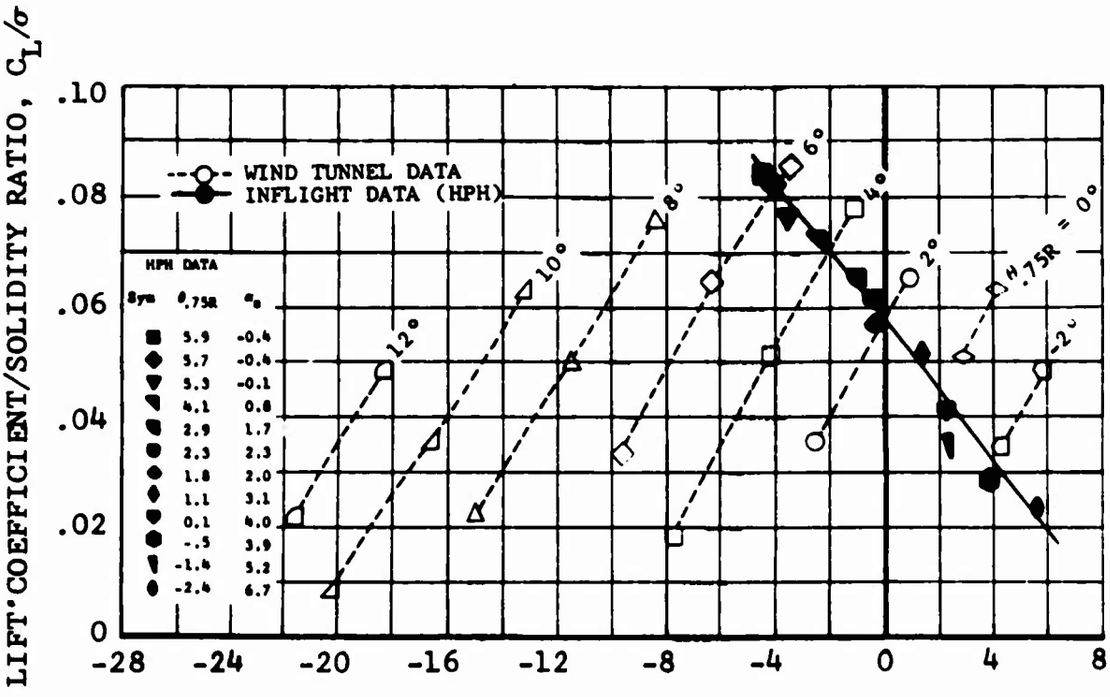

(a) C_L/σ vs α_c

Figure 21. Nondimensional Comparison of Inflight HPH Rotor Performance With Full-Scale UH-1B (Modified) Wind-Tunnel Performance, $\mu = 0.40$, $M_{(1.0,\ 90)} = 0.83$.

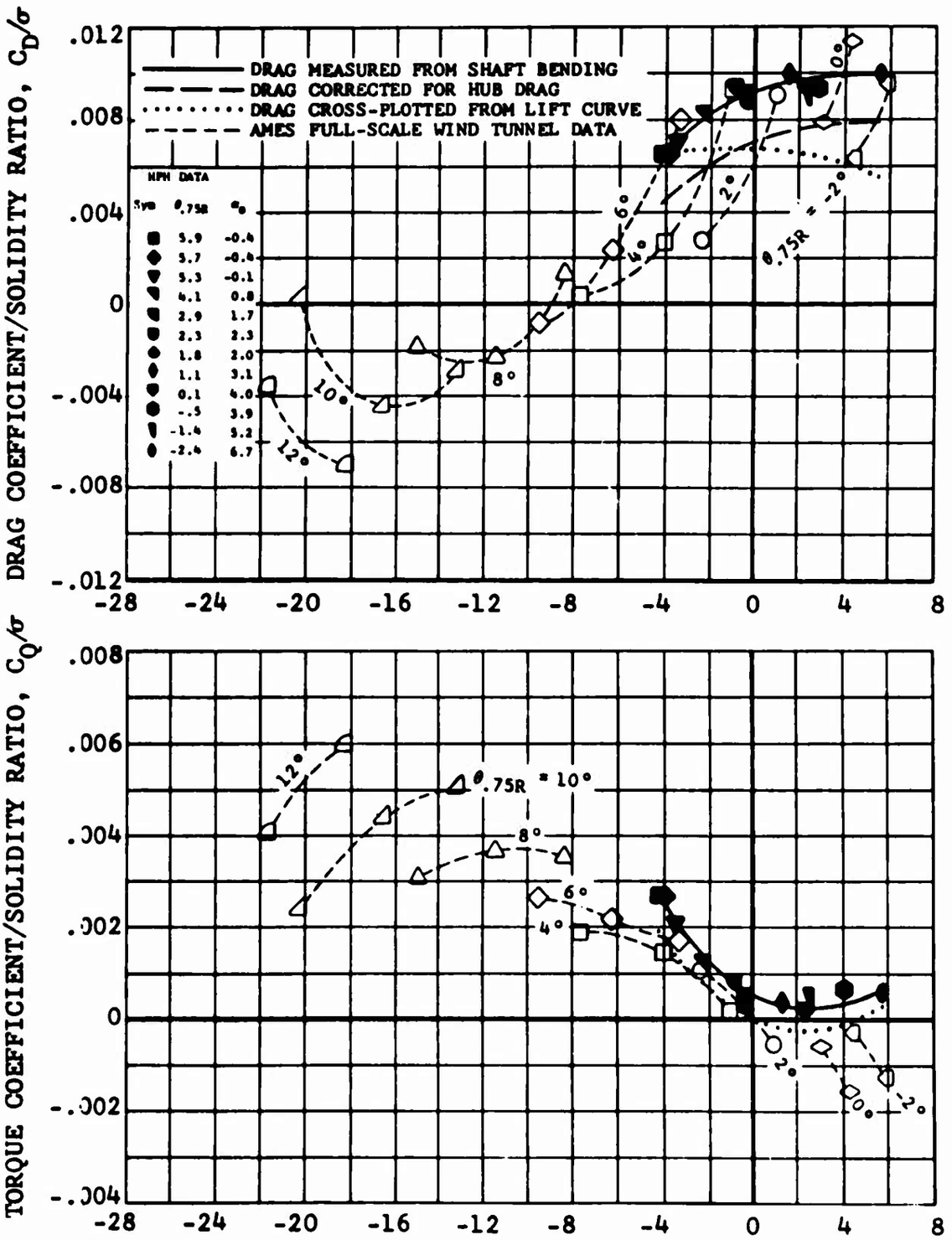

(b) C_D/σ vs a_c, C_Q/σ vs a_c

Figure 21. Concluded.

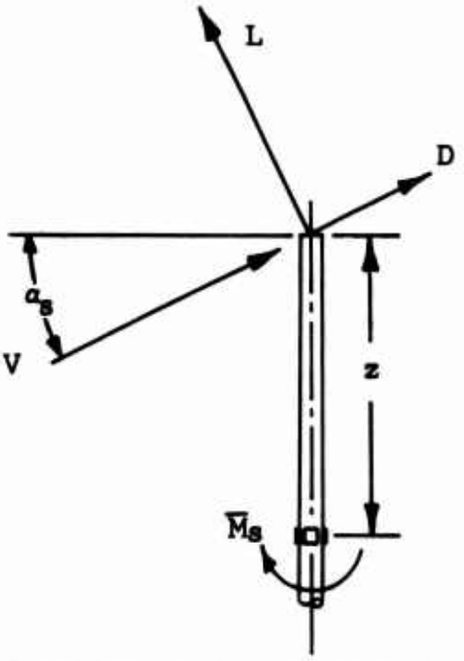

(a) Bending Moment in Fixed-Axis System Created at Strain Gage Location by Lift and Drag Forces.

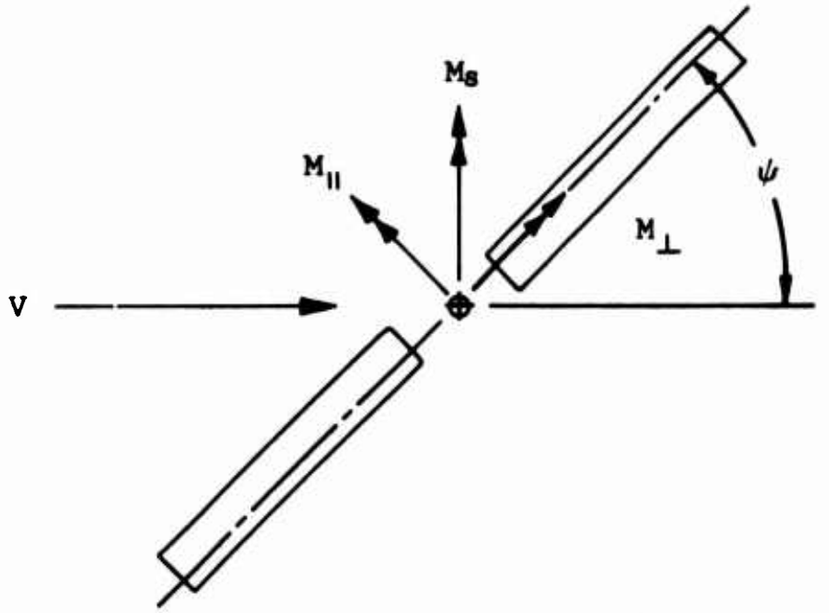

(b) Bending Moment in Rotating-Axis System Resolved into Parallel and Perpendicular Components.

Figure 22. Method of Determining HPH Rotor Drag Force From Measured Shaft Bending Moments.

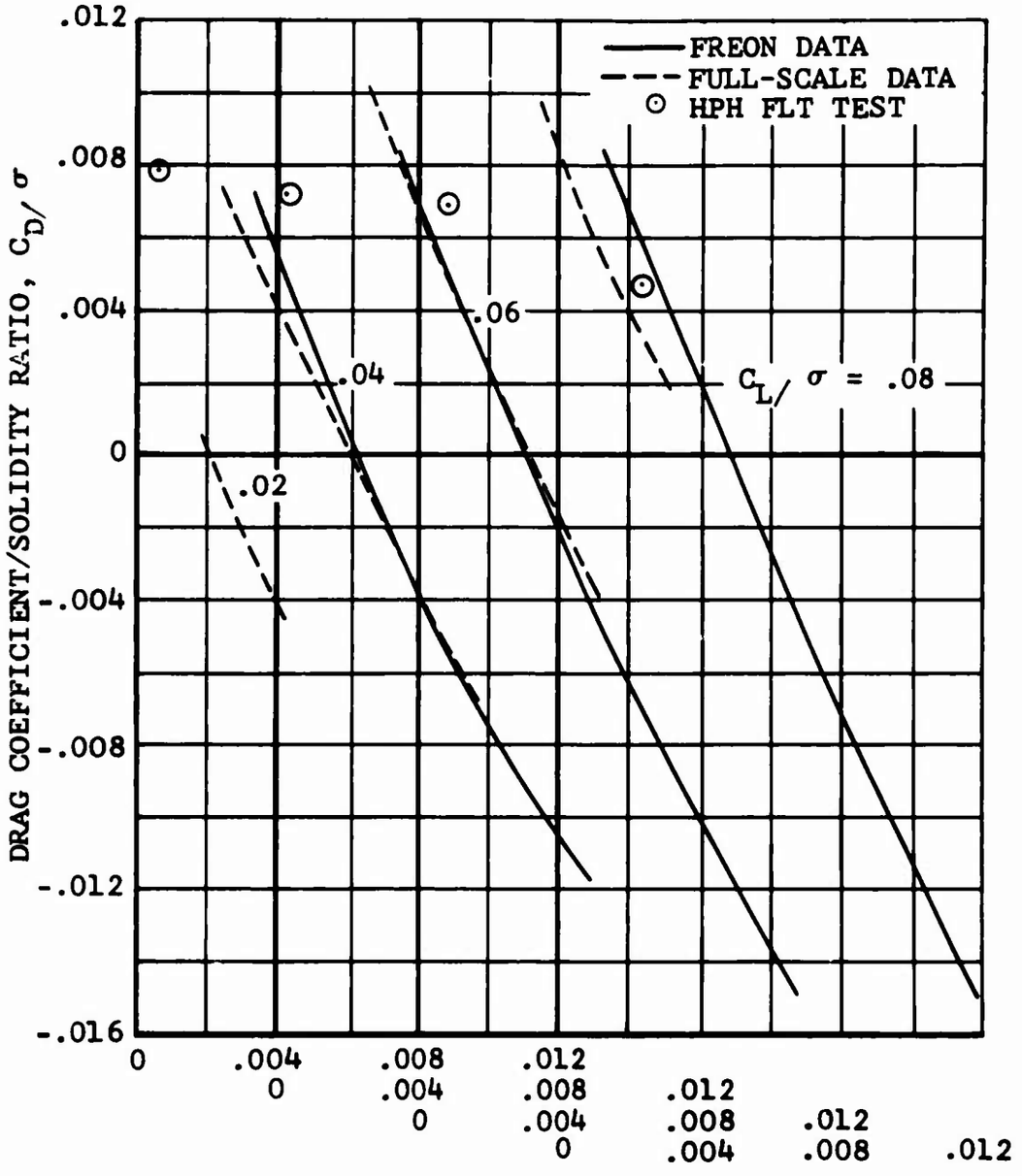

(a) μ = 0.40, $M_{(1.0,\ 90)}$ = 0.83

Figure 23. Nondimensional Comparison of the 0-Degree-Twist Model Rotor Performance With the Wind-Tunnel and Flight-Test Performance of the -1.83-Degree-Twist 44-Foot-Diameter Thin-Tip Rotor at Various Advance Ratio/Advancing-Tip Mach Number Combinations.

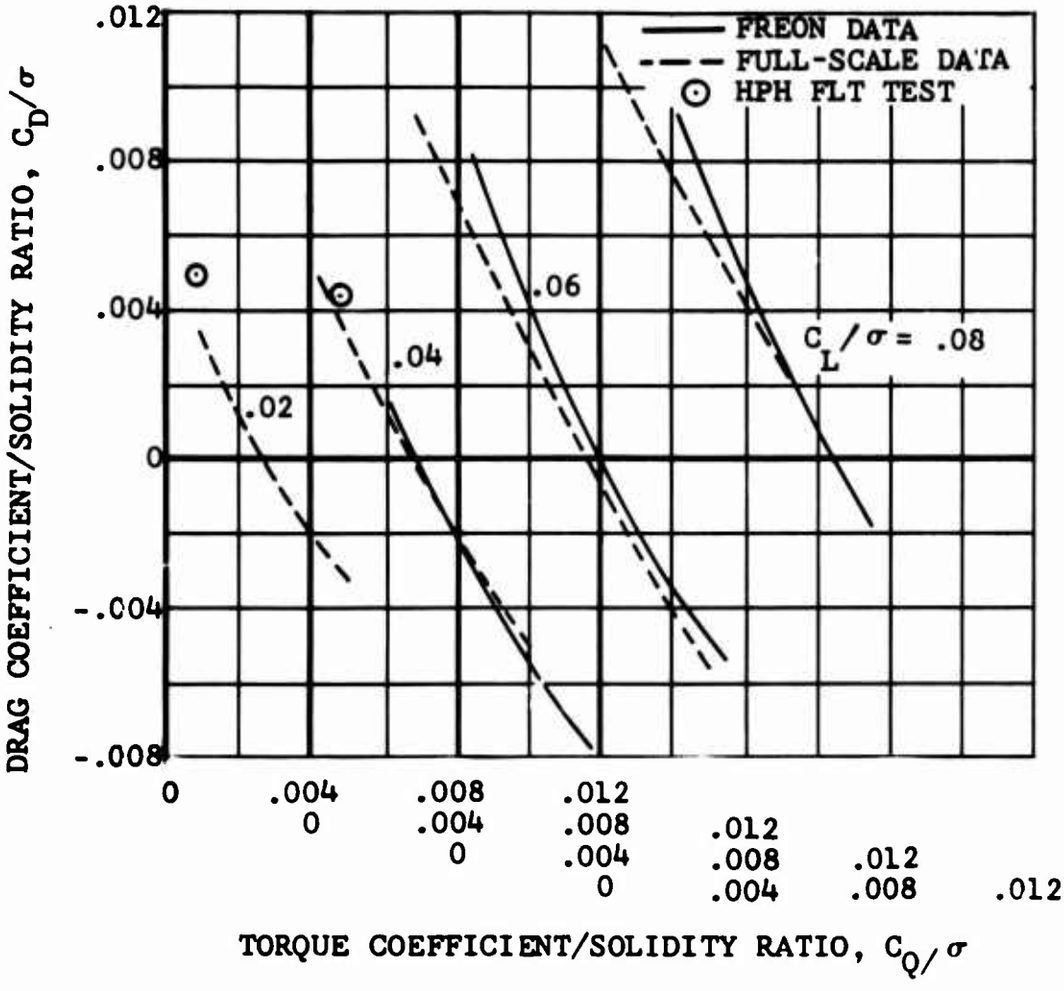

(b) $\mu = 0.41$, $M_{(1.0,\ 90)} = 0.94$

Figure 23. Continued.

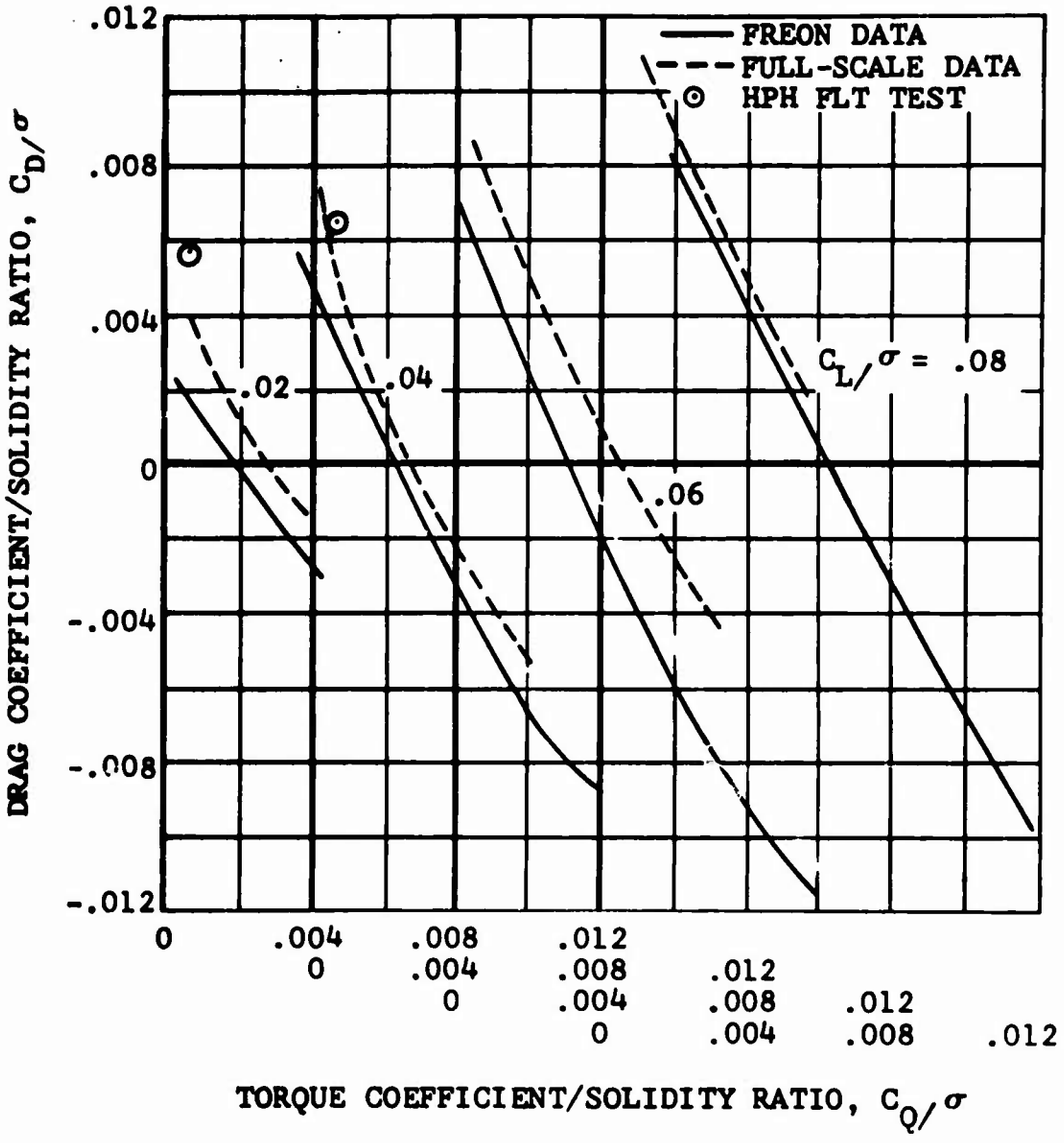

(c) $\mu = 0.45$, $M_{(1.0,\ 90)} = 0.90$

Figure 23. Concluded.

APPENDIX I
0-DEGREE-TWIST MODEL ROTOR EXPERIMENTAL AND THEORETICAL PERFORMANCE

Experimental performance of the 1/4-scale, 0-degree-twist Bell 540 rotor is shown in Figure 24. The data (presented in Reference 1) have been graphed and crossplotted in a carpet plot format for various combinations of advance ratio and advancing-tip Mach number. Theoretical calculation of the 0-degree-twist model performance using the uniform-inflow analysis is also shown for comparison purposes.

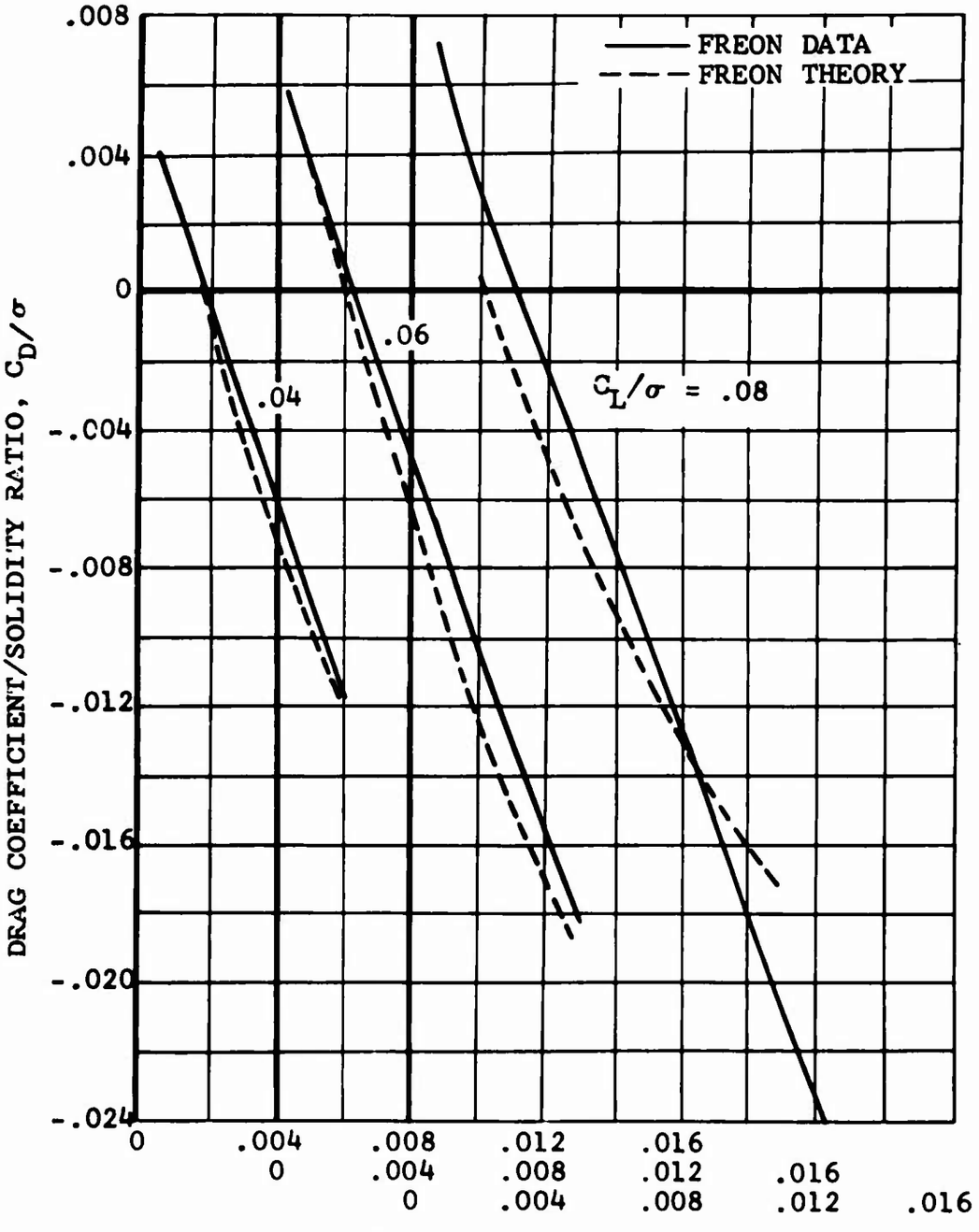

(a) μ = 0.30, M(1.0, 90) = 0.80

Figure 24. Test-Theory Comparison, Nondimensional Performance of Freon 0-Degree-Twist Rotor at Various Combinations of Advance Ratio and Advancing-Tip Mach Number.

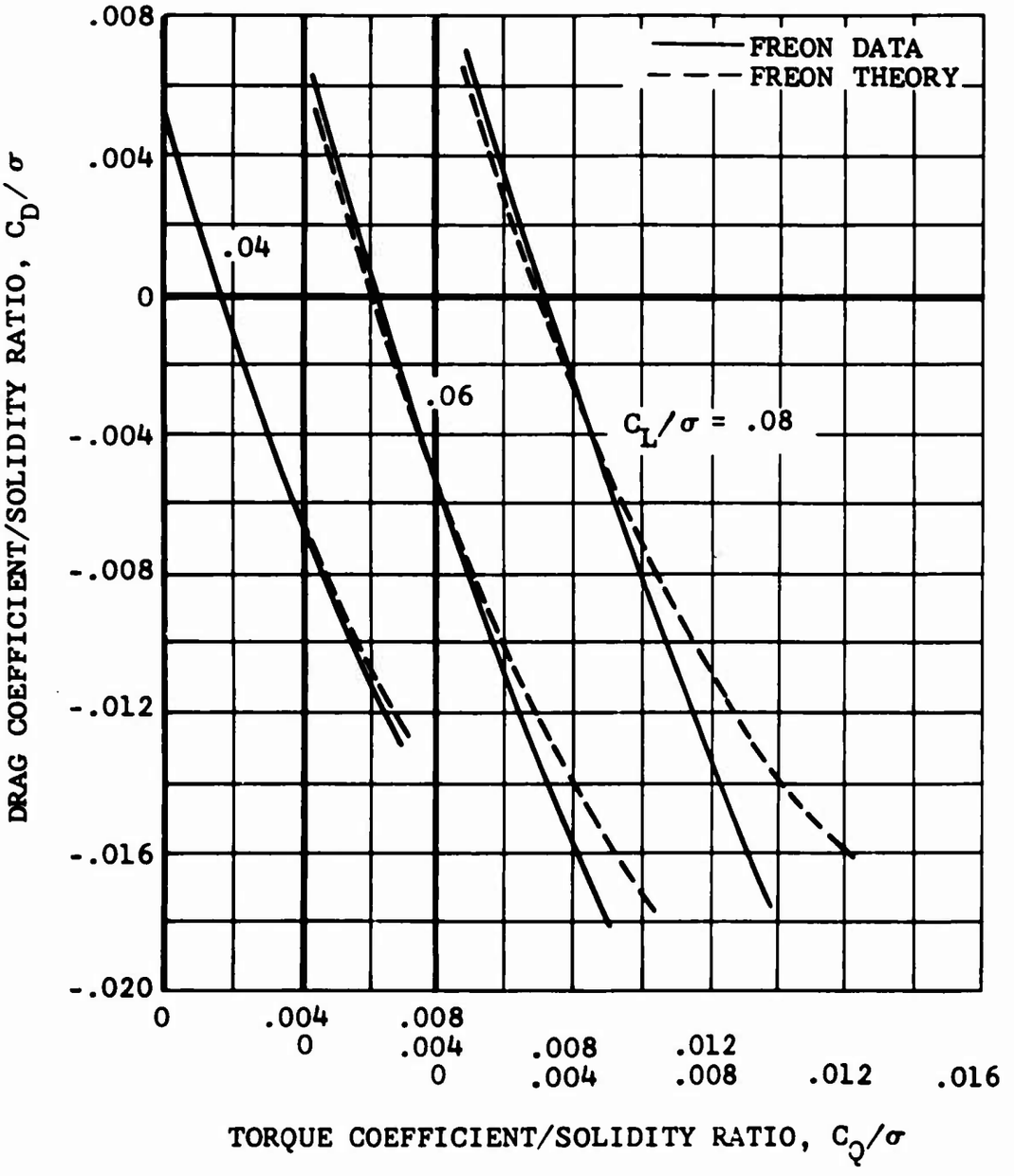

(b) μ = 0.30, $M_{(1.0,\ 90)}$ = 0.86

Figure 24. Continued.

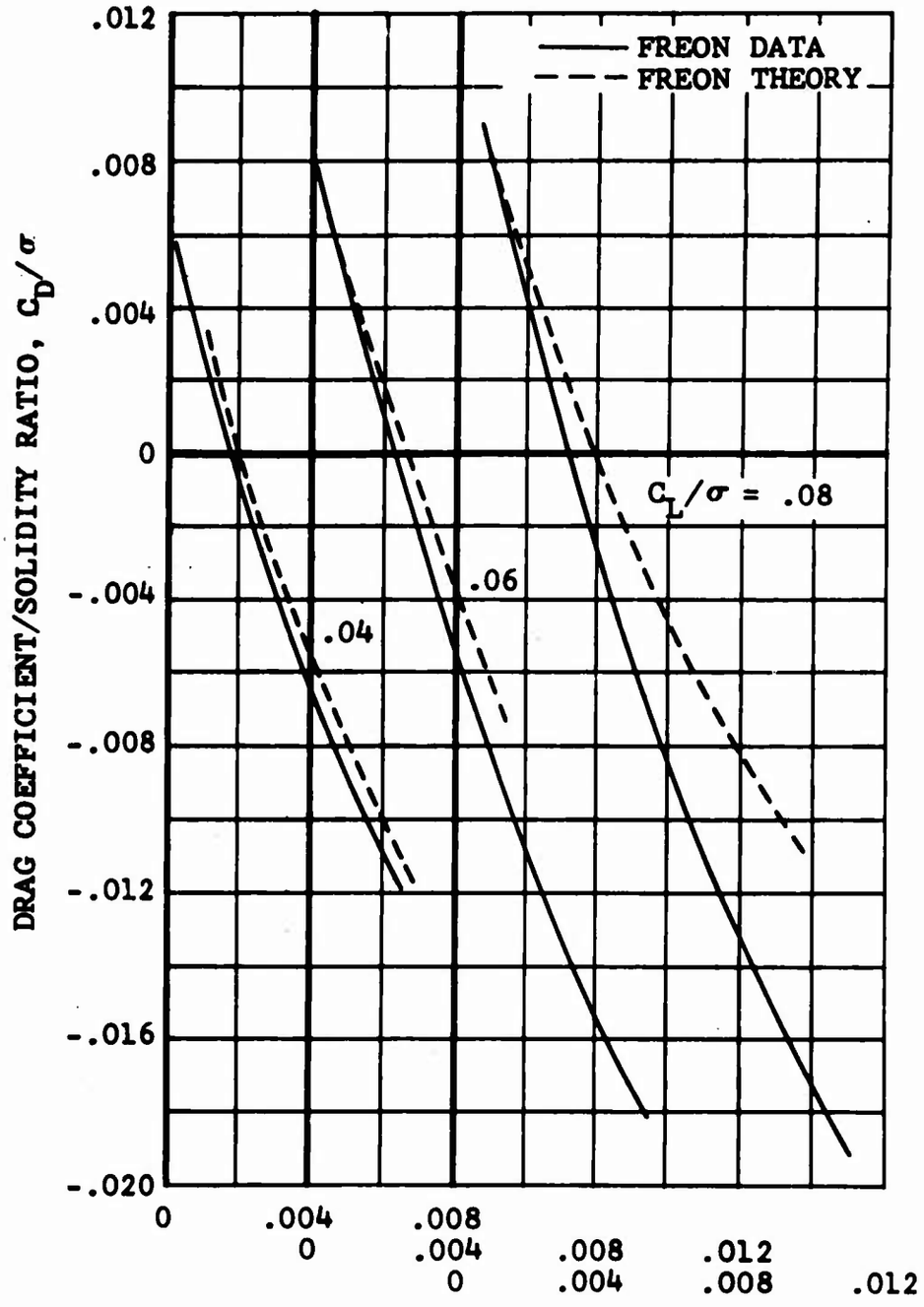

(c) $\mu = 0.30$, $M_{(1.0,\ 90)} = 0.91$

Figure 24. Continued.

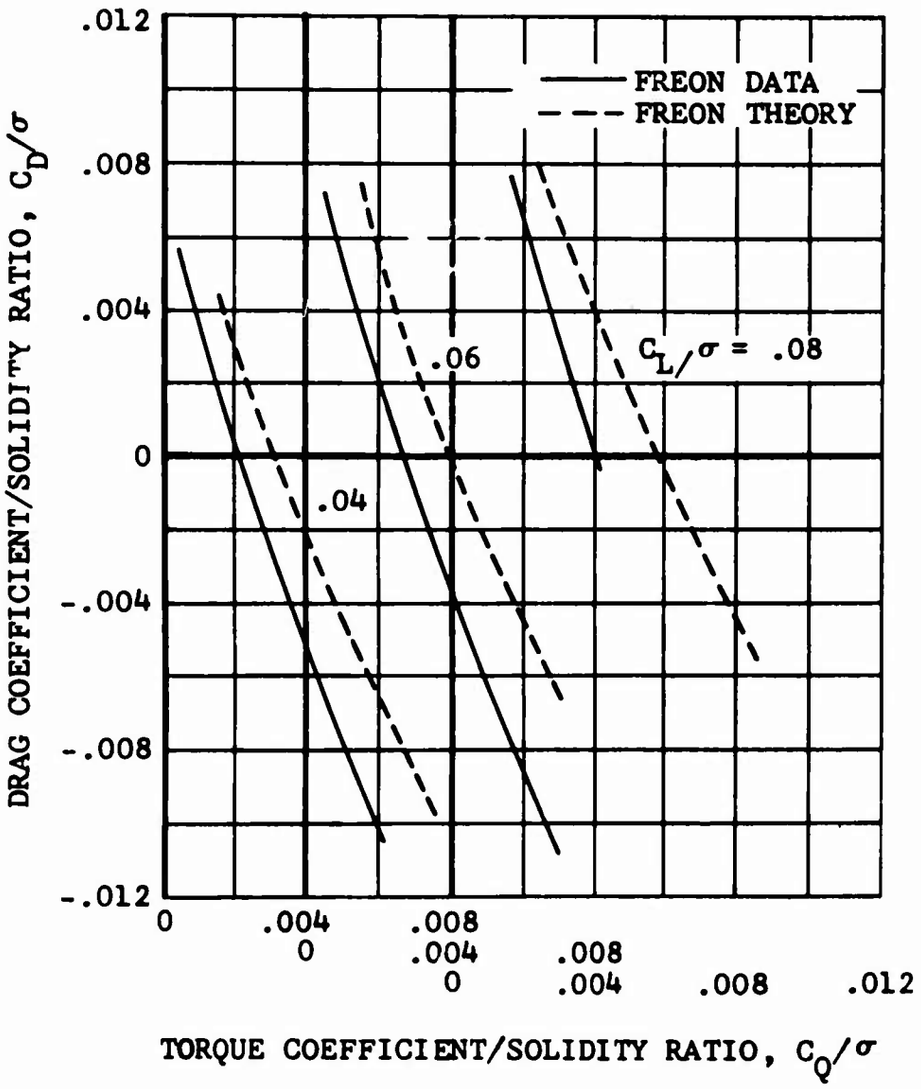

(d) $\mu = 0.30$, $M_{(1.0,\ 90)} = 0.96$

Figure 24. Continued.

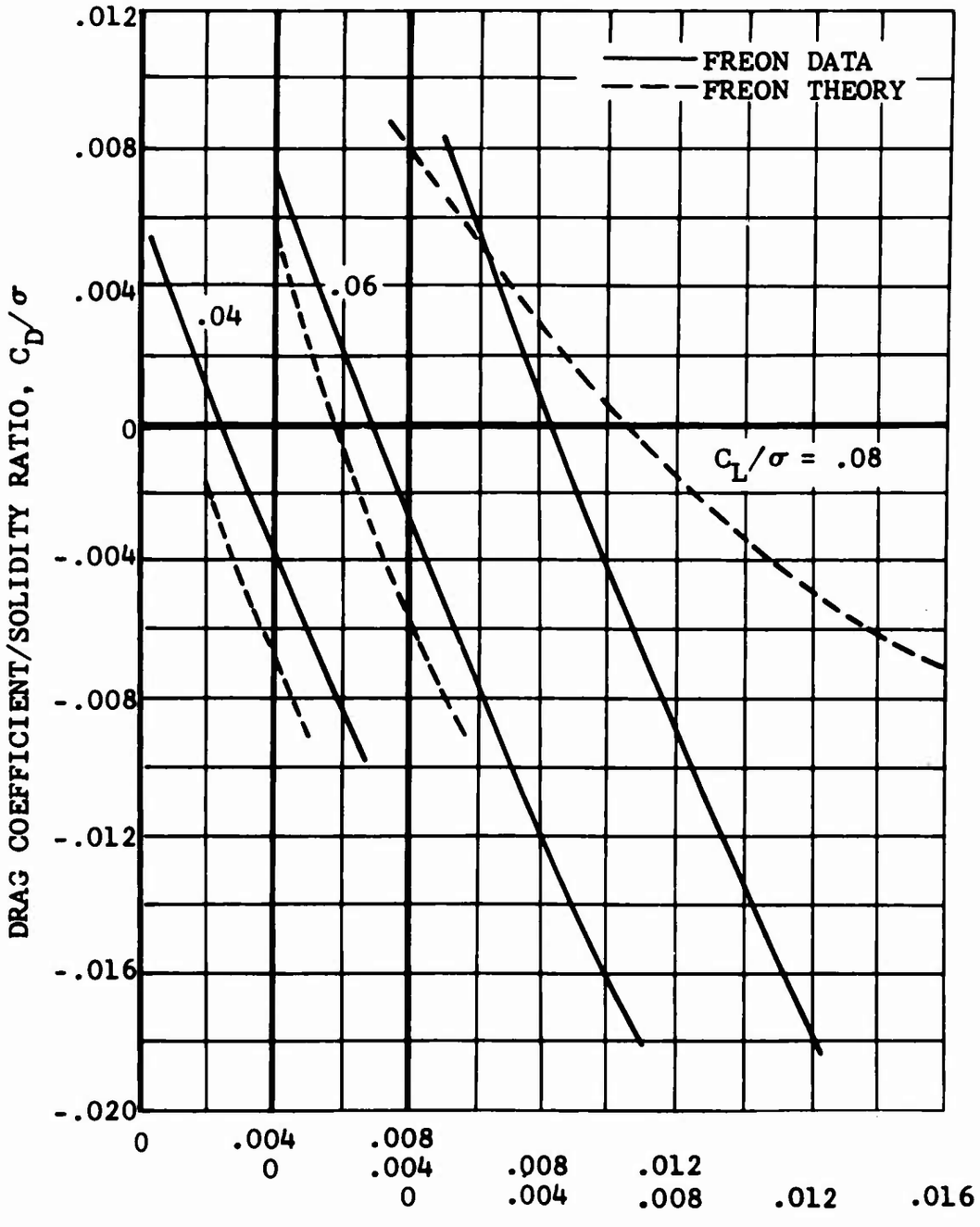

(e) $\mu = 0.34$, $M_{(1.0,\ 90)} = 0.81$

Figure 24. Continued.

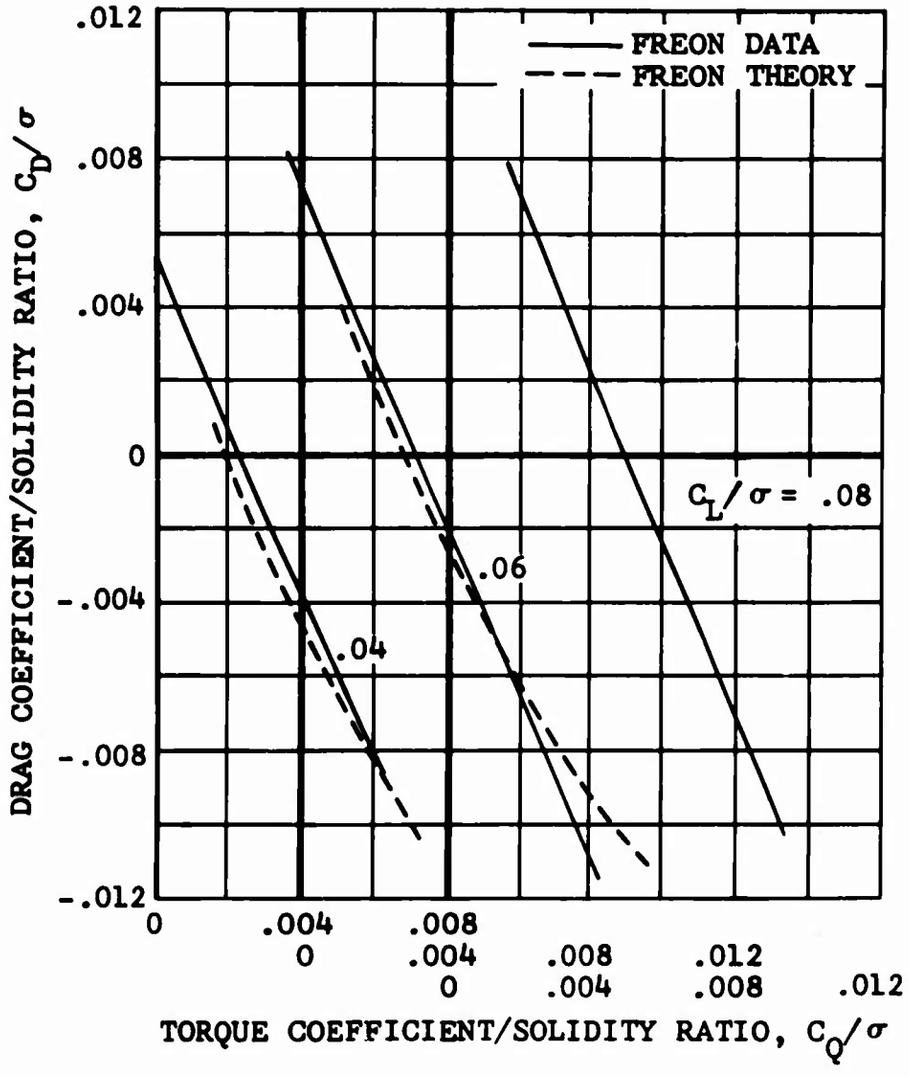

(f) $\mu = 0.36$, $M_{(1.0,\ 90)} = 0.91$

Figure 24. Continued.

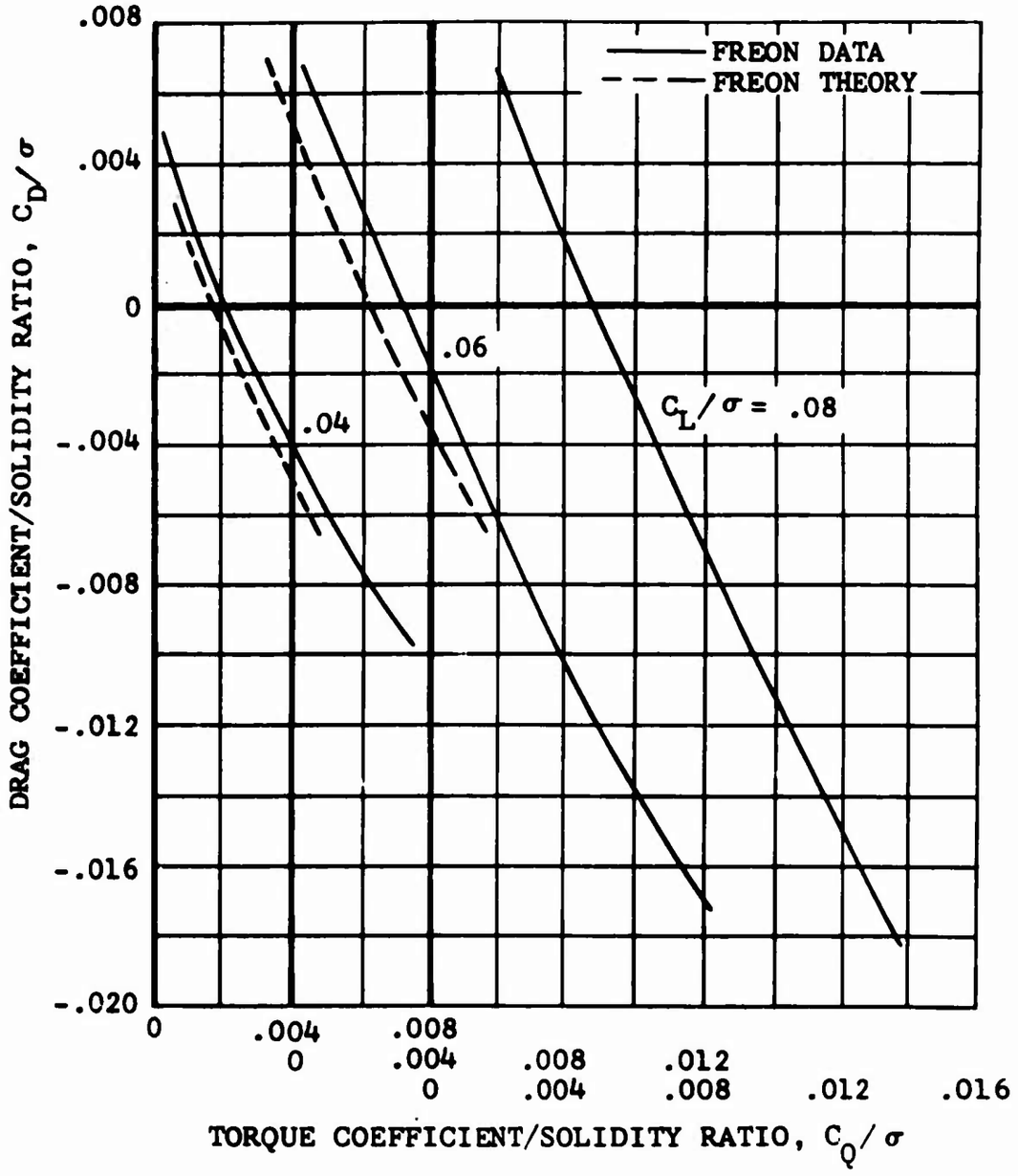

(g) $\mu = 0.39$, $M_{(1.0,\ 90)} = 0.84$

Figure 24. Continued.

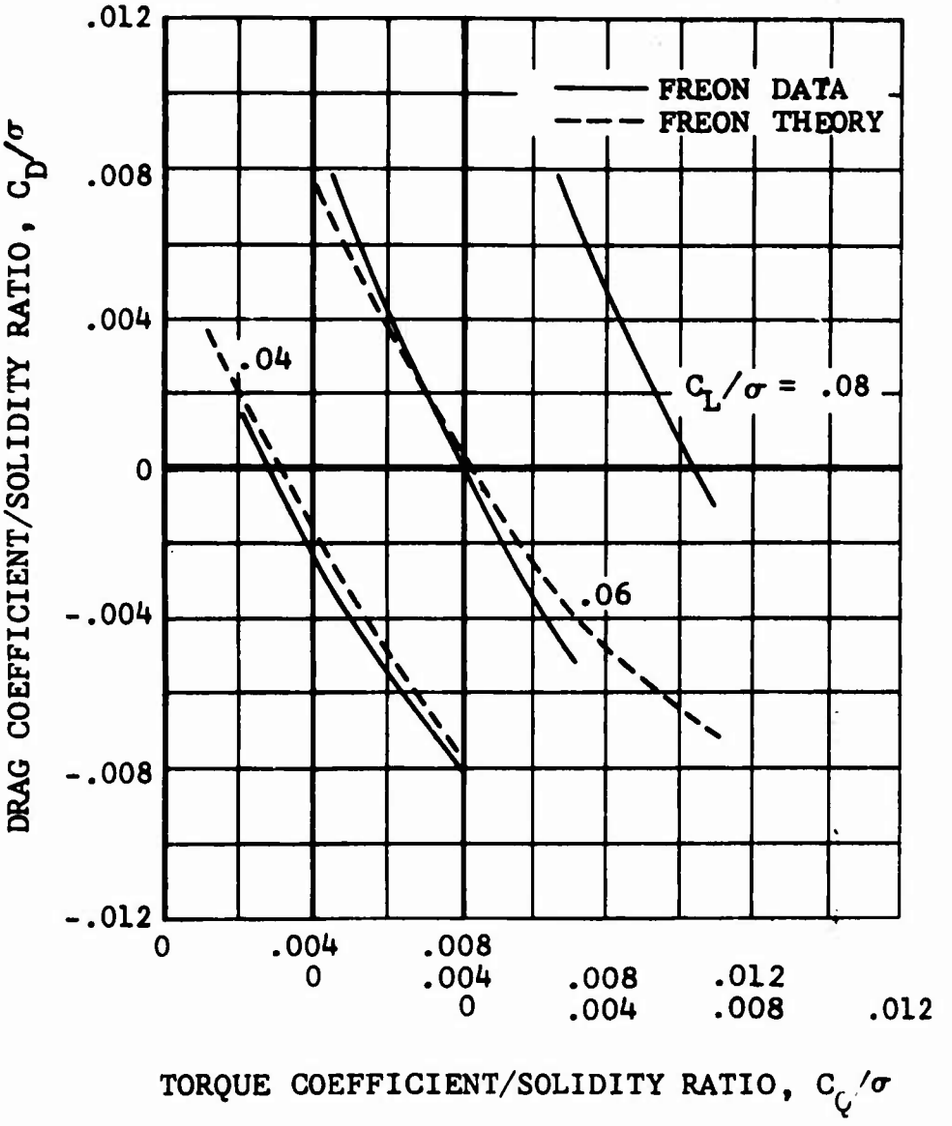

(h) $\mu = 0.41$, $M_{(1.0,\ 90)} = 0.95$

Figure 24. Continued.

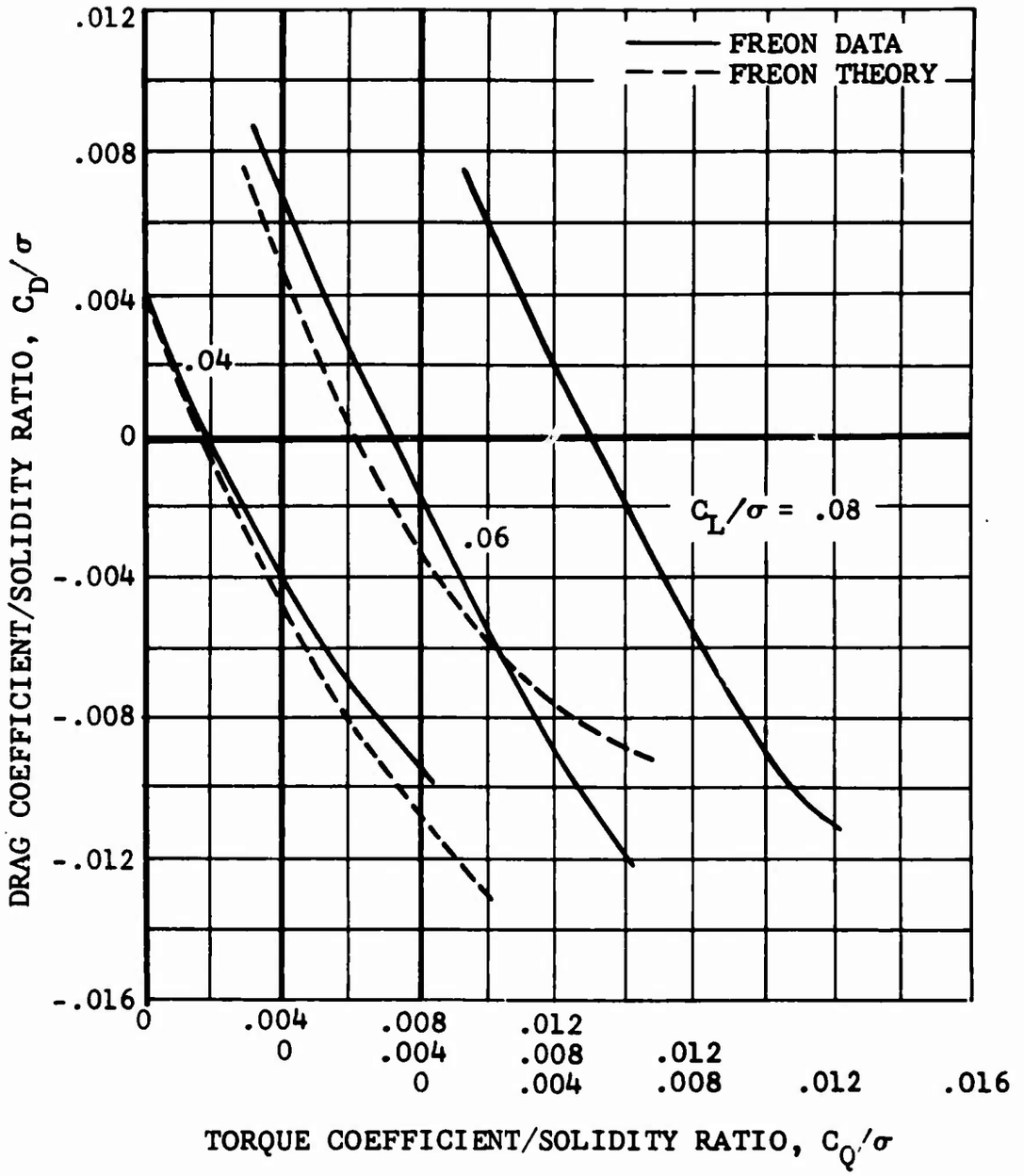

(i) μ = 0.43, $M_{(1.0,\ 90)}$ = 0.80

Figure 24. Continued.

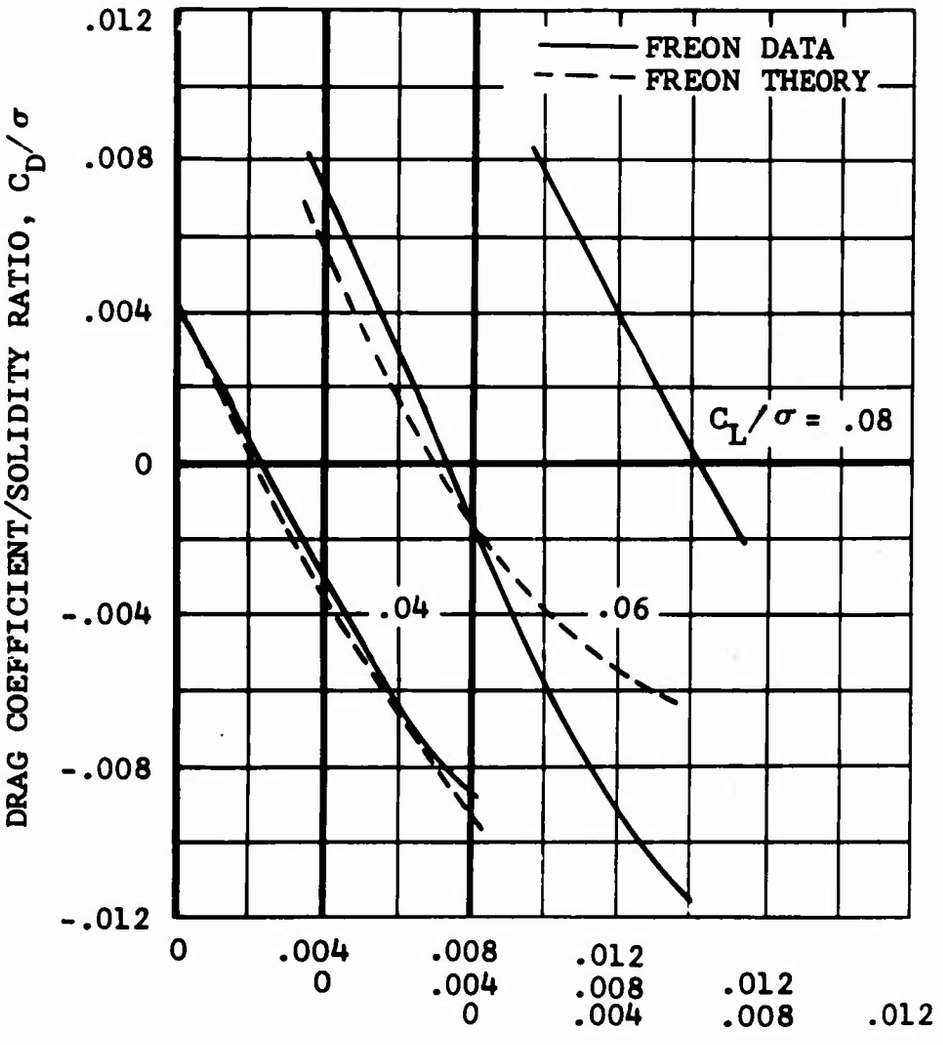

(j) $\mu = 0.43$, $M_{(1.0,\ 90)} = 0.91$

Figure 24. Continued.

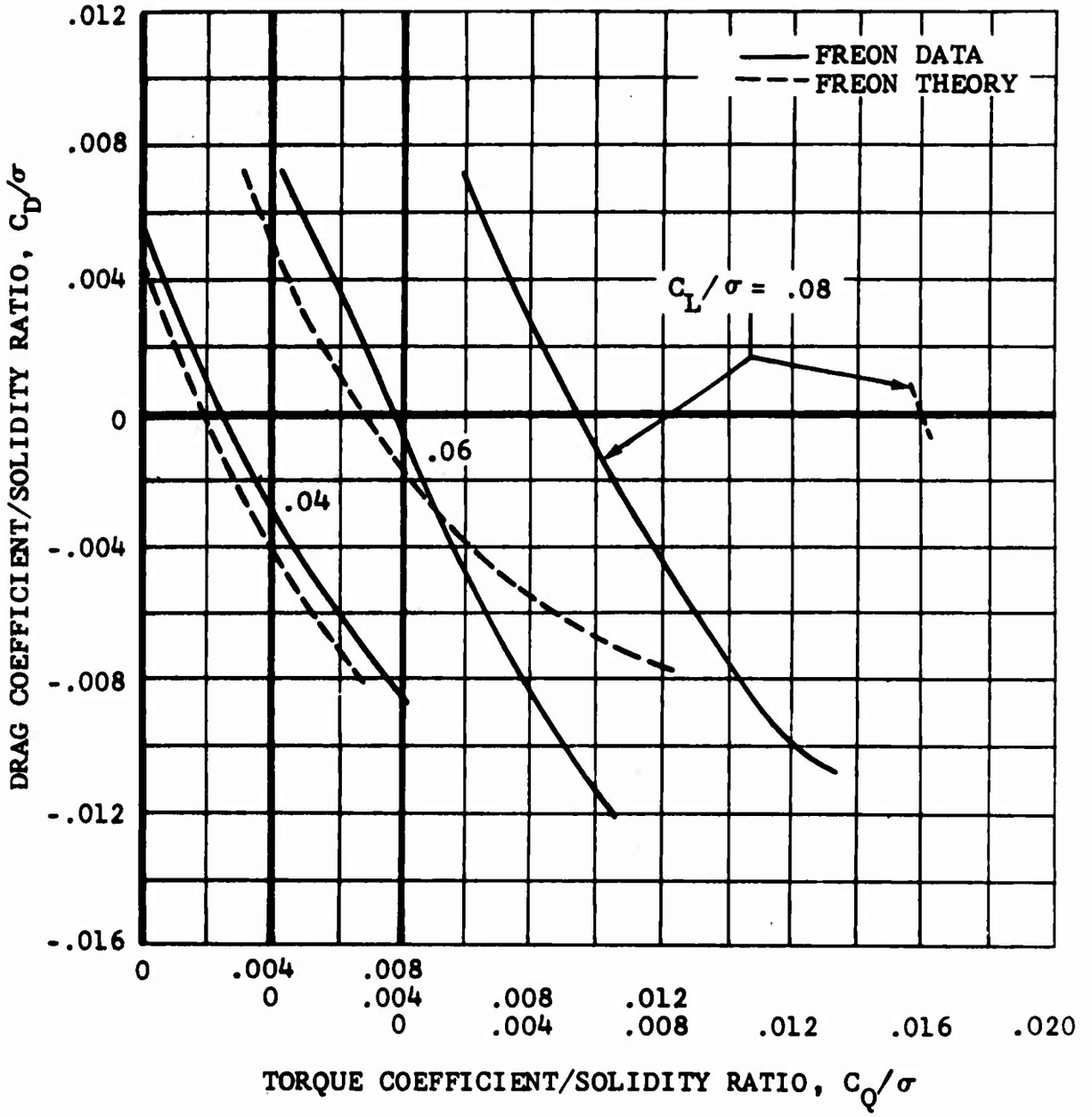

(k) $\mu = 0.44$, $M_{(1.0,\ 90)} = 0.86$

Figure 24. Continued.

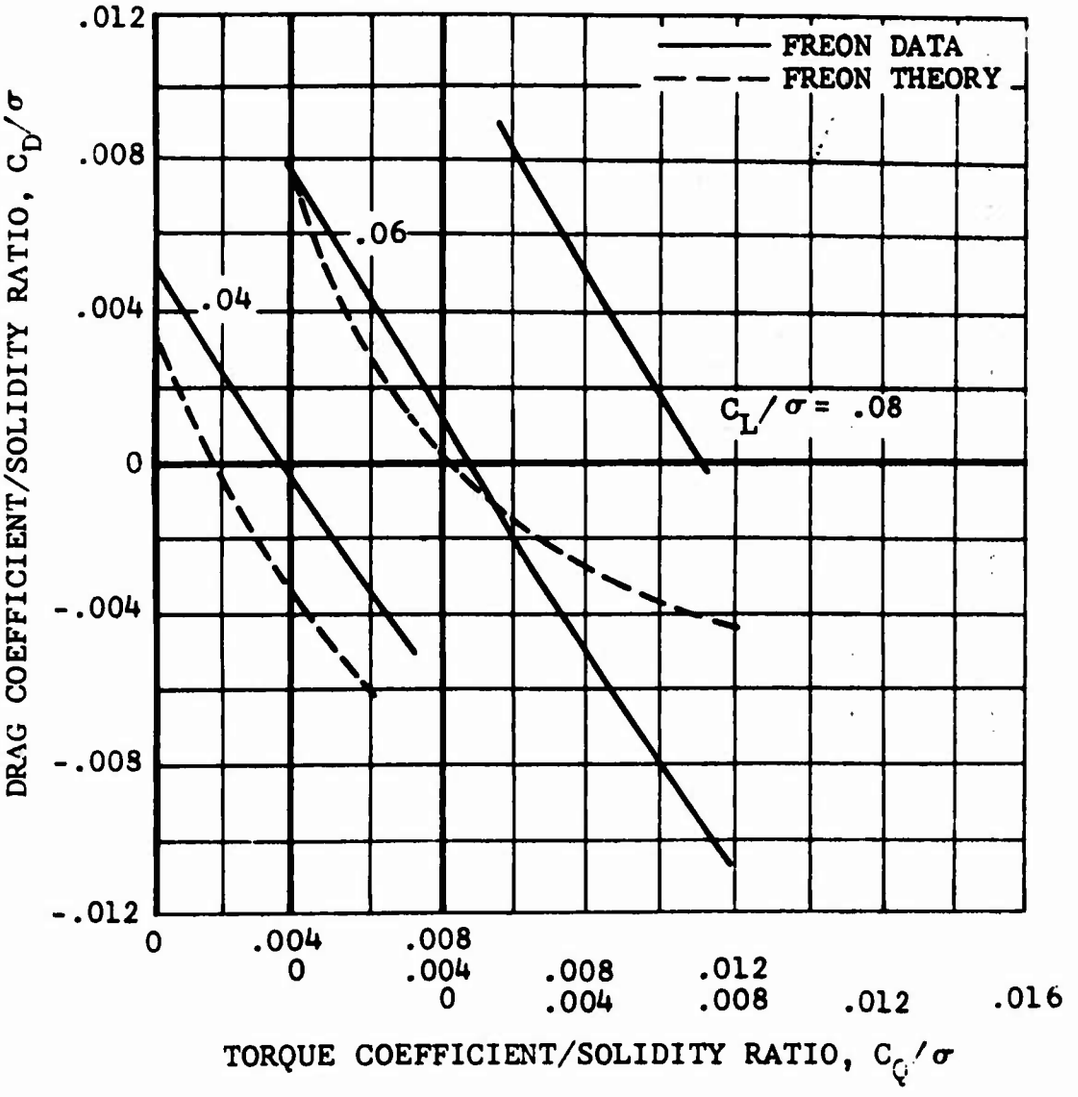

(1) μ = 0.49, $M_{(1.0,\ 90)}$ = 0.80

Figure 24. Continued.

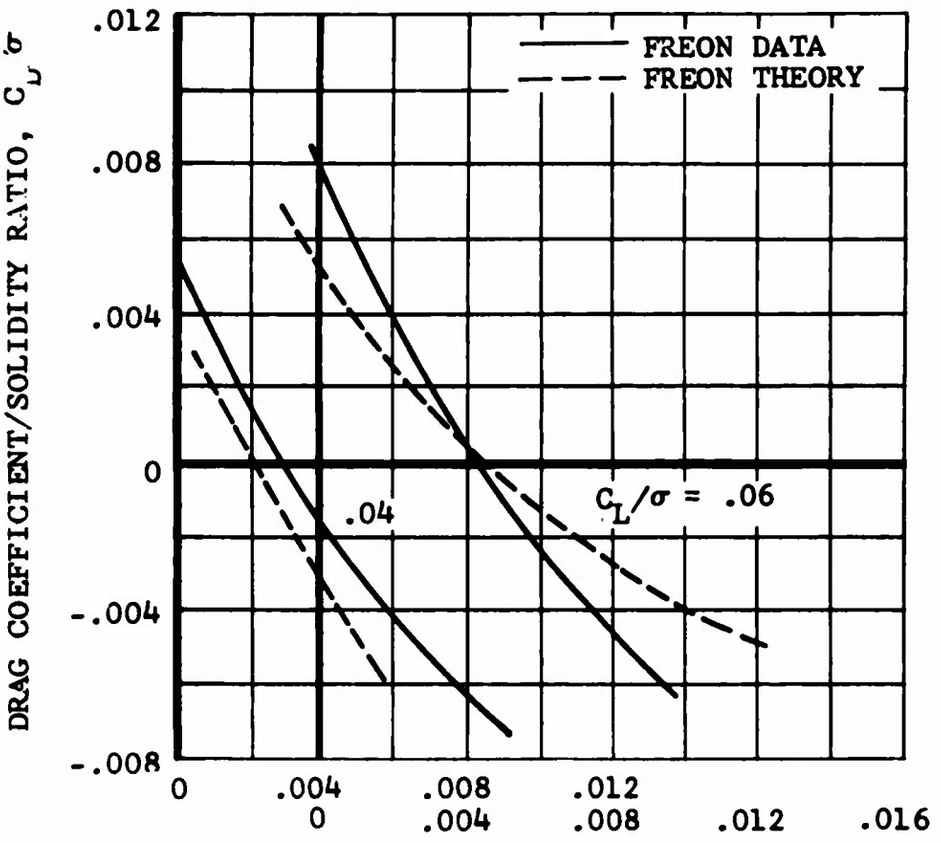

(m) $\mu = 0.48$, $M_{(1.0,\ 90)} = 0.85$

Figure 24. Continued.

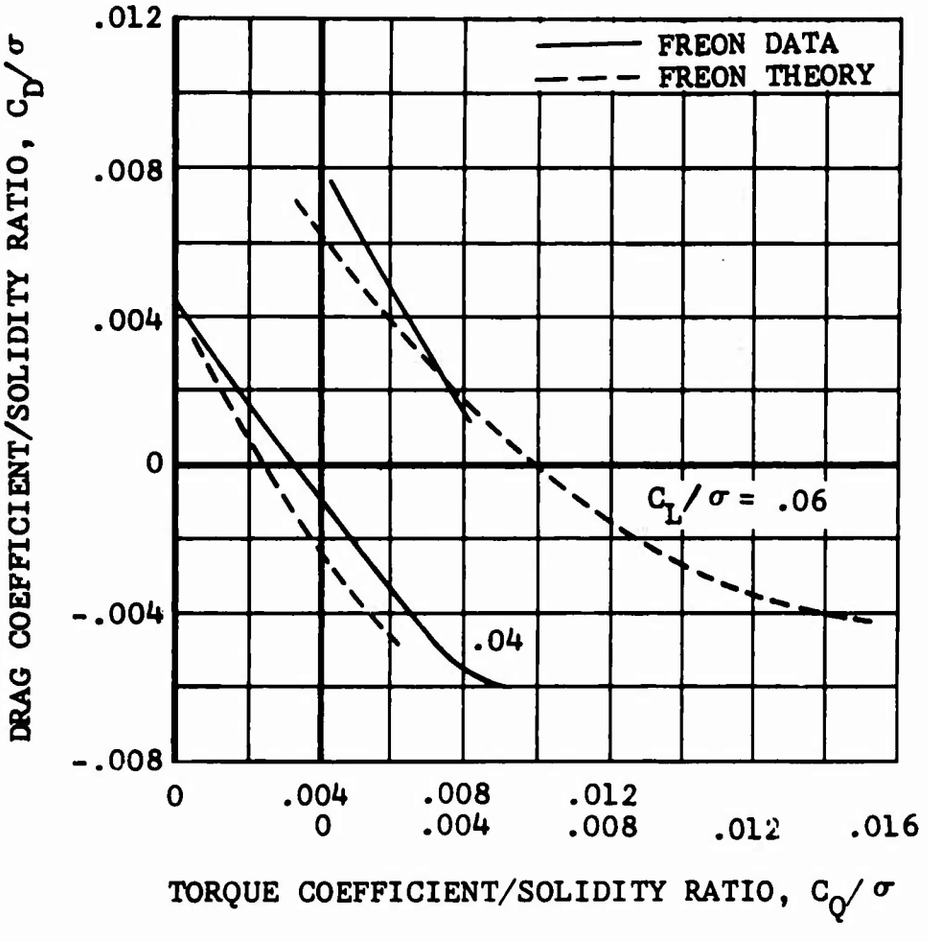

(n) $\mu = 0.49$, $M_{(1.0,\ 90)} = 0.90$

Figure 24. Continued.

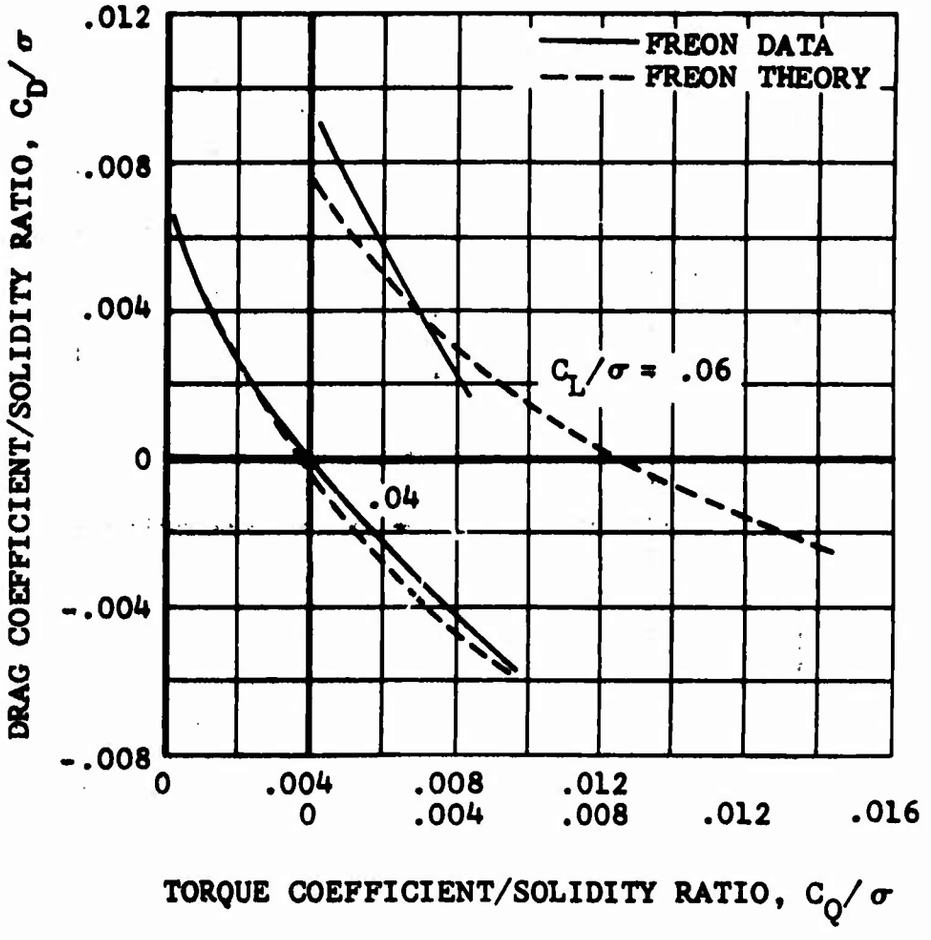

(o) $\mu = 0.49$, $M_{(1.0,\ 90)} = 0.95$

Figure 24. Continued.

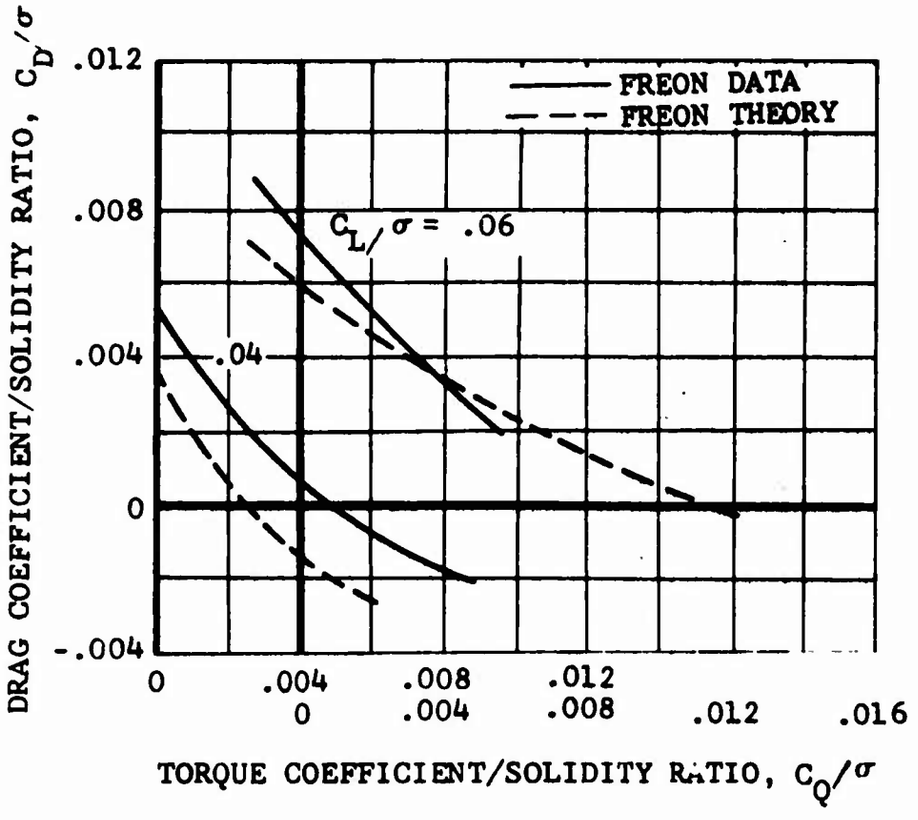

(p) $\mu = 0.58$, $M_{(1.0,\ 90)} = 0.80$

Figure 24. Continued.

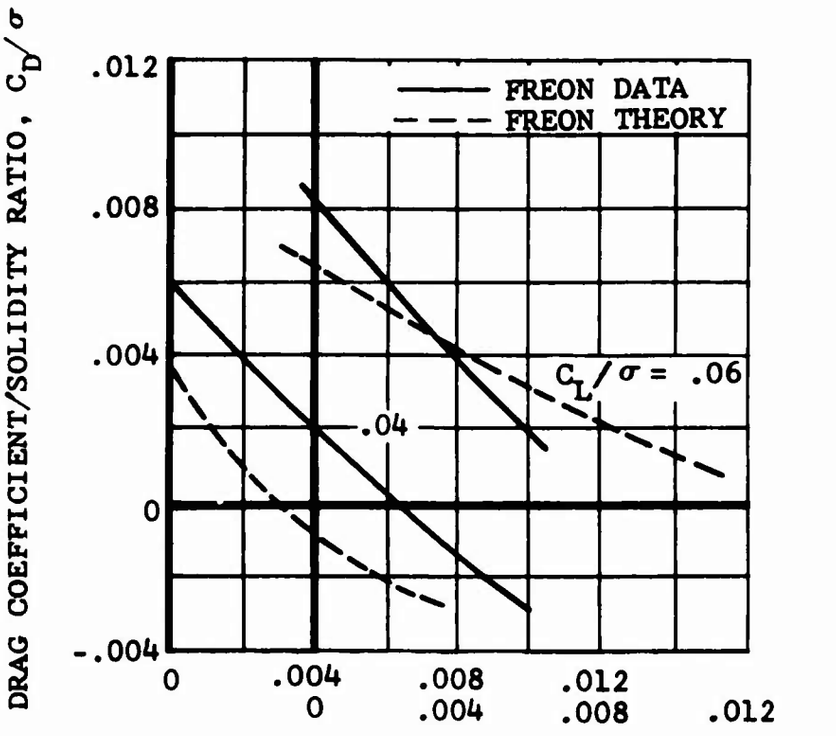

(q) $\mu = 0.58$, $M_{(1.0,\ 90)} = 0.85$

Figure 24. Continued.

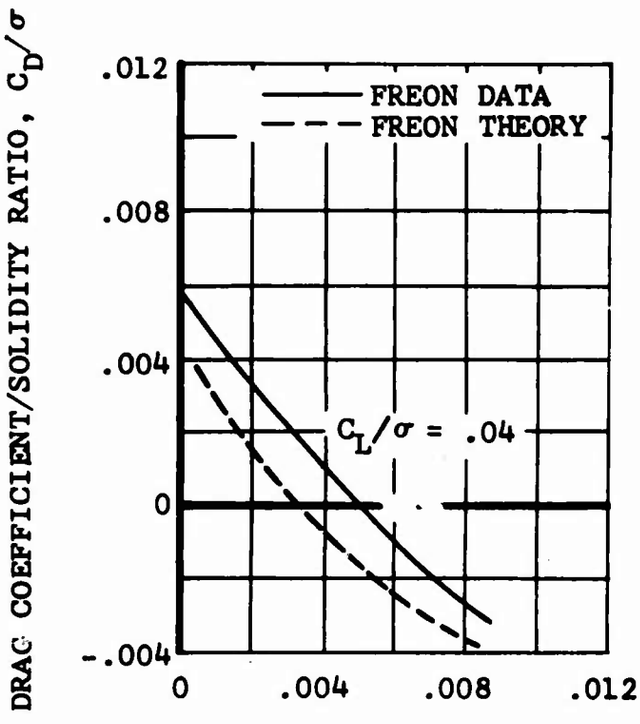

(r) $\mu = 0.55$, $M_{(1.0,\ 90)} = 0.91$

Figure 24. Continued.

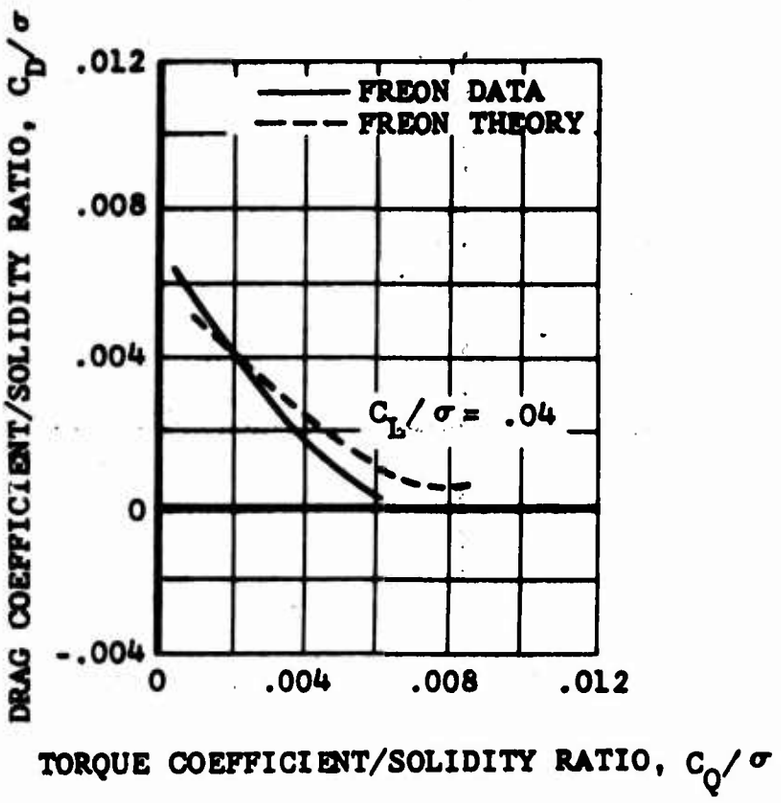

(e) $\mu = 0.56$, $M_{(1.0,\ 90)} = 0.96$

Figure 24. Continued.

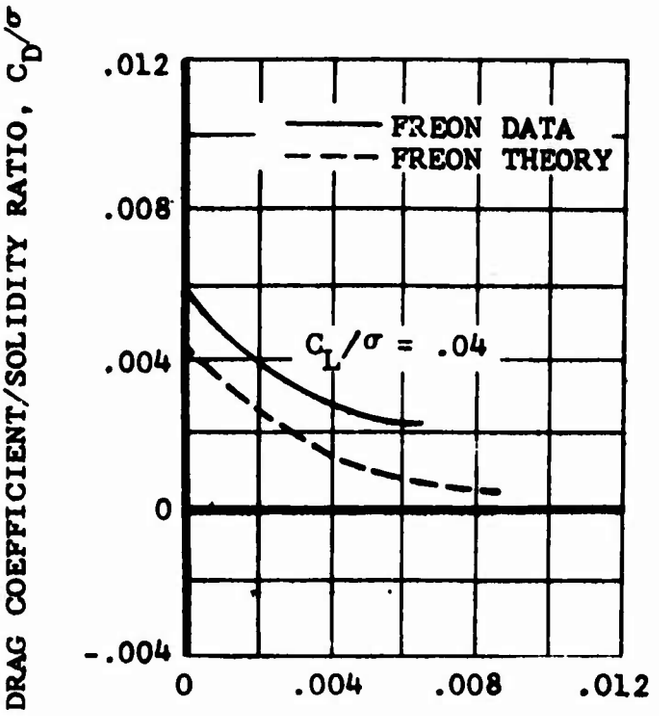

(t) $\mu = 0.63$, $M_{(1.0,\ 90)} = 0.91$

Figure 24. Concluded.

APPENDIX II
FULL-SCALE UH-1B (MODIFIED) EXPERIMENTAL ROTOR PERFORMANCE

Full-scale wind-tunnel performance of the UH-1B (modified) rotor is presented in Figure 25 for various advance ratios and advancing-tip Mach numbers. Data for the conditions shown are included in Reference 3.

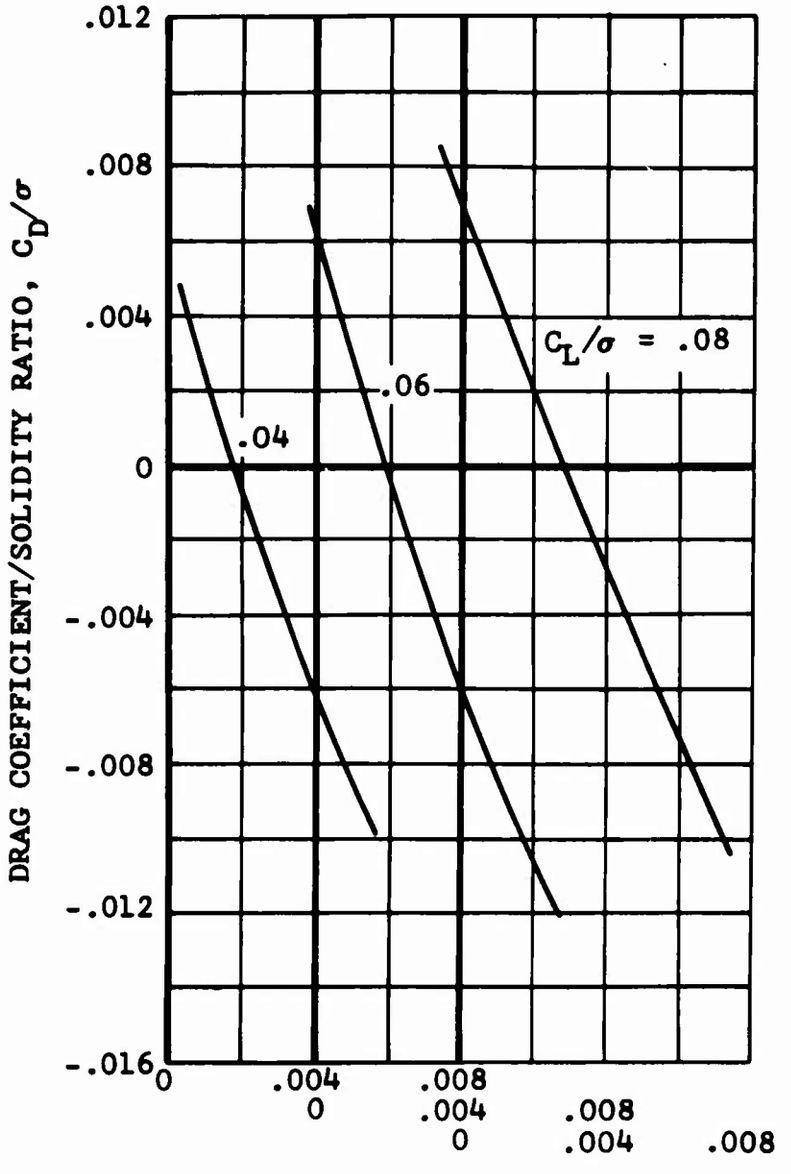

(a) $\mu = 0.31$, $M_{(1.0,\ 90)} = 0.88$

Figure 25. Nondimensional Performance of Full-Scale UH-1B (Modified) Rotor at Various Combinations of Advance Ratio and Advancing-Tip Mach Number.

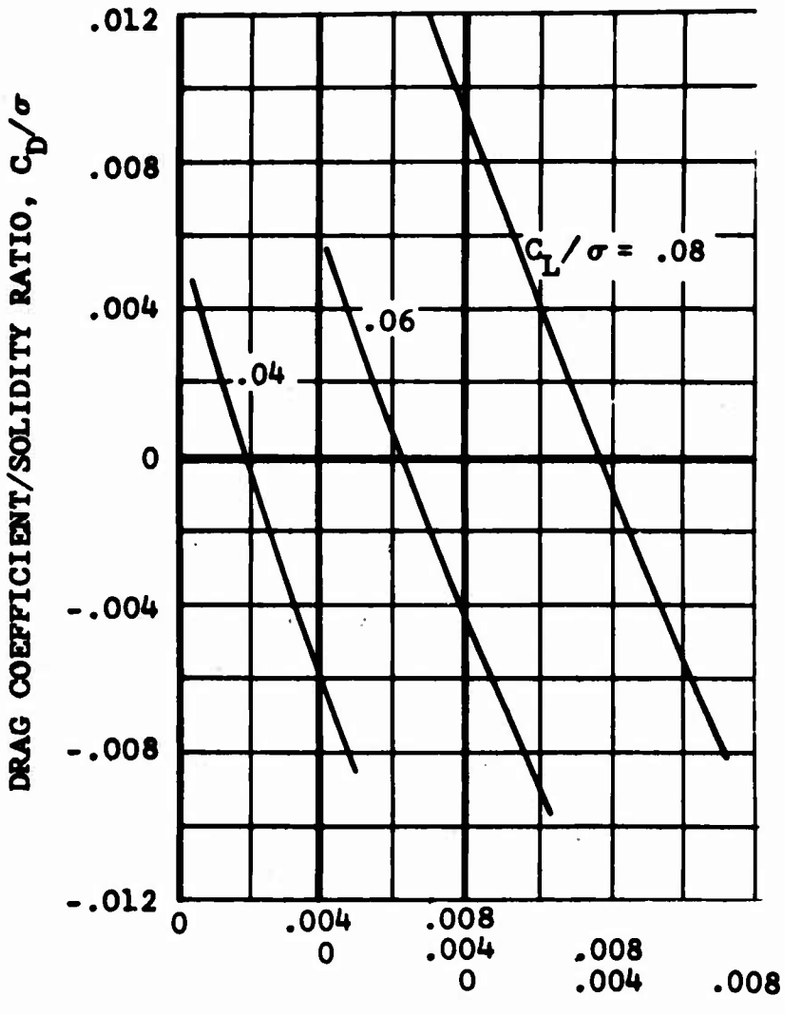

(b) $\mu = 0.36$, $M_{(1.0,\ 90)} = 0.80$

Figure 25. Continued.

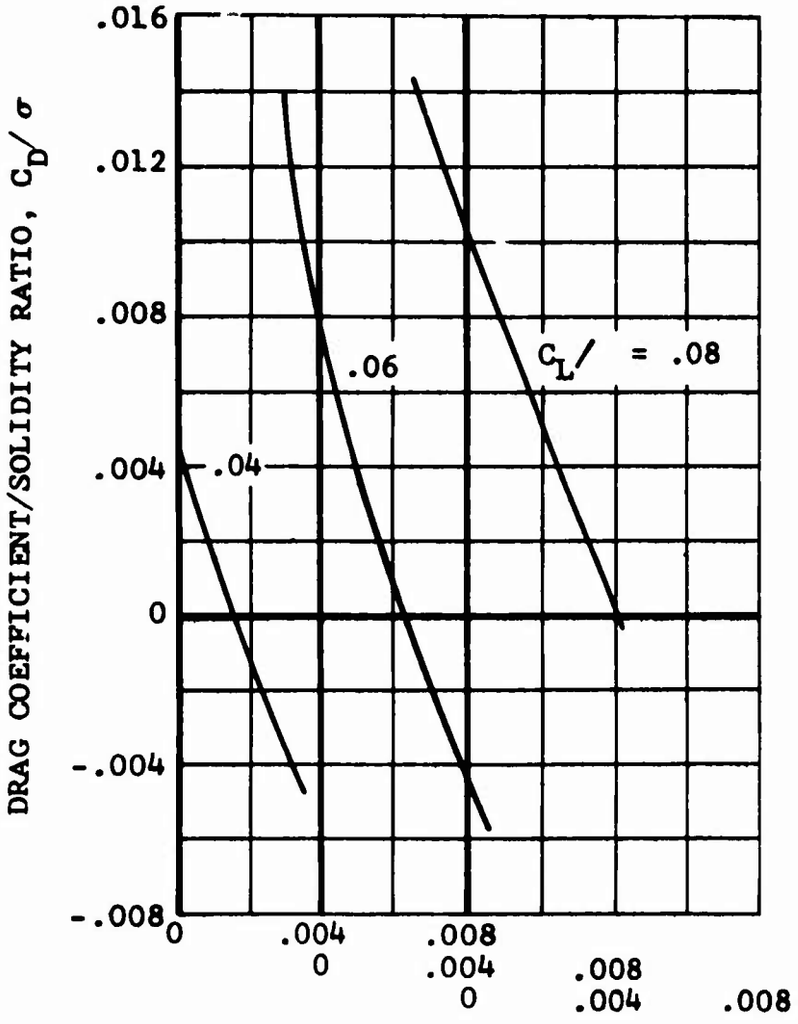

(c) $\mu = 0.36$, $M_{(1.0,\ 90)} = 0.90$

Figure 25. Continued.

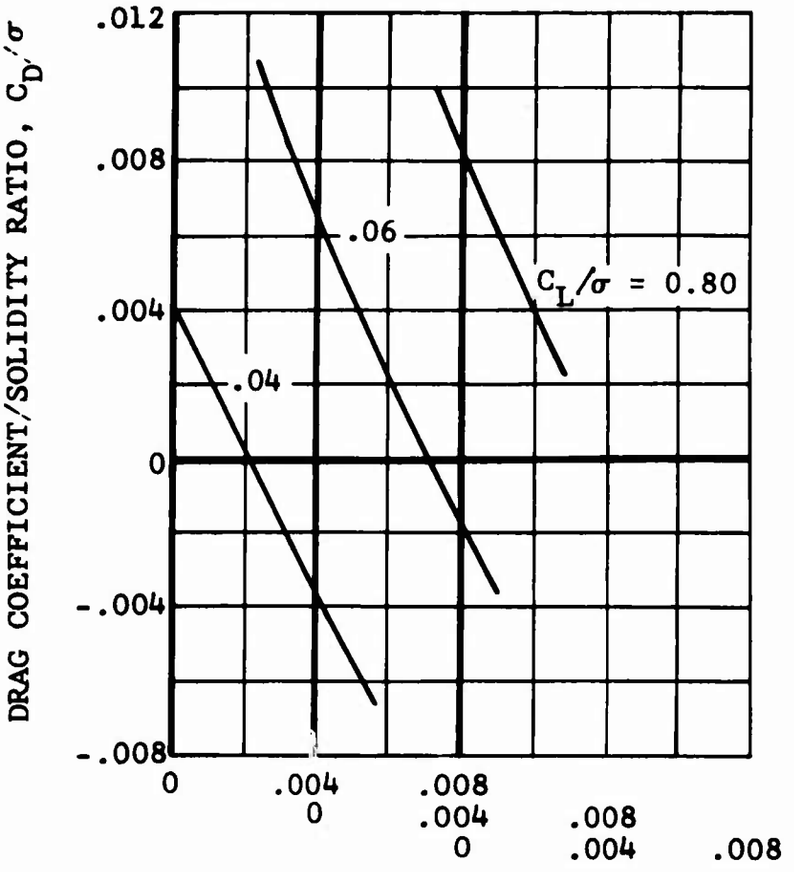

(d) μ = 0.41, $M_{(1.0,\ 90)}$ = 0.83

Figure 25. Continued.

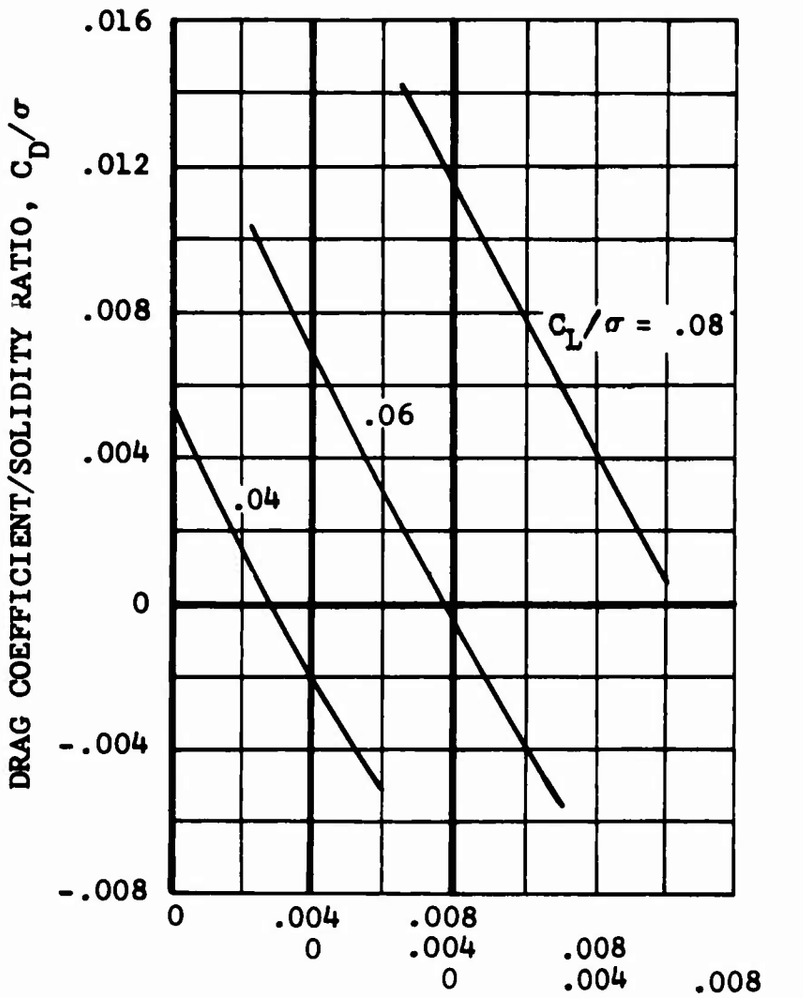

(e) $\mu = 0.41$, $M_{(1.0,\ 90)} = 0.94$

Figure 25. Continued.

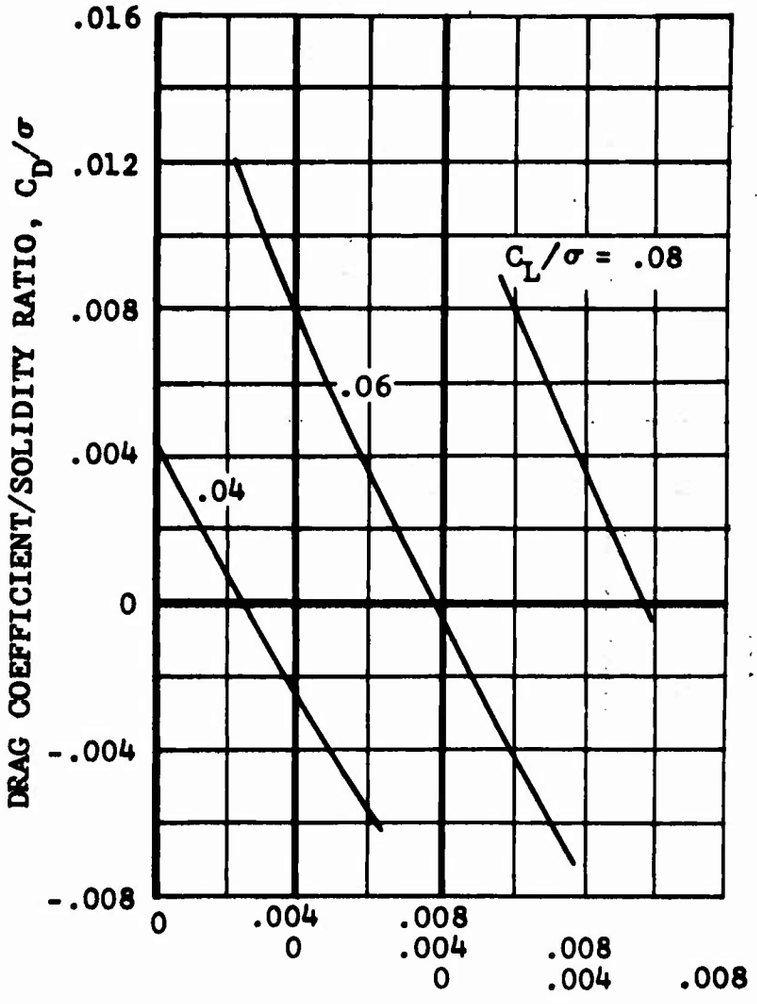

(f) $\mu = 0.45$, $M_{(1.0,\ 90)} = 0.77$

Figure 25. Continued.

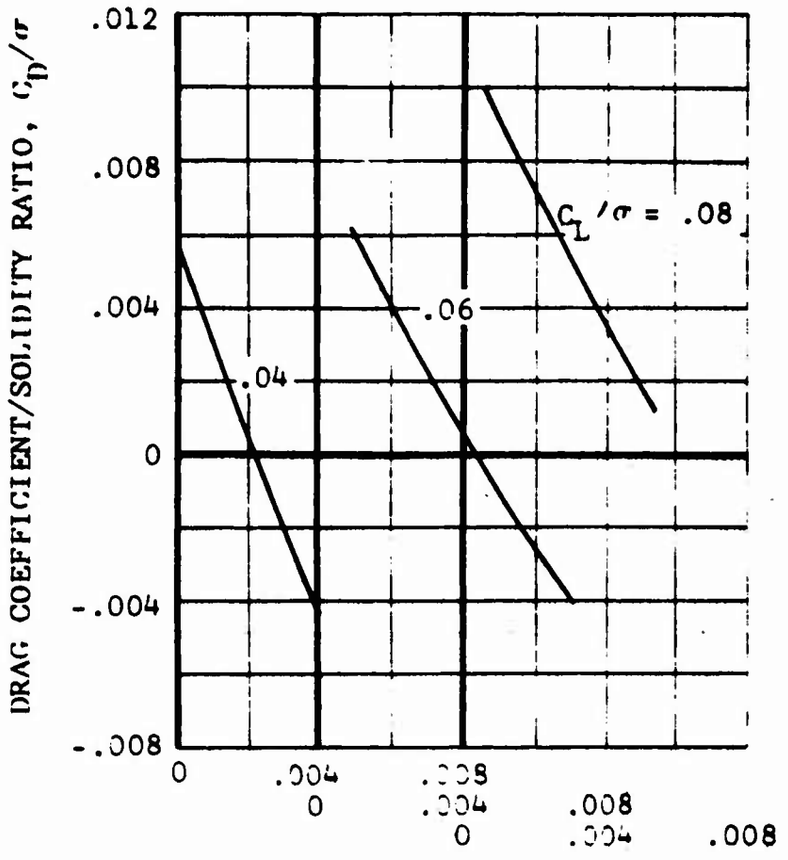

(g) μ = 0.46, $M_{(1.0,\ 90)}$ = 0.96

Figure 35. Continued.

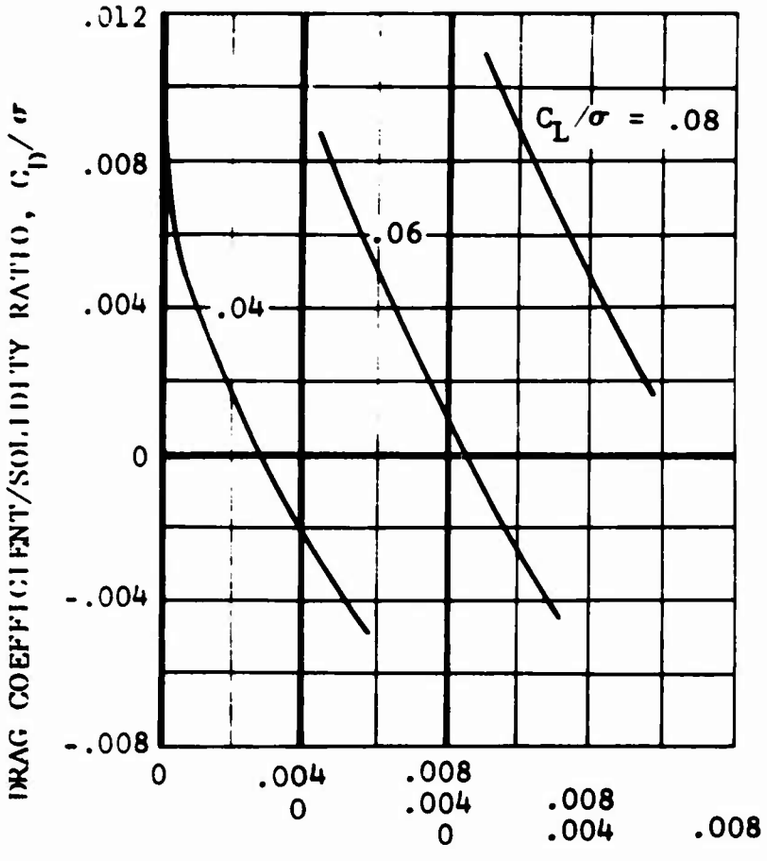

(h) μ = 0.45, $M_{(1.0,\ 90)}$ = 0.90

Figure 25. Continued.

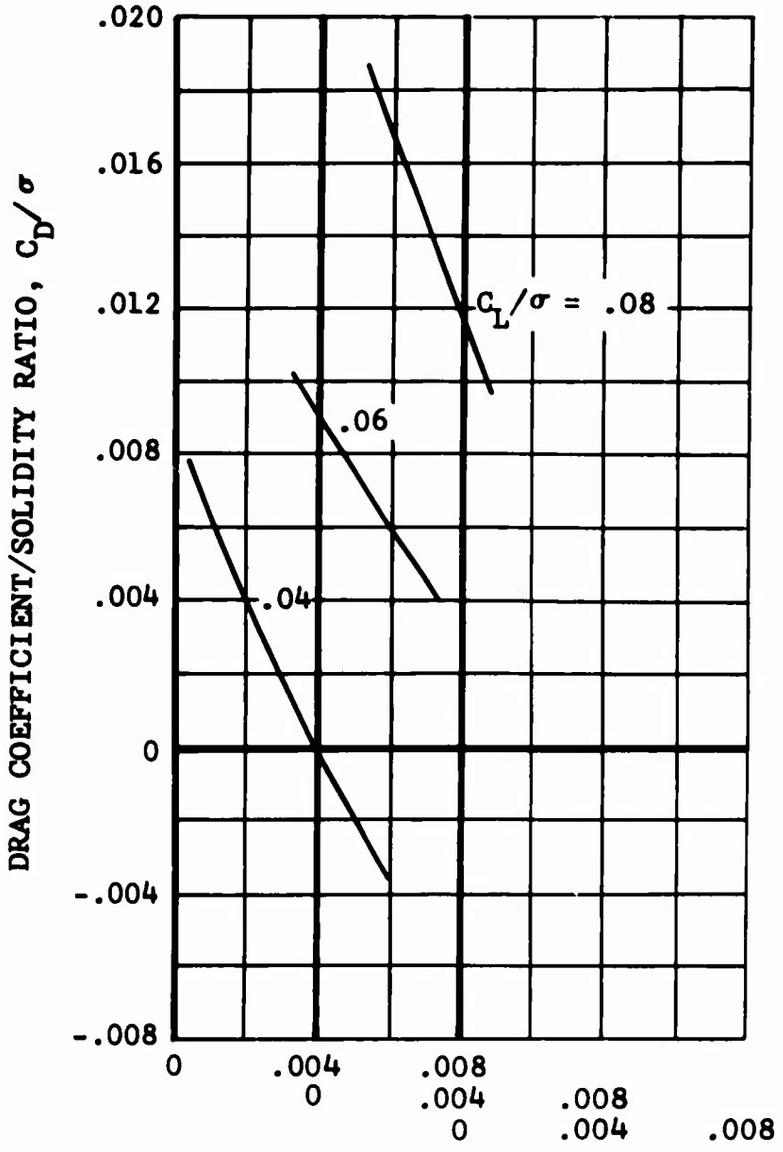

(i) μ = 0.51, $M_{(1.0,\ 90)}$ = 0.80

Figure 25. Concluded.

APPENDIX III
-10-DEGREE-TWIST MODEL ROTOR EXPERIMENTAL AND THEORETICAL PERFORMANCE

Experimental performance of the -10-degree-twist Bell 540 model rotor is presented in Figure 26 for various advance ratios and advancing-tip Mach numbers. The data from which these graphs were derived are available in Reference 1. Theoretical model performance calculations using the uniform-inflow analysis are included for comparison.

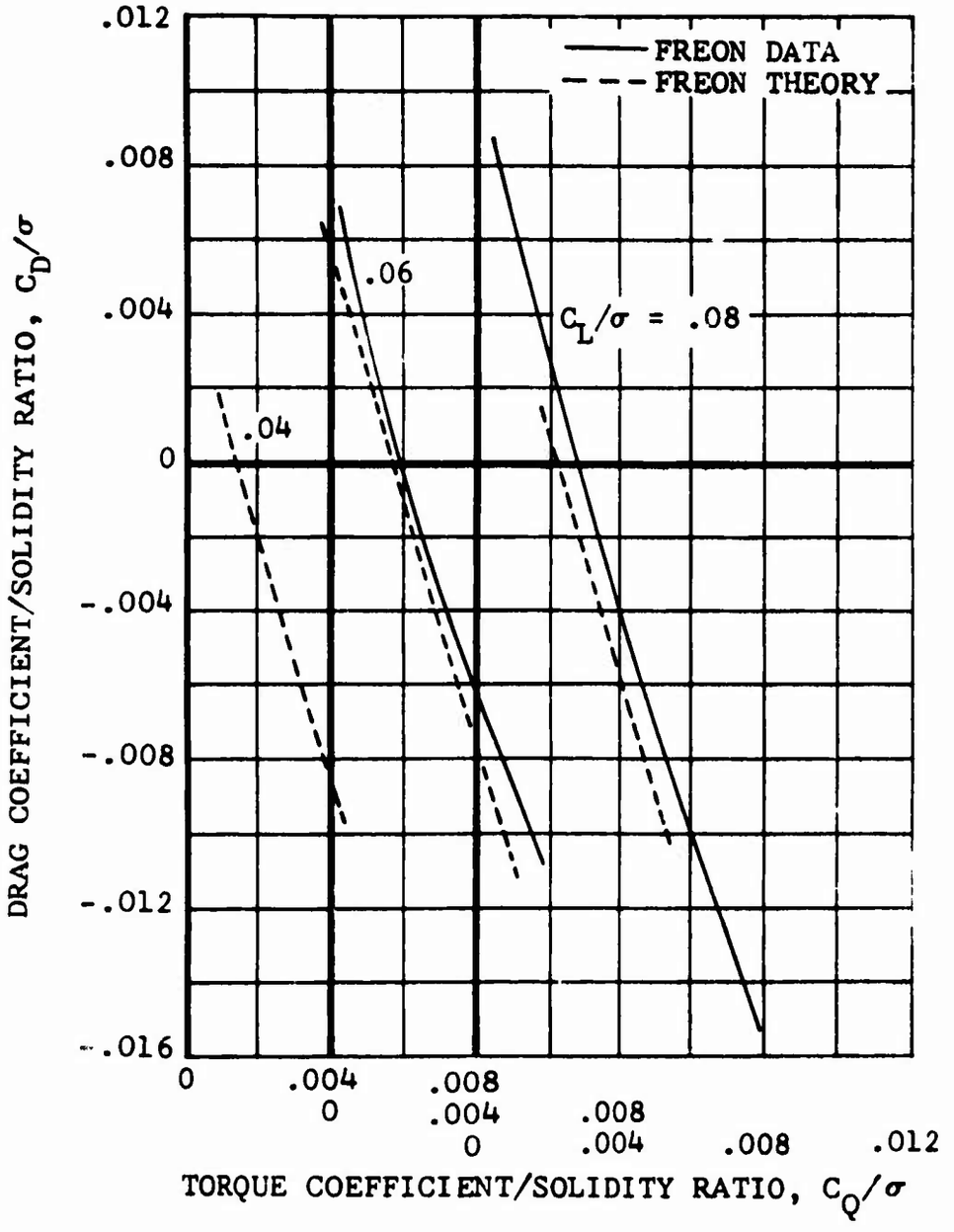

(a) μ = 0.30, $M_{(1.0,\ 90)}$ = 0.73

Figure 26. Test-Theory Comparison, Nondimensional Performance of Freon -10-Degree-Twist Rotor at μ = 0.30 and Various Advancing-Tip Mach Numbers.

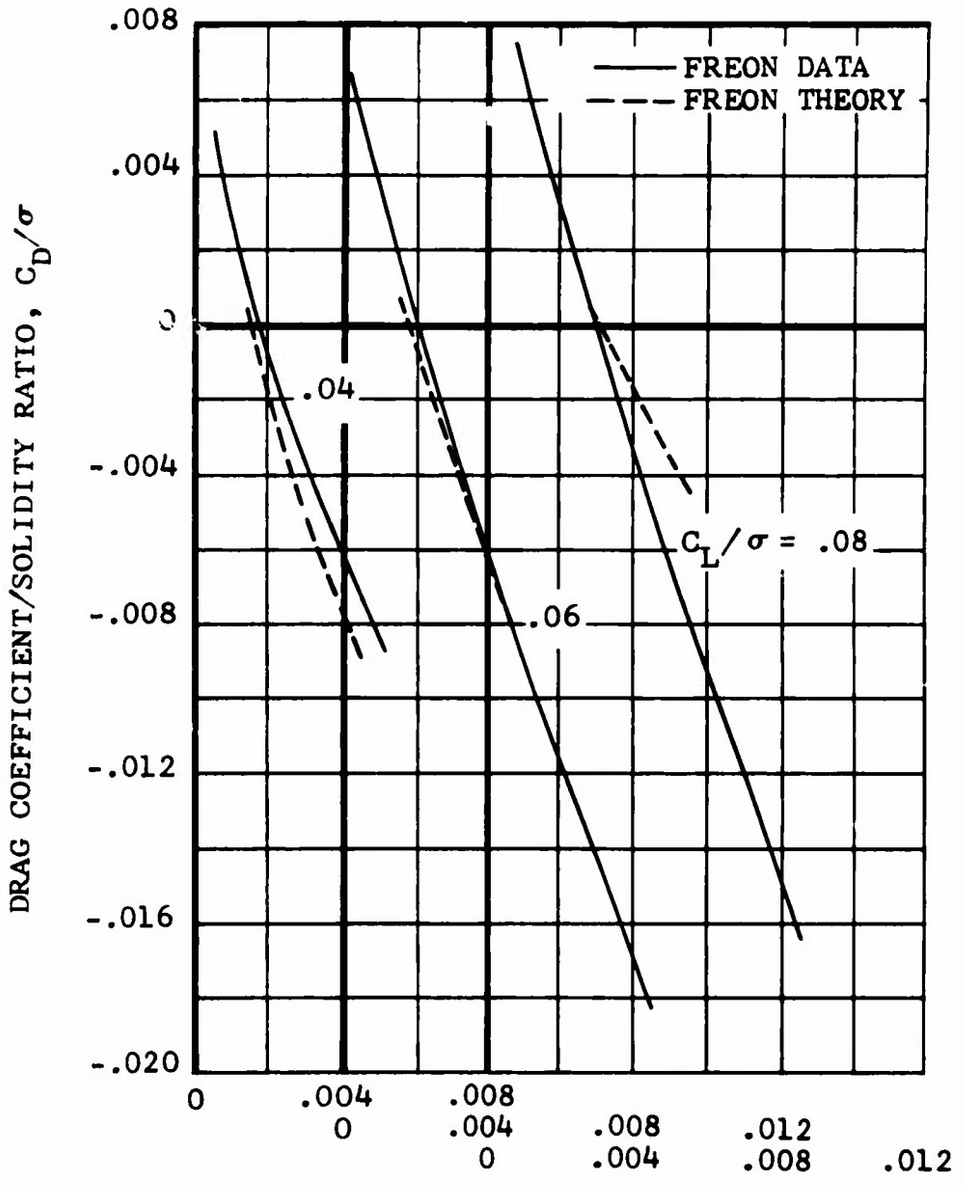

(b) μ = 0.30, $M_{(1.0,\ 90)}$ = 0.80

Figure 26. Continued.

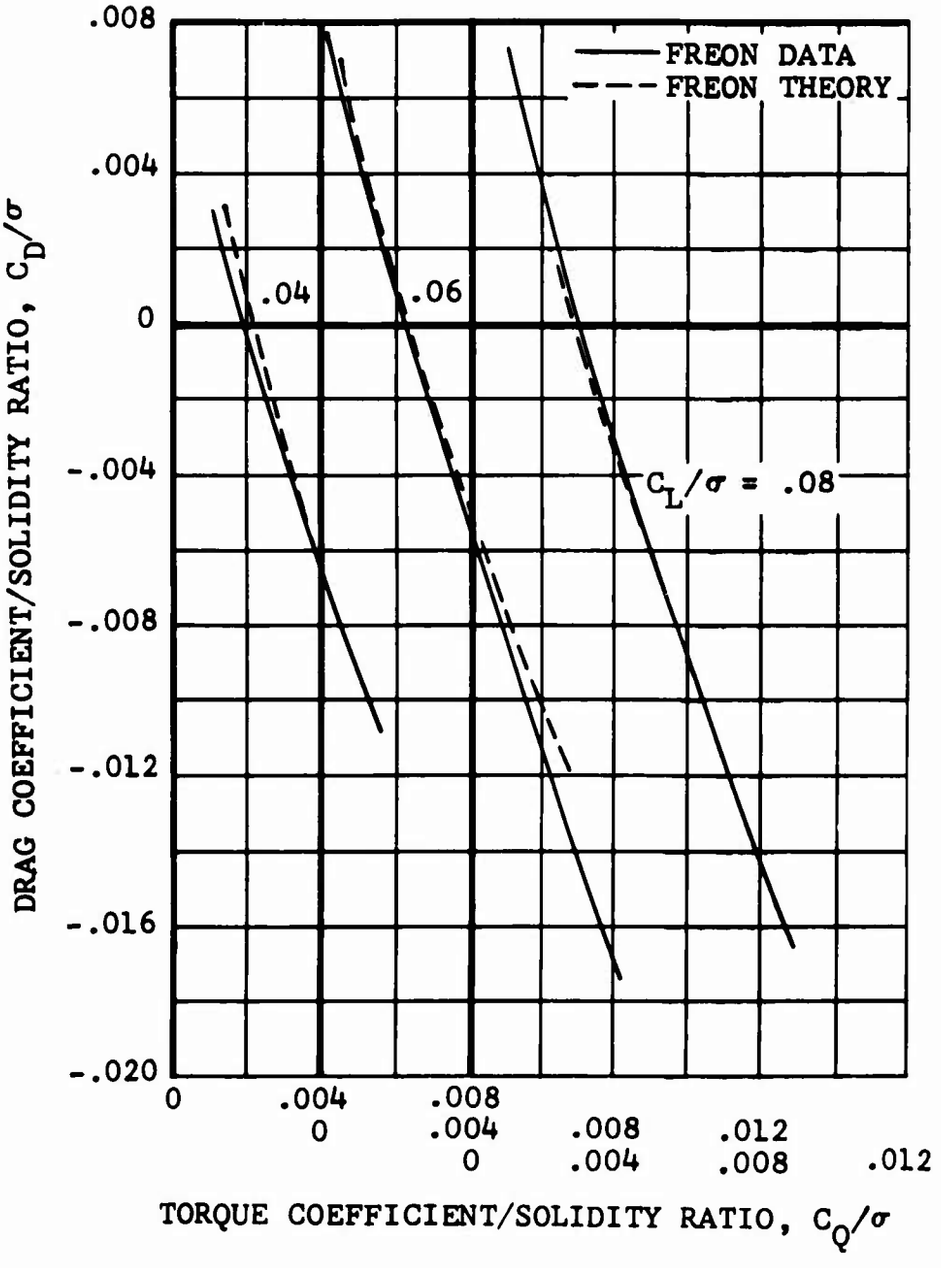

(c) = 0.30, $M_{(1.0,\ 90)}$ = 0.87

Figure 26. Continued.

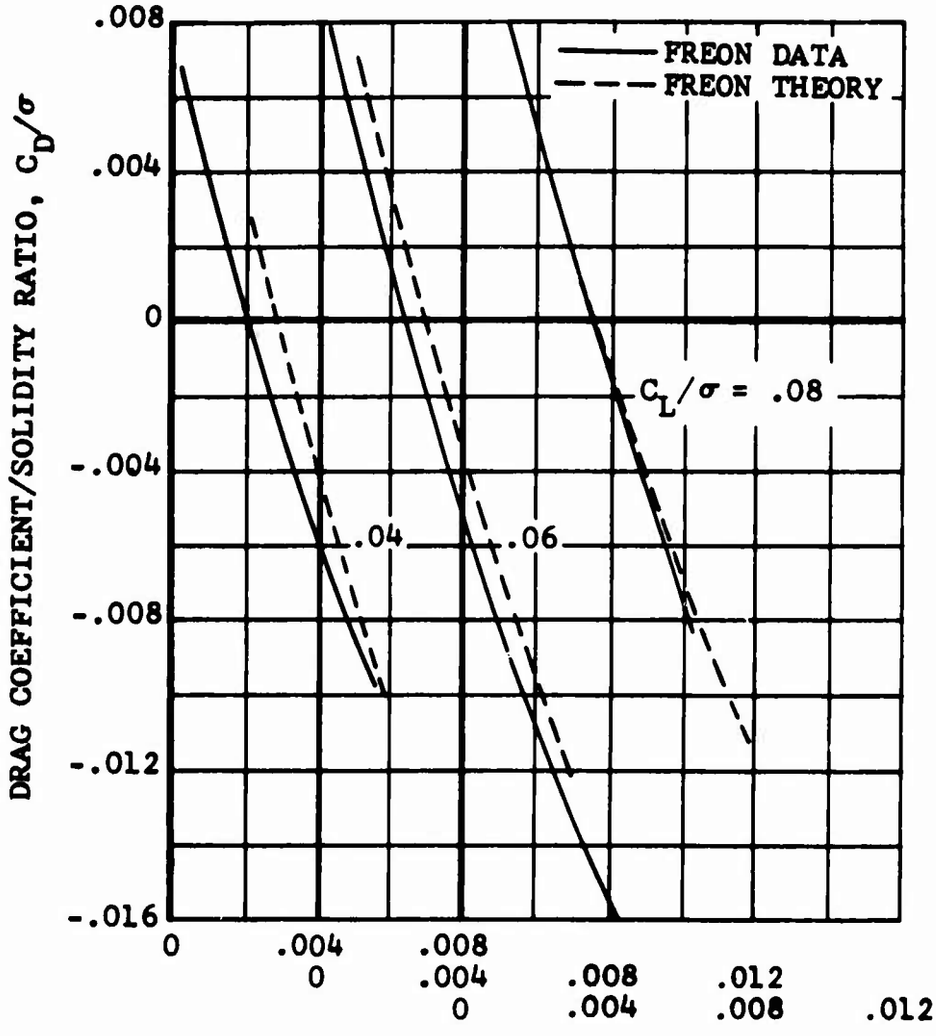

(d) $\mu = 0.30$, $M_{(1.0,\ 90)} = 0.91$

Figure 26. Continued.

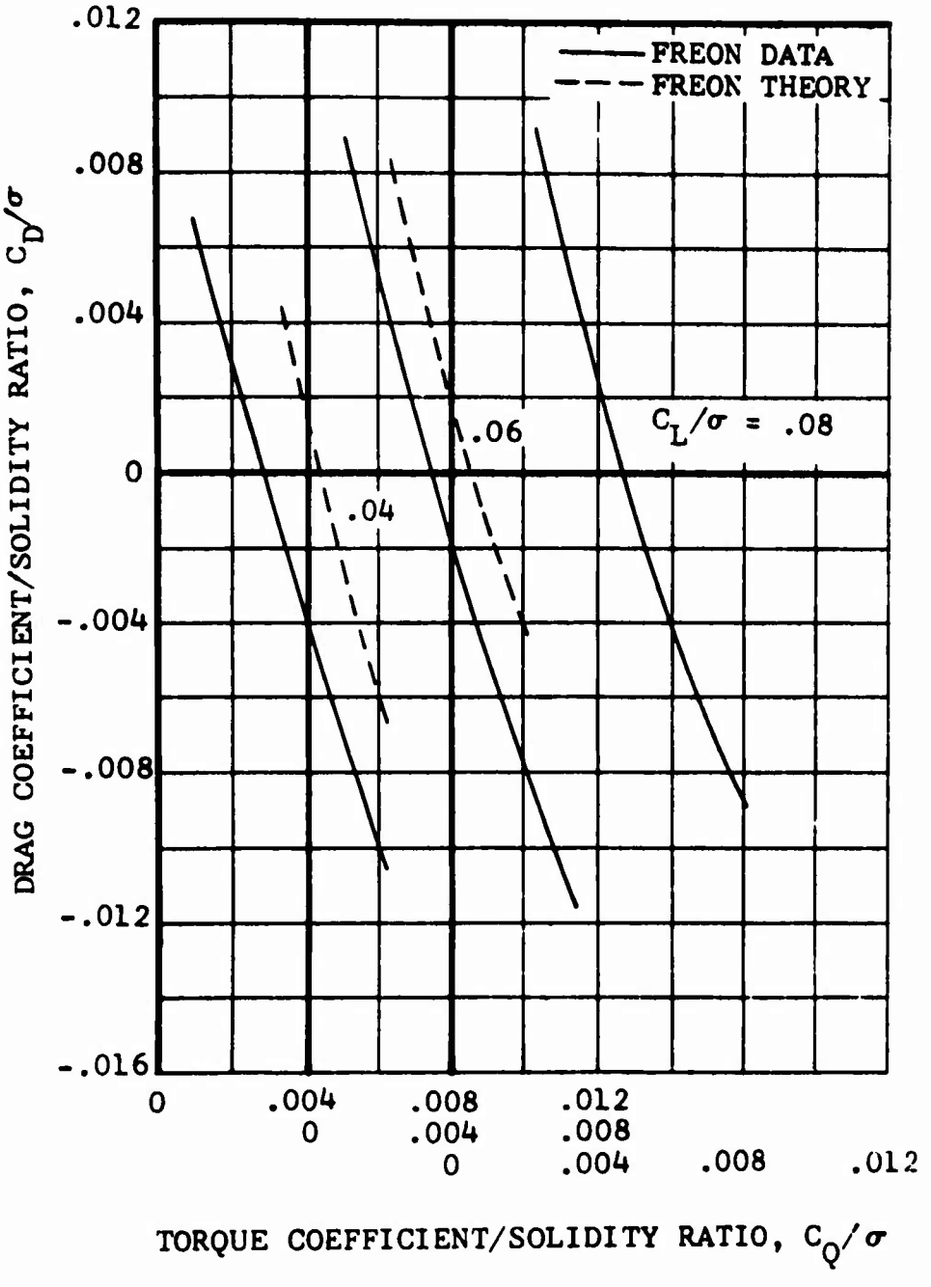

(e) $\mu = 0.30$, $M_{(1.0,\ 90)} = 0.96$

Figure 26. Concluded.

APPENDIX IV
FULL-SCALE STANDARD AND THIN-TIP UH-1D EXPERIMENTAL ROTOR PERFORMANCE

Full-scale performance of standard UH-1D (Figures 27 a-c) and thin-tip UH-1D (Figures 28 a-c) rotors is presented for 0.30 advance ratio and various advancing-tip Mach numbers. The performance is shown graphed in a carpet plot format using data obtained from Reference 2.

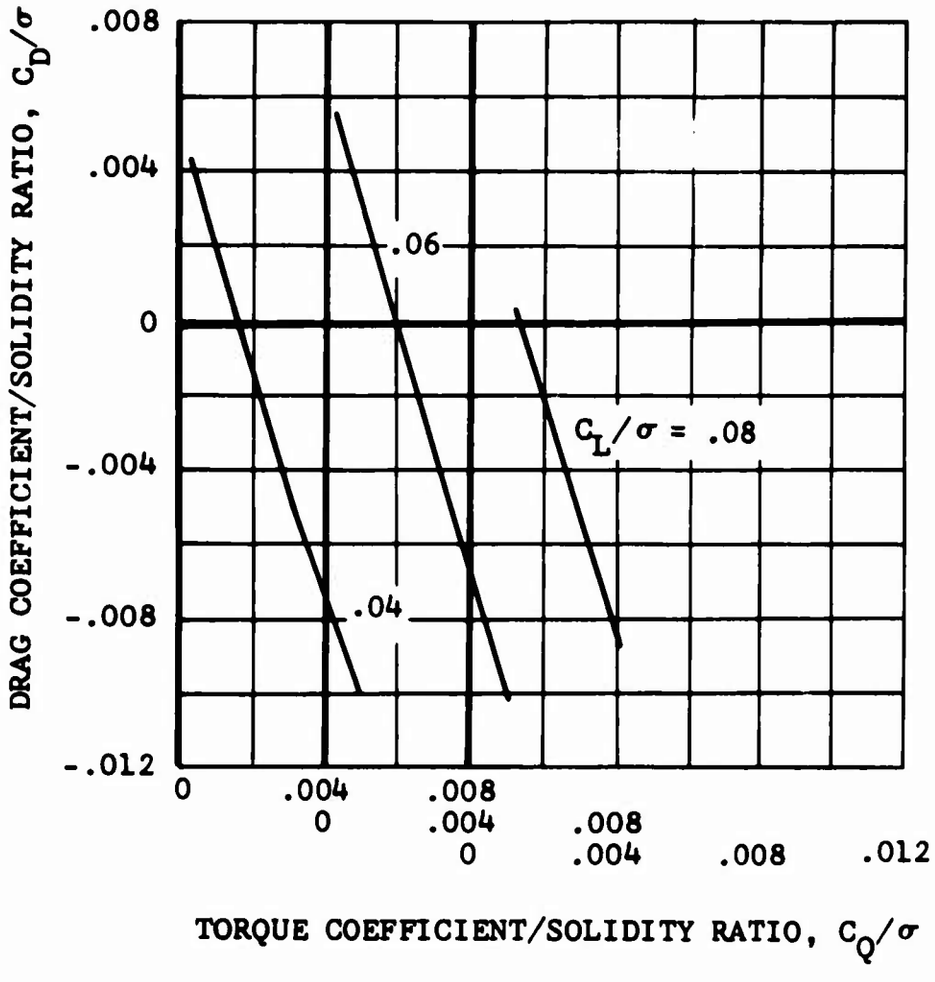

(a) $M_{(1.0,\ 90)}$ = 0.79

Figure 27. Nondimensional Performance of Standard and Thin-Tip UH-1D Rotors at μ = 0.30 and Various Advancing-Tip Mach Numbers.

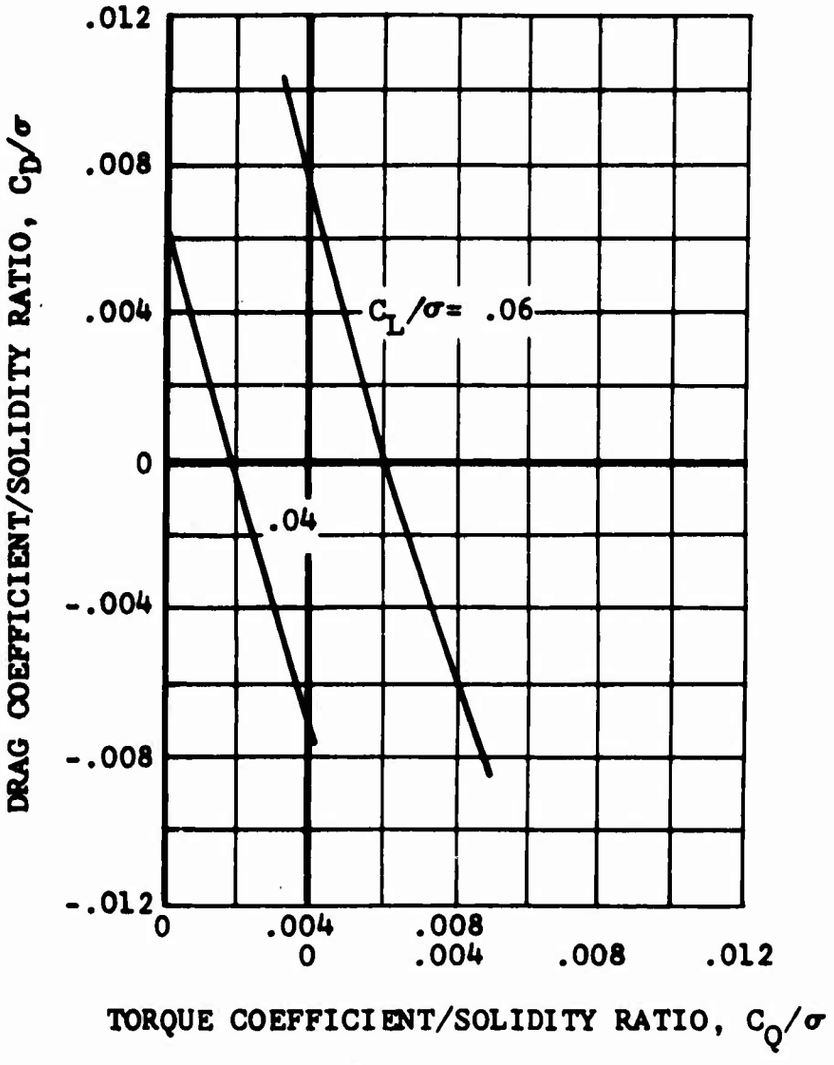

(b) $M_{(1.0,\ 90)} = 0.85$

Figure 27. Continued.

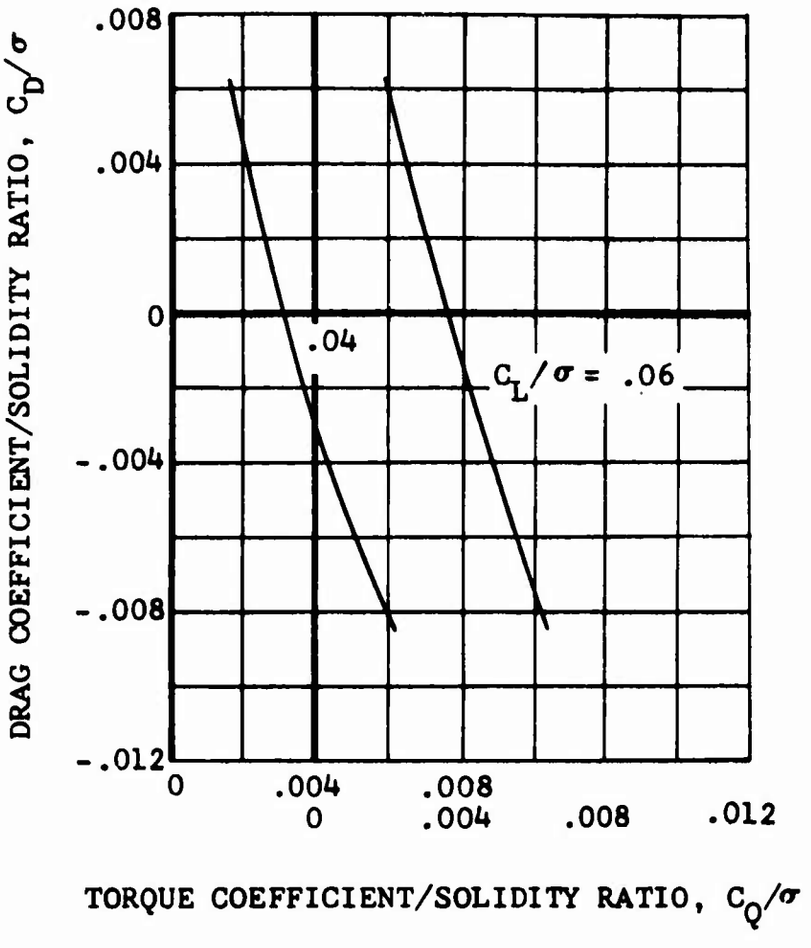

(c) $M_{(1.0,\ 90)} = 0.95$

Figure 27. Concluded.

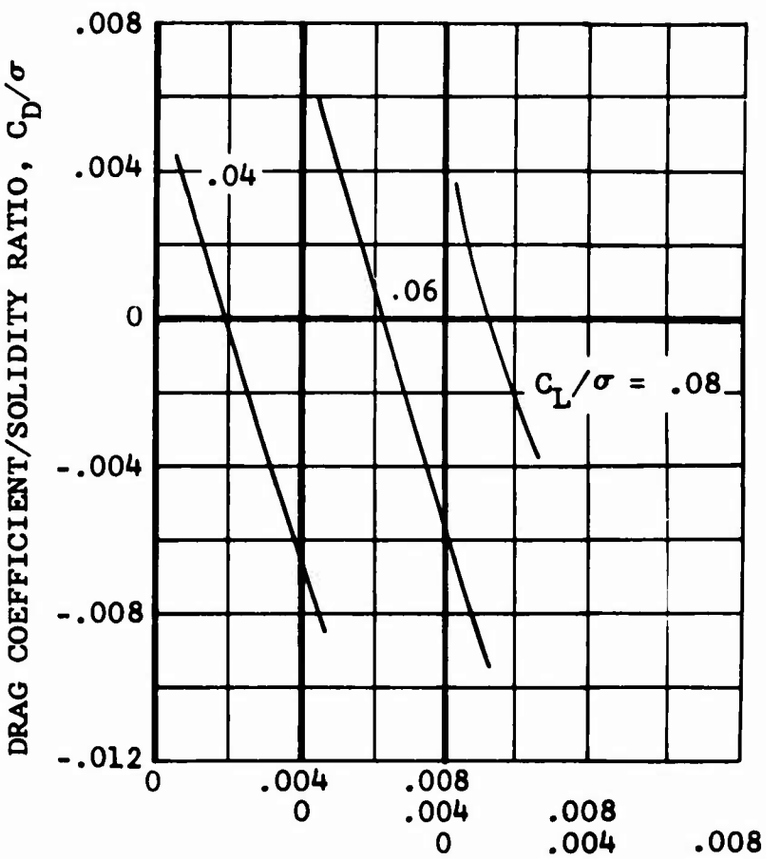

(a) $M_{(1.0,\ 90)} = 0.79$

Figure 28. Nondimensional Performance of Thin-Tip UH-1D Rotors at $\mu = 0.30$ and Various Advancing-Tip Mach Numbers.

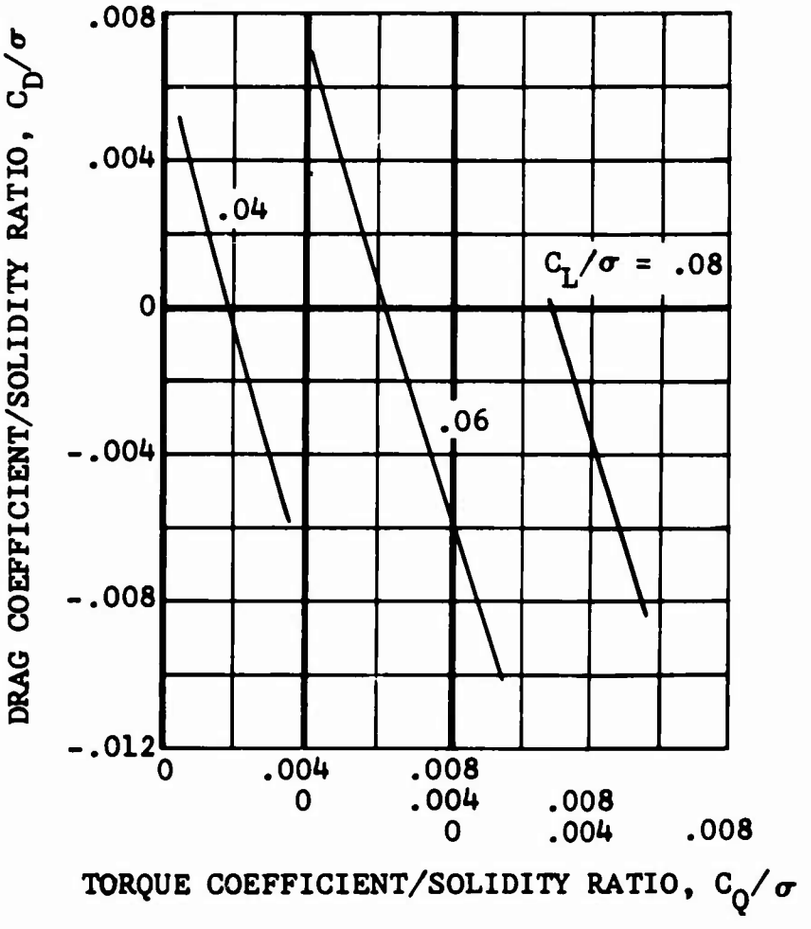

(b) $M_{(1.0,\ 90)} = 0.85$

Figure 28. Continued.

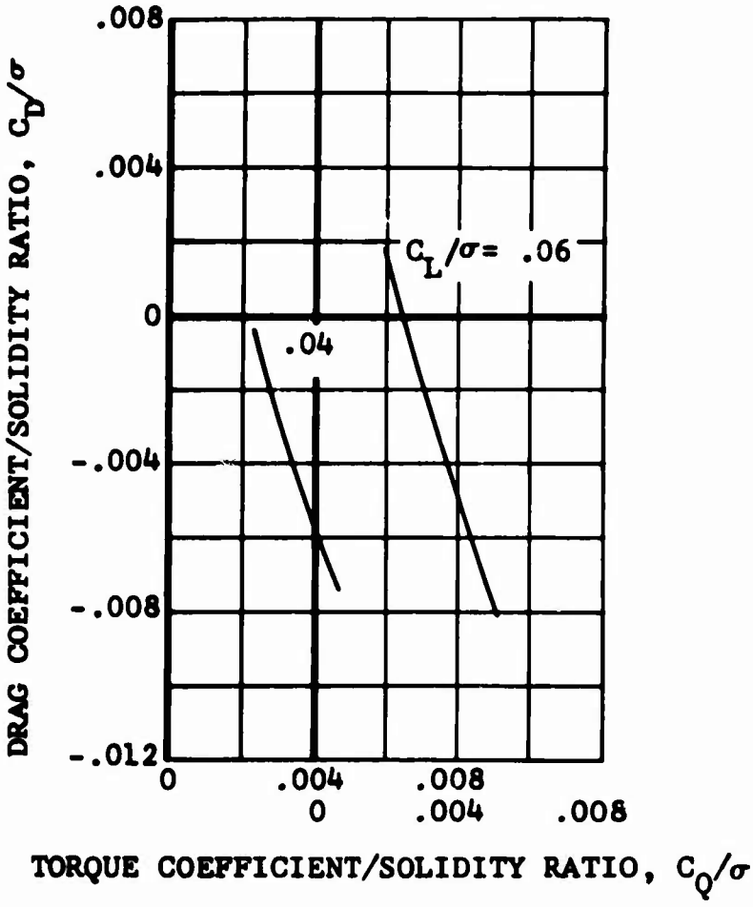

(c) $M_{(1.0,\ 90)} = 0.95$

Figure 28. Concluded.

Unclassified

Security Classification

DOCUMENT CONTROL DATA - R & D

(Security classification of title, body of abstract and indexing annotation must be entered when the overall report is classified)

1. ORIGINATING ACTIVITY (Corporate author)	2a. REPORT SECURITY CLASSIFICATION
Bell Helicopter Company Fort Worth, Texas	Unclassified 2b. GROUP

3. REPORT TITLE

AN EXPERIMENTAL/THEORETICAL CORRELATION OF MODEL AND FULL-SCALE ROTOR PERFORMANCE AT HIGH ADVANCING-TIP MACH NUMBERS AND HIGH ADVANCE RATIOS

4. DESCRIPTIVE NOTES (Type of report and inclusive dates)

Final Report

5. AUTHOR(S) (First name, middle initial, last name)

Bruce D. Charles

6. REPORT DATE	7a. TOTAL NO. OF PAGES	7b. NO. OF REFS
January 1971	127	13

8a. CONTRACT OR GRANT NO.	9a. ORIGINATOR'S REPORT NUMBER(S)
DAAJ02-69-C-0098 NEW b. PROJECT NO 1F162204A13903 c. d.	USAAVLABS Technical Report 70-69 9b. OTHER REPORT NO(S) (Any other numbers that may be assigned this report) BHC Report 576-099-055

10. DISTRIBUTION STATEMENT

This document is subject to special export controls, and each transmittal to foreign governments or foreign nationals may be made only with prior approval of Eustis Directorate, U.S. Army Air Mobility R&D Laboratory, Fort Eustis, Virginia 23604.

11. SUPPLEMENTARY NOTES	12. SPONSORING MILITARY ACTIVITY
	Eustis Directorate U.S. Army Air Mobility R&D Laboratory Fort Eustis, Virginia

13. ABSTRACT

Aerodynamic performance of two reduced-scale model rotors has recently been obtained in a Freon atmosphere in the NASA-Langley Transonic Dynamics Tunnel. The results are compared with the existing full-scale wind tunnel and inflight rotor performance data to substantiate this method of testing rotors. Additionally, current-state-of-the-art analytical techniques are employed to calculate the model performance. Overall, the model and full-scale results show good agreement when compared nondimensionally on an equal resultant force coefficient basis. Expected differences (due to rotor airfoil section differences) at conditions near rotor stall and at high advancing tip Mach numbers were not found in the test data. Possible implications are that a rotor tested in Freon may experience less severe stall and compressibility effects than would be shown by a corresponding rotor tested in air.

DD FORM 1 NOV 68 1473 REPLACES DD FORM 1473, 1 JAN 64, WHICH IS OBSOLETE FOR ARMY USE.

Unclassified

Security Classification

14. KEY WORDS	LINK A		LINK B		LINK C	
	ROLE	WT	ROLE	WT	ROLE	WT
Scale model rotor performance in a Freon atmosphere						
Thin-tip main rotor blades						
High advancing-tip Mach number						
High advance ratio						